Open-Dissipative Mean-Field Theory for Photon Bose-Einstein Condensates

Diplomarbeit in Theoretischer Physik

durchgeführt von

Enrico Stein

am Fachbereich Physik der TU Kaiserslautern

unter Anleitung von

Priv.-Doz. Dr. Axel Pelster

Juli 2018

Abstract

In the last two decades the phenomenon of Bose-Einstein condensation, where the ground state of a quantum system of many bosons gets macroscopically occupied, has been studied extensively. One of the latest systems, where such a phase transition can occur, is a photon Bose-Einstein condensate. The core of the system is a dye solution filling a microcavity in which the photons are effectively harmonically trapped. Due to cyclic absorption and reemission processes of photons the dye leads to a thermalisation of the photon gas at room temperature. Furthermore, as a consequence of a nonideal quantum efficiency, those cycles yield in addition a heating of the dye solution, which results in a change of the refractive index and, thus, in an effective thermo-optic photon-photon interaction. A second mechanism providing a photon-photon interaction is the Kerr-effect, i.e. a nonlinearity of the refractive index that is directly proportional to the light intensity of the photon condensate.

In this thesis we set up a mean-field theory that is able to describe a photon Bose-Einstein condensate under influence of these two possible kinds of interaction. For this purpose we derive on heuristic grounds a system of two equations, one for the condensate mean-field wave function and one for the temperature that is produced by the photons diffusing through the dye solution in the cavity. These two equations are coupled in the sense that the condensate amplitude is the source of the temperature, whereas the temperature changes the refractive index of the dye solution and, thus, shifts the chemical potential of the photons. We will show that this already describes the thermo-optic effect and that pump and loss effects play an important role for the temporal evolution of the condensate. Moreover, we make use of the fact that longitudinally trapped photons behave as massive particles in the remaining two transversal degrees of freedom. As the photon equation is now purely stated in two dimensions, we also eliminate the longitudinal degree of freedom from the temperature equation.
Equipped with this system of both two-dimensional differential equations, our aim is to look on the imprints of the thermo-optic photon-photon interaction upon the collective excitations of the photon Bose-Einstein condensate. Thus, we start our analysis by calculating the dispersion relation of the homogeneous condensate. We find that, in contrast to a Bogoliubov spectrum that is based on a closed Gross-Pitaevskii equation, here also damping and instabilities occur.
Afterwards we look into the frequencies of the lowest-lying collective excitations of the harmonically trapped condensate via a linear stability analysis. Due to the open-dissipative character of the system its energy is not conserved and, thus, it is not possible to investigate its dynamical properties within a usual variational approach by using an action. Instead, we work out an approximation which is based on determining the equations of motion for the first two cumulants under the assumption that both the condensate wave function and the temperature distribution are Gaussian shaped. In particular, we find that the Kohn theorem is broken due to the thermo-optic interaction, i.e. the frequency of the dipole mode turns out to depend on the photon-photon interaction and, thus, is shifted to smaller frequencies.
Finally we eliminate the temperature degrees of freedom by using the Green's function of the temperature diffusion equation. By doing this we recover a single open-dissipative Gross-Pitaevskii equation with an interaction that is nonlocal in both space and time due to the interplay of temperature diffusion and thermo-optic interaction. With this equation at hand, we revisit again both the homogeneous and the trapped case. Whereas in the homogeneous case the same results as for the previous approach come out, it turns out in the trapped case that the former Gaussian ansatz for the temperature fails for strong diffusion.

Zusammenfassung

In den vergangenen beiden Jahrzehnten wurden Bose-Einstein Kondensate, bei denen der Grundzustand eines quantenmechanischen Systems aus vielen Bosonen makroskopisch besetzt wird, ausführlich untersucht. Eines der jüngsten Systeme, in denen ein solcher Übergang erzeugt wurde, ist ein Bose-Einstein Kondensat aus Photonen. In nuce besteht das System aus einem mit einer Farbstofflösung gefüllten Mikroresonator, in welchem die Photonen harmonisch gefangen sind. Da diese mehrere Male vom Farbstoff absorbiert und wieder in die Kavität emittiert werden, bevor jene den Resonator verlassen, kann das Photonengas zur Raumtemperatur thermalisieren. Da die Quanteneffizienz des Farbstoffs limitiert ist, führen diese Absorptions- und Emissionsprozesse zu einer Erwärmung des Farbstoffs, wodurch sich dessen Brechungsindex ändert, was zu einer effektiven thermooptischen Wechselwirkung zwischen den Photonen führt. Der Kerr-Effekt, der eine Nichtlinearität des Brechungsindex proportional zur Lichtintensität beschreibt, ist eine weitere Möglichkeit, eine solche Wechselwirkung herbeizuführen.

Diese Arbeit behandelt eine Molekularfeldtheorie, die in der Lage ist, ein Photonenkondensat, das eben diese beiden Wechselwirkungsprozessen unterliegt, phänomenologisch zu beschreiben. Dafür wird unter heuristischen Gesichtspunkten ein System bestehend aus zwei Gleichungen hergeleitet, von denen eine das Kondensat und die andere die Temperatur beschreibt. Dieses ist derart gestaltet, dass die Photonendichte als Quelle der Temperatur dient und jene über den Brechungsindex das chemische Potential der Photonen beeinflussen kann. Es wird gezeigt, dass diese Annahmen sowie die Beachtung von Pump und dissipativen Prozessen genügen, um den thermooptischen Effekt zu beschreiben. Darüber hinaus wird ausgenutzt, dass sich Photonen, die in einer Raumrichtung gefangen sind, als massive Bosonen in den verbleibenden beiden Richtungen verhalten. Da die Kondensatgleichung nun zweidimensional ist, wird auch der longitudinale Freiheitsgrad der Temperaturgleichung eliminiert.
Das Ziel besteht nun darin, die Auswirkungen der thermooptischen Wechselwirkung auf die kollektiven Anregungen des Photonenkondensates zu untersuchen. Zu Beginn wird die Dispersionsrelation des homogenen Kondensates berechnet. Diese weicht vom bekannten Bogoliubov-Spektrum einer geschlossenen Gross-Pitaevskii-Gleichung dahingehend ab, dass nun die Anregungen gedämpft sind und auch Instabilitäten auftreten können.
Hernach werden durch eine lineare Stabilitätsanalyse die kollektiven Anregungen des harmonisch gefangenen Kondensats untersucht. Hierbei muss beachtet werden, dass aufgrund der Offenheit des Systems keine Wirkung existiert, so dass der übliche Variationszugang nicht zur Verfügung steht. Stattdessen wird ein Verfahren benutzt, das auf den Bewegungsgleichungen der Kumulanten beruht. Dazu wird angenommen, dass sowohl Kondensatwellenfunktion als auch die Temperaturverteilung einem Gauß'schen Profil entsprechen. Damit lässt sich unter anderem zeigen, dass das Kohn-Theorem aufgrund der thermooptischen Wechselwirkung nicht mehr gilt, dass also die Frequenz der Dipolmode nicht mehr identisch der Fallenfrequenz ist und durch diese Wechselwirkung reduziert wird.
Zuletzt wird die Temperaturgleichung formal durch eine Green'sche Funktion gelöst, woraus sich eine einzelne Kondensatgleichung gewinnen lässt, die nun Nichtlokalitäten sowohl im Raum als auch in der Zeit aufweist. Während dies im homogenen Falle zu denselben Ergebnissen führt, stellt sich heraus, dass durch die Anwesenheit der harmonischen Falle der Gauß'sche Ansatz bei starker Diffusion nicht mehr gültig ist.

Contents

Introduction

In nova fert animus mutatas dicere formas
corpora: di, coeptis (nam vos mutastis et illas)
adspirate meis primaque ab origine mundi
ad mea perpetuam deducite tempora carmen.

P. Ovidius Naso, Metamorphoseon, ll. 1-4

My soul is wrought to sing of forms transformed
to bodies new and strange! Immortal Gods
inspire my heart, for ye have changed yourselves
and all things you have changed! Oh lead my song
in smooth and measured strains, from olden days
when earth began to this completed time!

This thesis is devoted to the theoretical understanding of an exotic state of light, it is about what is called a Bose-Einstein condensate of light. Light, as the historic development of its understanding shows, has been a source of new concepts through all the decades of human thinking.

1. A Historic Introduction

Already the curiosity driven ancient Greeks spent many thoughts on the true nature of light. In their reception light per se was at first not a phenomenon by itself but a tool for seeing the surrounding. The philosopher Empedocles (ca. 495-435 AC), who claimed the existence of the four roots of the being are fire, water, earth and air, explained light produced by a fire in the eye and streaming as a ray out of the eye. But on the other hand he also expressed the view that light is produced by the things visible and streaming on rays to the eyes [1]. A century later the famous mathematician Euclid (about 300 AC), who brought to us the fundamentals of geometry, also explained light by rays coming out of one's eyes that travel at infinite speed. He was the first one who started to examine light in a scientific way by studying the law of refraction already by using mathematics [2]. But there was not only the school that treated light as rays, also the atomistic point of view was already present at that time. For instance, the Roman philosopher Lucretius (99-55 AC) claimed that light, as the remaining nature (cf. the work of Democrit), consists of smallest particles that are non dividable [3]. As we see, already in the ancient days the wave-particle duality was a topic to discuss upon, although it was not guided by what is nowadays called exact reasoning.

The modern understanding of the nature and the mathematical description of light began with

Descartes. He understood light as a mechanical property of luminous bodies and the medium in that it propagates. In the course of this he compared light to sound waves and was able to describe refraction by assuming a change of its propagation velocity. He followed the analogy between sound waves and light although he was convinced by the corpuscular theory [4]. After him Fermat claimed that light always follows a route that takes the least time [4]. That is what is today called Fermat's principle and is a special case of the least action principle. In the same century fundamental new experiments by Newton [5], who found the spectral decomposition of light passing through a prism, and Roemer, who estimated in 1676 the light velocity to being finite [4], were followed by new theoretical ideas. On the one hand there was Huygens with his proposal of light being a wave that propagates through a medium that he called aether. With this perception of light he was able to explain the findings of reflection, refraction and interference, but he was not able to cover the straightforward movement of light in free space [6]. On the other hand, by taking a corpuscular view on light Newton was able to describe exactly this movement in free space as well as the occurrence of colour that he explained with the existence of many light particles of different weight. Moreover, he was still able to describe reflection and refraction, but he failed to describe interference effects, since this is an intrinsic property of linear waves. In order to treat this phenomenon he expressed some thoughts on a theory that mixes some wave-like behaviour in his corpuscular theory [5, Book III]. Thus, Newton showed volens nolens that light cannot completely be described by only taking the one or the other point of view.

In the following century Young was able to conduct detailed experiments on interference phenomena. The most famous of those experiments is his double-slit experiment. He then was able to propose the interference principle that underlined the wave nature of light as Huygens proposed. Governed by the findings of Young and Huygens, Fresnel was able to formulate a mathematical rigorous wave theory of light that was in reasonable agreement with the experiment. But there was the problem of the deeper understanding why light can be described in exactly that way since attempts to formulate the wave theory in terms of an collectively oscillating aether were not successful. More insight into the physical foundations was given by the electromagnetic theory developed by Maxwell that is based on the experiments of Faraday [7, 8]. In this theory the existence of electromagnetic waves follows directly from the equations postulated by Maxwell. Due to the coincidence of the propagation velocity of the Maxwell waves with the one of the light waves people were able to identify those electromagnetic waves with light. Concerning the propagation medium the experiments by Michelson and Morley suggested that no aether exists and consequently light is able to propagate through vacuum as Einstein concluded in Ref. [9]. Thus, it seemed that all questions concerning the nature of light have been answered or will be answered in the near future. Two experimental facts that were not answered so far, however, are the black-body radiation and the photoelectric effect.

In the beginning of the twentieth century Planck was able to solve the riddle of the black-body radiation [10–12]. He introduced oscillators carrying energy quanta that are multiples of the eigenfrequencies of the oscillators. With that approach he was able to justify his heuristic interpolation of the Wien and the Rayleigh-Jeans law that described so far either the small or long wavelength regime of the black-body radiation distribution, respectively. He was able to show that a quantisation of the light field was necessary to find a reasonable agreement between theory and experiment. Along those lines Einstein proposed the existence of light quanta and was able to solve the mystery concerning the photoelectric effect [13]. From now on it was clear that light - as the remainder of the fundamental phenomena - is in a need to be described quantum

mechanically. With the upcoming wave mechanics, as it was suggested by de Broglie [14] and formulated by Schrödinger [15,16], the old conflict between the followers of the atomistic view on light and the ones appreciating the wave approach to light were showed to be combinable and the compromise solution that Newton formulated in an embryonic state seems to be a forethought of these new ideas.

In 1927 Dirac formulated at first a full quantum mechanical theory of radiation [17] and paved the way for quantum electrodynamics. With the progress of this very theory, one was also able to understand the interaction between light and matter at heart. This development led in the 1960s to the invention of the laser [18]. This was nothing but a taming of light as with the technical process of this apparatus it became very easy to prepare light in some certain state and to tweak with that light-atom interaction. Now light turned from a phenomenon worth to be examined to a tool in the laboratories. In the spirit of this the laser cooling mechanism was been invented and driven forward by Chu, Phillips and Cohen-Tannoudji.

It turned out, that laser cooling is one of the basic techniques needed to get a Bose-Einstein condensate (BEC). Within this state of bosonic matter, where apart from the thermal cloud, the bosons occupy the same quantum mechanical state and behave collectively as a quantum liquid. The first BEC was achieved by Cornell and Wieman [19] as well as by Ketterle [20] in 1995, since then the field of ultracold atoms evolved rapidly and soon the basic properties of BECs became well known facts.
In today's research BECs are used as a tool to simulate quantum mechanical systems that are not directly experimentally accessible or hard to prepare. One example is a BEC in an optical lattice. Here, one can show that the excitations of the BEC fulfil a dispersion relation that is analogue to that of electrons in a solid material [21].
A second example is the simulation of black-hole physics with BECs [22]. As the sound velocity in such a system is finite, one can construct an ereignishorizont in a supersonic BEC, as the sound velocity plays the role of light velocity in general relativity.
Thus, one can use BECs to simulate different physical systems and resembles physics as the "art of interchangeable" [23]. One can also ask the question about turning the point of view and let photons condensate due to the interaction with matter and not to use light as a technique that allows for tweaking matter.

2. Quantum Fluids of Light and Exciton-Polariton Condensates

Light in a cavity behaves as if it possesses a mass and obeys a two-dimensional Schrödinger equation, a behaviour that is introduced by the cavity cutoff. Moreover, if the cavity is filled with a nonlinear material, also photon-photon interactions exist and, depending on the material, become a relevant part of the temporal evolution. This is the point, where photons start to behave in a collective manner. Thus, with enough photons in the nonlinear cavity, they behave as a quantum fluid. Indeed, it was shown in [24] that the equations for an electromagnetic field in a cavity can be rewritten in a hydrodynamic form and that certain spatial patterns, which are expected from usual hydrodynamics, can occur. Moreover, it could be shown that in a nonlinear laser cavity the electric field undergoes a nonequilibrium second-order phase transition to the lasing behaviour and the nonlinearity of the cavity yields an effective photon-

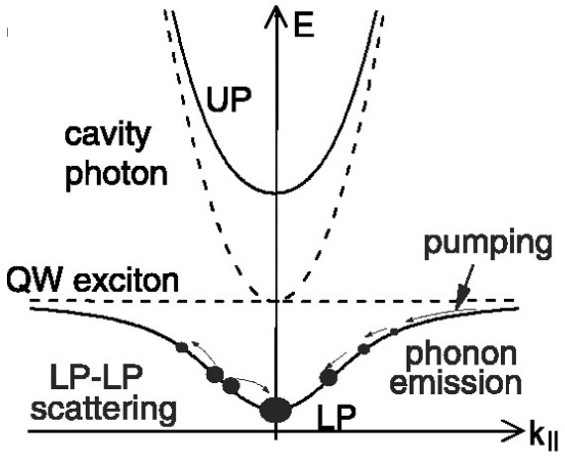

FIG. 1: Principle of the first exciton-polariton BEC [31]. The exciton-polariton gas is pumped by injecting coherently polaritons at a certain point of the dispersion relation indicated by the point pumping.

photon interaction [25].
Also superfluidity of light was observed. In [26] light was sent through a nonlinear bulk medium. By means of the paraxial approximation the propagation in the direction of the bulk medium can be mapped to the time evolution of a two-dimensional superfluid of light. In this system stable vortices have been observed. Today a similar experimental setup is used to simulate astronomical effects like the creation of Bose stars [27]. A similar experiment, in which lights behaves as a superfluid, was recently reported in [28]. In this setup light passed through a cell filled with atomic vapour. Since the vapour responds nonlinear to the light moving through the cell, also here a nonlinear photon fluid emerges.

Therefore, the question arises whether light can also undergo an equilibrium phase transition to a Bose-Einstein condensate. However, the first condensate of light was not a condensate of pure light, but a nonequilibrium condensate of exciton-polaritons. For a detailed review on this topic, we refer to [29, 30]. These are condensates of quasi-particles, which are built up of electron-hole pairs and cavity photons. This was achieved for the first time in the experiment of [31], whose principle is shown in Figure 1. Here, the cavity is pumped coherently, i.e. resonantly near the dispersion minimum. The injected excitations can then relax towards the minimum of the lower polariton dispersion. Above a certain pump threshold a parametric oscillation occurs that is due to a spontaneous $U(1)$ symmetry breaking, [32]. However, this leads to a nonthermalised condensate.
In order to achieve thermalisation of the condensate one needs to inject polaritons incoherently into the cavity, since under this circumstance interactions with the environment are much more relevant in order to relax to the ground state, see Figure 2. Therefore, a quasithermal state can evolve and, if the pump power exceeds the BEC threshold, even a thermalised BEC can occur, as was successfully demonstrated in [33]. Therefore, one gets an open-dissipative condensate, since it is coupled to a reservoir and polaritons can also be emitted. One year later, a heuristic mean-field model was introduced in order to describe this condensate [34]. This model consists of a Gross-Pitaevskii equation for the condensate that has also an imaginary part acting on

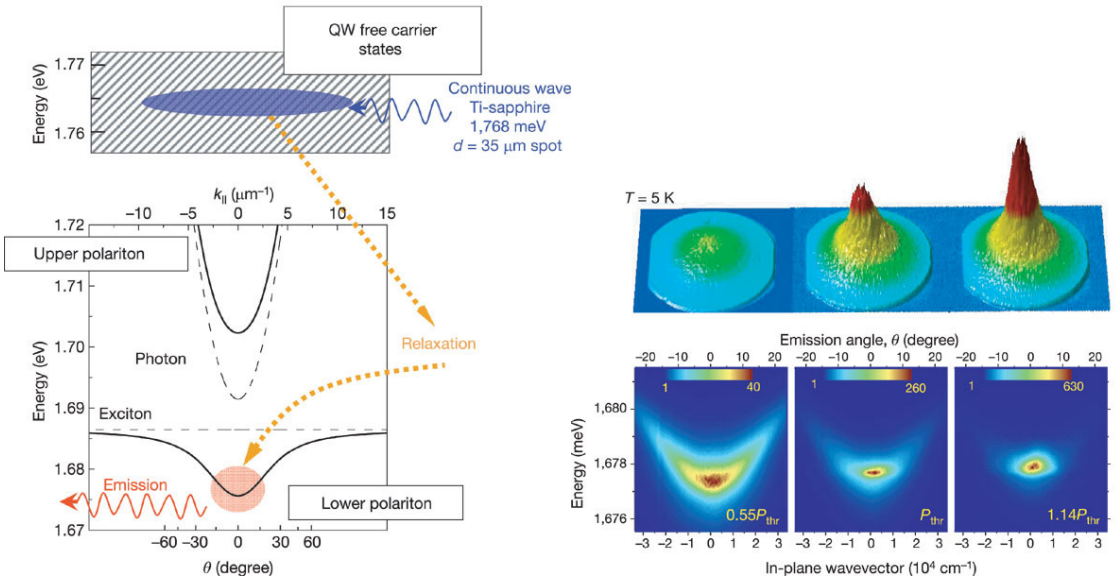

FIG. 2: Experimental principle from [33]. Panel **(a)** shows the dispersion relation of the polaritons and the incoherent excitation principle. The laser excites free carrier states at high energy, which then decay into polariton states. If the pump intensity is high enough, a BEC can form in the lowest polariton state. Panel **(b)** shows the creation of the condensate.

the amplitude of the condensate wave function in order to take pump and loss into account. Moreover, also the reservoir is modelled by a diffusion equation, that is coupled to the Gross-Pitaevskii equation. With this model it becomes possible to answer fundamental questions as the condensate dispersion and also examine the condensate in a double well potential.

Finally one can ask the question whether pure photons can condensate. This question was tackled in 2010 by the group of Martin Weitz [35] and already brings us to the topic of the present thesis.

3. Outline

In this thesis the question is formulated, whether a mean-field model for the photon BEC exists that is as easy as the one presented in [34] for the exciton-polariton BEC. For this purpose the thesis consists of three parts. The first part is dedicated to the experimental and theoretical foundations of the experiment. In Chapter 1 basic physical mechanisms and the experimental setup, which is needed to achieve a photon BEC, is explained. Following that, an overview over the recent results is also given. As we will see, the debate on the origin of the effective photon-photon interaction is still going on. The nature of the interaction is the second question that underlies this thesis. We will assume that a thermo-optic interaction dominates and then peal out what are the signs of this very interaction. In particular, we examine the effect of this interaction upon the frequencies of the collective modes of the condensate.

Equipped with the experimental knowledge we proceed in deriving the equation of motion of

the photon BEC in Chapter 2. The essence of this equation is already encoded in Maxwell's equations. But, as the aim is to describe the photon BEC in presence of a thermo-optic interaction, it turns out that also an evolution equation for the temperature is needed, which is produced by ongoing absorption and reemission processes of light in the dye solution and spreading through this solution. That equation is provided by the thermal diffusion equation, where the photon condensate appears as the source. After projecting the resulting equations to the longitudinal cavity modes, we argue that only one mode of the condensate wave function and one of the temperature, respectively, is relevant. The resulting two equations for the remaining transversal degrees of freedom are then shown to be formally equivalent to similar equations in the exciton-polariton case.

In the second part of the thesis the equations, that have been derived in the first part, are analysed in detail. In Chapter 3 we deal with the homogeneous system and determine its spectrum. As the system is open-dissipative, we find that this spectrum does not only consist of eigenfrequencies for a given wave number but also of corresponding eigendampings. In the same analysis we are able to peal out the effective photon-photon interaction. Moreover, it turns out that for small wave vectors an instability occurs.

In the fourth Chapter we will finally calculate the lowest-lying collective frequencies of the harmonically trapped condensate. The usual way to approximately derive those frequencies is to write down the action and insert a suitable ansatz for the wave function into the action. Then Hamilton's principle of least action is applied in order to gather the evolution equation for the variational parameters of the ansatz. As the photon Bose-Einstein condensate is, however, an open-dissipative system, meaning that the energy is not conserved, this approach cannot be used, since no action exists and therefore Hamilton's principle is not available. Hence, we use a different approach that is based on determining the equations of motion for the cumulants of both the condensate wave function and the temperature distribution. Due to this no action is needed anymore and we can derive the collective modes. At first we determine the steady state. We find that the usual steady state, that is known from a closed Gross-Pitaevskii equation, is modified by both the pump of the condensate and by the diffusion of the temperature. In the dynamic case it turns out that the dipole mode is also effected by the thermo-optic interaction and, thus, breaks the Kohn theorem. We show even that it can break down completely, meaning that no centre-of-mass oscillation is possible anymore, beyond a critical photon number. Also for the breathing and quadrupole mode we find that the frequencies are reduced due to the thermo-optic interaction.

The third part of the thesis deals with eliminating the temperature equation in order to get rid of the necessity to assume a certain shape of the temperature function. As a consequence, we will see that the mathematical description gets much more involved. For this purpose in Chapter 5 the Green's function of the temperature equation from Chapter 2 is calculated. We encounter that this leads to an effective photon-photon interaction that is nonlocal in space and in time in form of a partial-integro differential equation of second kind for the condensate wave function. Furthermore we find that the mathematical methods of choice to deal with these nonlocalities are on the one hand the Fourier transformation in order to deal with the spatial one and on the other hand the Laplace transformation for the temporal one. With this at hand we revisit the homogeneous case again in Chapter 6, where we encounter basically the same results for the collective modes. By analysing again the case of a trapped condensate in Chapter 7, we derive the specifications in which the ansatz with two seperate equations is valid and obtain some shift

in the collective frequencies and the emergence of damping, which, however, turn out to be small for the experimental parameters.

Part I.

Experimental and Theoretical Foundations

1. Experimental Foundations

In the beginning was the Word, and the Word was with God, and the Word was God.
He was with God in the beginning.
Through him all things were made; without him nothing was made that has been made.
In him was life, and that life was the light of all mankind.
The light shines in the darkness, and the darkness has not overcome it.

John 1,1-5

As the aim of this thesis is to find an appropriate phenomenological mean-field model of a photon Bose-Einstein condensate, the knowledge of the underlying experimental setup is crucial. Therefore, this Chapter reviews the experimental work done so far. For a detailed review on the topic of photon BECs we refer to [36] and to the tutorial [37]. We begin in Section 1.1 with an overview of the fundamental principles and of the experimental setup as it is used in the current experiments in Bonn, London and Utrecht. Also the thermalisation procedure is explained. After that the different experimental results obtained so far are reviewed. Section 1.2 deals with the phase transition from a thermal cloud to the Bose-Einstein condensate itself. A comment on the polarisation of the photon BEC is given in Section 1.3. In Section 1.4 an experimental procedure, that is able to produce arbitrary potentials, is described. Especially, the possibility of creating and measuring the double well potential is mentioned. Finally, the Chapter closes with a discussion on the effective photon-photon interaction in Section 1.5.

1.1. Physical Principles and Experimental Setup

The first step in realising a Bose-Einstein condensate of photons is to establish thermal equilibrium in the photon gas. Photons do no interact directly with each other but via absorption and emission processes with matter. In this way an effective photon-photon interaction as well as a thermalisation mechanism can be generated.
According to Einstein [38] there are three elementary processes on how a single light mode interacts with two-level systems. On the one hand a corresponding photon can be absorbed with the rate $B_{12}N_1n$, where N_1 denotes the number of two-level systems in equilibrium and n describes the number of photons. Whereas on the other hand a photon can also be emitted in the light mode by the N_2 excited two-level systems, once via spontaneous emission with the rate AN_2 and once by stimulated emission with the rate $B_{21}N_2n$. The respective rate factors B_{12}, A and B_{21} represent the Einstein coefficients. The rate equation for the photon number is, thus, given by

$$\dot{n} = AN_2 + B_{21}N_2n - B_{12}N_1n \tag{1.1}$$

yielding the equilibrium photon number

$$n = \frac{1}{\frac{B_{12}N_1}{B_{21}N_2} - 1}, \tag{1.2}$$

where $A = B_{21}$ is assumed [39]. Accordingly, the photon distribution is determined by the ratio of total absorption and total stimulated emission rate.
If one considers instead of simple two-level systems dye molecules, that can be seen as two-level systems dressed by phononic decay channels, the Kennard-Stepanov relation [39–42]

$$\frac{B_{12}(\omega)}{B_{21}(\omega)} = e^{-\frac{\hbar(\omega-\omega_{\mathrm{ZPL}})}{k_{\mathrm{B}}T}} \tag{1.3}$$

has to be applied. For a heuristic derivation of the Kennard-Stepanov relation see Appendix A. Here ω_{ZPL} is the so called zero-phonon line frequency, which is the transition frequency of the bare two-level system. This relation connects the emission and absorption coefficient by assuming a thermal equilibrium of the phononic excitations is achieved before the emission or the absorption process, respectively. In the experimental situation usually Rhodamine 6G is used as a dye.
In [37,43] it is shown that the Kennard-Stepanov relation together with the chemical equilibrium between the photon gas and the (un-)excited molecules results in the Bose-Einstein distribution of the equilibrium photon number

$$n = \frac{1}{e^{[\hbar(\omega-\omega_{\mathrm{cutoff}})-\mu]/k_{\mathrm{B}}T} - 1}, \tag{1.4}$$

where μ stands for the chemical potential of the photons stemming from the photon-dye interaction and ω_{cutoff} represents the cutoff frequency of the cavity.
This already indicates that the cavity is the second crucial part of the experiment. As the free-space dispersion relation is linear in the absolute value of the wave vector $\mathbf{k}$, it is not possible to cool a free photon gas to the lowest state since this is already the vacuum of the electrical field. But, by means of a cavity one can introduce a quadratic dispersion relation with a well defined cutoff frequency due to the paraxial approximation [44], see Figure 1.1. This cutoff frequency is selected by the interplay of cavity spectrum and dye spectrum, both are shown in Figure 1.2. Thus, the cavity provides a ground state for the photon gas. Moreover, since the dispersion relation is quadratic, the photons behave as massive particles. It is also possible to introduce a trapping potential for the photons by using curved cavity mirrors. Usually, those mirrors are curved spherically, thus, yielding a harmonic trapping potential [44].
The second advantage of using a cavity is, that the intracavity field can directly be measured, as photons from inside the resonator are leaking out. However, this means, that an external photon source is needed, making the system open-dissipative. In order to not destroy the coherence of the intracavity photon gas, the dye molecules are pumped far off the cavity cutoff frequency. Thus, basically the same pump mechanism occurs as in the case of an incoherently pumped exciton-polariton condensate, see Figure 2.
Those three points are the main ingredients that are needed to create a photon Bose-Einstein condensate. The concrete experimental setup is shown in Figure 1.3.

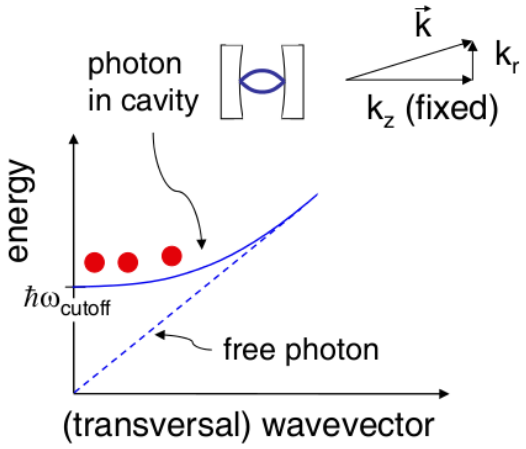

FIG. 1.1: Dispersion of photons in a cavity compared to the dispersion of free photons. The photons can condense to the ground state with energy $\hbar\omega_{\mathrm{cutoff}}$. The picture is taken from [45]

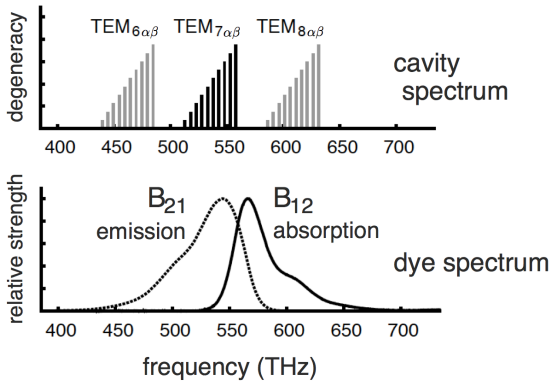

FIG. 1.2: Cavity spectrum (top) together with the absorption $\alpha(\nu)$ and emission $f(\nu)$ coefficients of Rhodamine 6G (bottom). In the Bonn experiment the highlighted TEM_7 mode is selected. The picture is taken from [44].

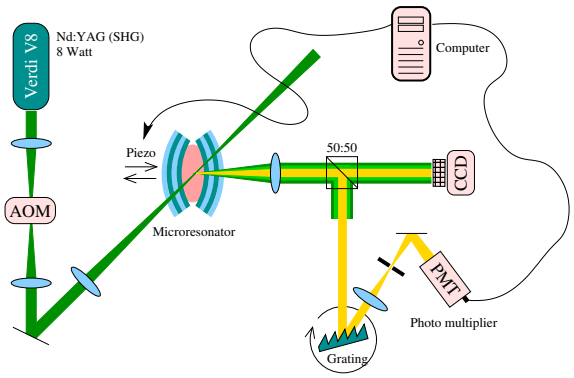

FIG. 1.3: Complete experimental setup. The dye-filled microresonator is pumped by a Nd:YAG laser. The light leaking out of the cavity is due to the beamsplitter analysed at the same time in both real space and Fourier space. The picture is taken from [44].

1.2. Phase Transition

The first experimental realisation of a photon Bose-Einstein condensate was achieved by the Weitz group in Bonn [35]. They were able to show that the above mechanism is, indeed, suitable for providing a thermalised photon gas and that it can be brought to the Bose condensed range by tuning the photon number above criticality. As the two-dimensional photon gas experiences a harmonic trapping potential, the thermalisation as well as the phase transition can be seen in real space. In Figure 1.4 real colour pictures of the condensate are shown. The thermalised photon gas below the threshold of Bose-Einstein condensation can be seen in panel (a). The red light comes from the middle of the trap, whereas green light comes from the areas far away from the centre. This indicates the thermalisation of the gas in a harmonic trapping potential, as the lowest energy states are centred in the middle and the higher energy states show up on the outside. As the pump intensity is increased beyond the threshold for condensation, a bright spot in the trap centre occurs, as can be seen in panel (b) of Figure 1.4. This means that the lowest energy state gathers a high photon population, i.e. the photon gas undergoes a transition to a Bose-Einstein condensate. One can confirm thermalisation and condensation of the photon gas by observing its spectra as shown in Figure 1.5.

With the same techniques it became possible to measure the crossover between a thermalised state and a lasing state [46] and to show that the final state crucially depends on the thermal contact to the dye. Also experiments concerning the statistical [47,48] and the caloric properties [49] of the photon gas have been conducted, see Figure 1.6. The latter show that the photon gas mainly behaves as a gas of ideal bosons. With this it was, indeed, demonstrated, that a second-order phase transition occurs by exceeding the BEC threshold. Whereas the group of Martin Weitz aimed to have large photon condensates of about 10,000 photons, more recently, in experiments in the group of Robert Nyman in London BECs of only seven photons [50] were achieved.

1.3. Polarisation

The group of Dries van Oosten in Utrecht published recently measurements of the four Stokes parameters showing a clear occurrence of polarisation in the BEC cloud, whereas the thermal cloud is not polarised [51]. The degree of polarisation in dependence of the total photon number is shown in Figure 1.7. There both the degree of polarisation in the trap centre, i.e. the polarisation of the condensate, and the corresponding quantity at the edge of the trap, where the thermal cloud is located, are shown. As the photon number exceeds the critical point for Bose-Einstein condensation, polarised light comes out of the trap centre. This shows clearly, that the photon BEC is polarised. It was also demonstrated, that the polarisation of the condensate follows the polarisation of the pump beam.

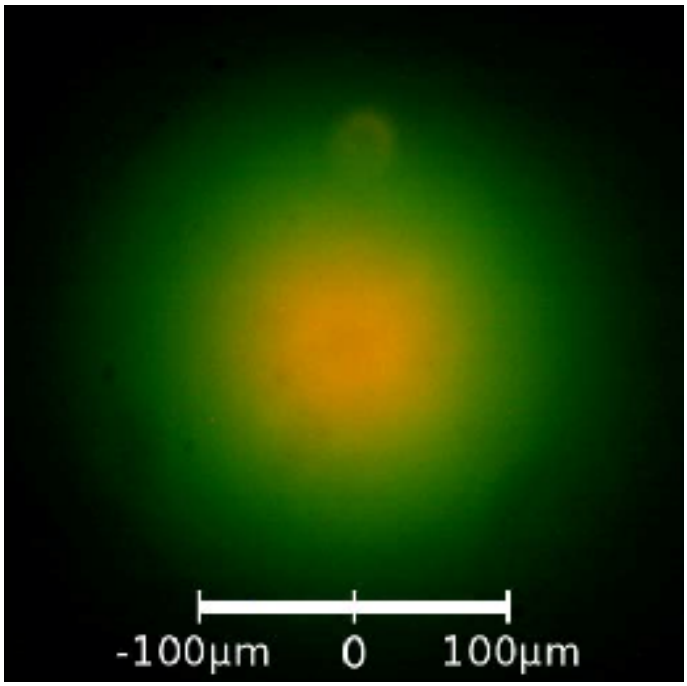

(a)

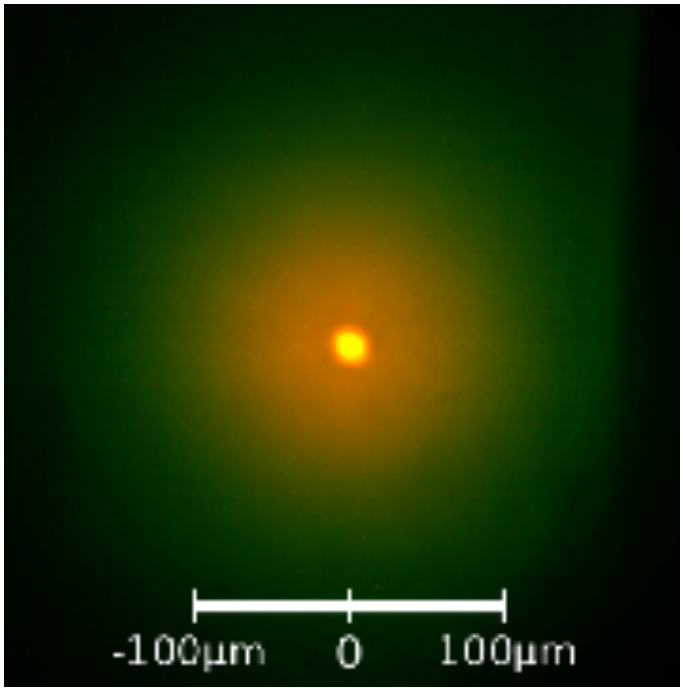

(b)

FIG. 1.4: Picture of the spatial photon distribution **(a)** below threshold showing the thermalised photon gas and **(b)** above threshold with the condensate in the trap centre and the thermal cloud around the condensate. Note, that the colours in these pictures are the real colours of the light leaking out the cavity. The red photons with the lowest energy are located in the trap centre, whereas the green photons with the higher energy are settled on the outside of the trap. In panel **(b)** the bright spot in the centre is the BEC. The pictures are taken from [35]

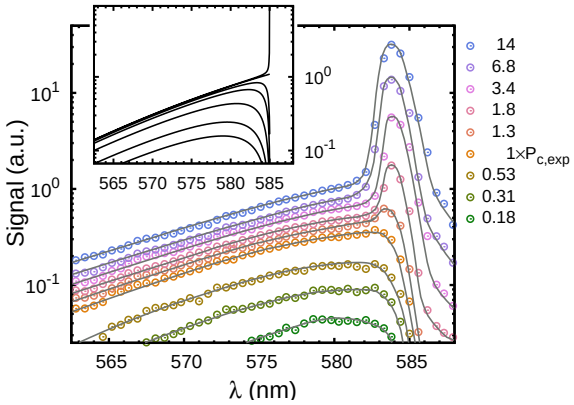

FIG. 1.5: Spectrum of the intracavity photon gas. The spectrum follows below and above the phase transition the Bose-Einstein distribution. Over the threshold the condensate peak occurs at the cutoff energy. The picture is taken from [44].

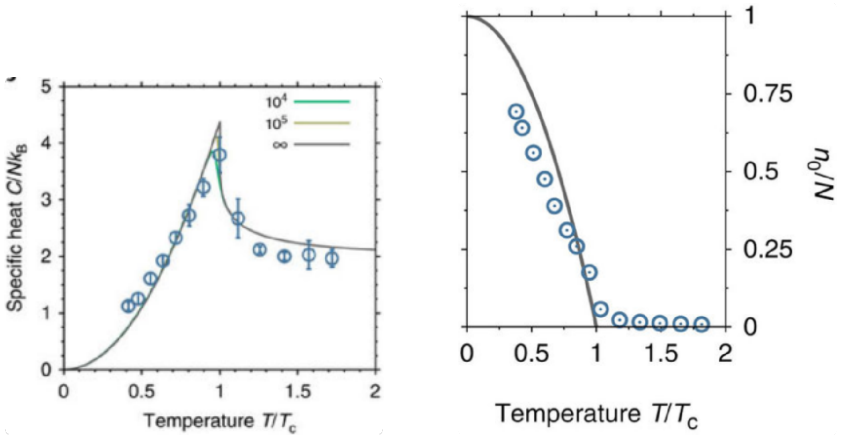

(a) **(b)**

FIG. 1.6: **(a)** Measured specific heat of the photon gas (blue circles) compared to the theory for noninteracting bosons suggesting a nearly ideal Bose gas. **(b)** Order parameter of the photon BEC. The circles show the measured quantities and the line shows the theoretical curve. The picture is taken from [49].

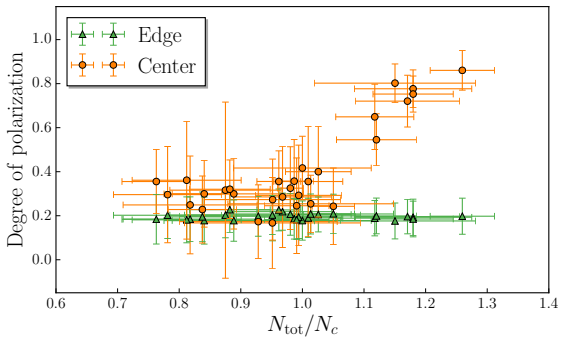

FIG. 1.7: Dependence of the polarisation of the photon gas in the microcavity on the total photon number. As one can see with the occurrence of a photon BEC the degree of polarisation increases. The picture is taken from [51].

1.4. Arbitrary Potentials and Double Well

Another promising experiment has recently been conducted by the Weitz group. It has been shown that it is possible to generate an arbitrary potential for the photons in the cavity [52]. To this end a layer of silicon, that absorbs the light of a separate laser well, is mounted on one of the cavity mirrors and a thermosensitive polymer is additionally included in the dye solution. Due to that absorption the silicon layer heats up in the vicinity of the laser spot yielding a phase transition of the polymer to a phase with higher refractive index, which has the effect of a additional trapping potential for the photons. Thus, one can generate an arbitrary potential by moving the spot of this extra laser over the silicon layer. In particular, one can create a double-well potential as has been done in [52]. However, detailed results on the oscillation of the condensate wave function between the two sites of the double well are not published yet.

1.5. Interaction

It is also observed that a repulsive photon-photon interaction is provided in the experiment, as the condensate width increases with increasing photon number [35, 53] as shown in Figure 1.8. Due to dimensional reasons the interaction strength in two-dimensional BECs corresponds to a dimensionless number $\tilde{g} = mg/\hbar^2$ [54]. The measurements in Bonn suggest for the dimensionless interaction constant the value $\tilde{g} = (7 \pm 3) \times 10^{-4}$ [44], whereas the corresponding measurements in Utrecht result in a value that is of the order 10^{-2} [53]. Moreover, the Utrecht experiments also show the interaction strength $\tilde{g}$ to depend on the dye concentration in such a way, that the interaction gets smaller as the dye concentration increases, see panel (b) in Figure 1.8. A comment on that counter-intuitive finding is given at the end of Section 9.1.

In the given system two interaction mechanisms have been identified [44]. On the one hand there is the Kerr interaction resulting from a nonlinear answer of the dye solution to ongoing absorption and emission processes. This results in a direct modification of the refractive index of the dye solution n by the photon intensity I itself

$$n = n_0 + n_2 I. \tag{1.5}$$

This yields a photon-photon interaction that is local in space and instantaneous in time. The second mechanism is provided by thermo-optical lensing. This means that the refractive index is varied by changing the dye-solution temperature. The dye-solution can, indeed, heat up during the experiment since the quantum efficiency of the dye molecules is less than 1, meaning that some absorbed photons are converted into vibronic dye excitations. Therefore, the change of refractive index varies according to

$$n = n_0 + \frac{\partial n}{\partial T} T, \tag{1.6}$$

where T describes the temperature produced by the absorption of photons themselves. This has the consequence that the photon-photon interaction, which is introduced by this mechanism, turns out to be nonlocal in space and retarded in time as the temperature excitations diffuse through the medium.

Thus, the question arises, which is the dominating interaction mechanism. In [44] it is pointed

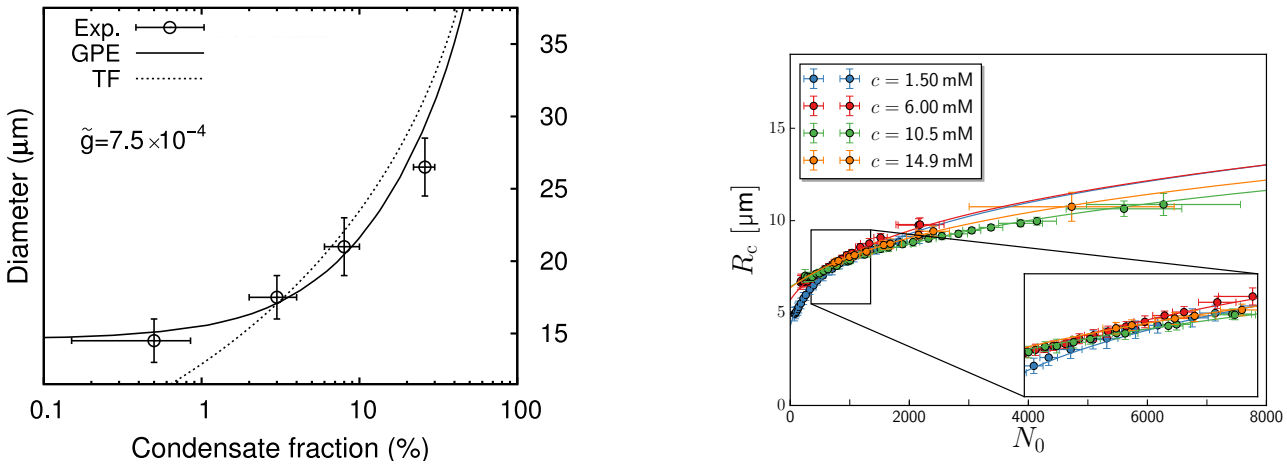

FIG. 1.8: Measurements of the condensate width from which the interaction constant can be derived: **(a)** Bonn experiment [44] and **(b)** Utrecht experiment [53]. Note that in **(b)** the interaction constant is measured to be two orders of magnitude higher than in **(a)**. Moreover, the concentration dependency is clearly visible.

out that the thermo-optic interaction is clearly dominating since the intracavity intensity is by far too small for the given Kerr coefficient to contribute to the interaction. Thus, basically the complete interaction comes from the thermo-optic effect. The group in Utrecht formulates this more cautious in [53]. They claim that the precise interaction mechanism is not known, but the thermo-optic one is a reasonable explanation.

2. Theoretical Foundations

Ich bin ein Teil des Teils, der anfangs alles war
Ein Teil der Finsternis, die sich das Licht gebar
Das stolze Licht, das nun der Mutter Nacht
Den alten Rang, den Raum ihr streitig macht [...]

Johann Wolfgang Goethe, Faust I, ll. 1349–1352

I'm part of the part, that once was - everything,
Part of the darkness, from which Light, issuing,
Proud Light, emergent, disputed the highest place
With its mother Night, the bounds of Space,[...]

In this Chapter our aim is to derive a macroscopic mean-field model that is able to describe a light field in a microcavity being filled with a thermo-optic medium, for greater detail on the experimental setup consult Chapter 1. As already explained in Section 1.5 the main contribution to the photon-photon interaction in such materials is caused by thermal lensing [44]. This necessitates to describe both the temperature diffusing through the dye-solution and the photon BEC. The former is modelled by a diffusion equation with the photon density as a source, whereas the photon BEC is described by its mean-field wave function fulfilling the wave equation in the cavity containing the dye solution. There are also several similar models that already have been discussed thitherto [52, 55, 56]. In Ref. [57] the authors work out a microscopic approach to the description of the system including only the Kerr effect as they do not include the heating and, thus, a dynamic change of the absorption and emission behaviour of the dye. The fundamentals of our concrete model go back to Martin Weitz [52,58], which are also the basis of [59]. There the authors take a three-dimensional Schrödinger equation and couple this to a three-dimensional diffusion equation in order to incorporate the thermo-optic effect. But this approach lacks of two problems. First, as we will show in following, the photon mass is only defined in two dimensions as it emerges due to the boundary conditions of the cavity. The second problem is that pump and loss processes are completely ignored. But as a thermo-optic interaction is based on the absorption of photons, this assumption is not valid. In the following derivation we will work upon these issues and derive a complete two-dimensional model, that also incorporates the intrinsic pump and loss processes.
We start by reviewing Maxwell's equations in absorptive and dispersive media and derive the electric-field wave equation in such materials in Section 2.1. To be able to further describe the thermo-optic interaction the dye-solution temperature is introduced with its own diffusion equation in Section 2.2. Afterwards we make use of the concrete geometry of the cavity by performing a paraxial approximation in Section 2.3. With its aid we are able to peal out the different time scales that are determining the dynamical behaviour of the photon BEC. Following that in Section 2.4, we carry out an expansion of both the electric field and the temperature field into the longitudinal modes by taking into account the underlying geometry,

which reduces the effective dimension of both fields from three to two. In case of the electric field this is accompanied by a slowly-varying amplitude approximation, which necessitates a subsequent rotating wave approximation in Section 2.5. In the wake of these steps we are in the right position to choose only one dominant longitudinal mode of both the temperature and the electrical field. In Section 2.6 we amend the last missing ingredient to the model by introducing a pump mechanism on heuristic grounds. Finally, in Section 2.7 we compare the equations of our model to the corresponding mean-field equations of the incoherently pumped exciton-polariton condensate.

2.1. Maxwell's Equations in Matter

We begin our derivation at the heart of electromagnetism, namely at Maxwell's equations in matter. In the following we denote as usual with $\mathbf{E}$ the electrical field and its matter analogue, the displacement field, by $\mathbf{D}$ and the magnetic field is referred to as $\mathbf{B}$. Note, that we do not introduce a matter analogue for the magnetic field, since the dye solution is not magnetic at all. Thus, we start with [60]:

$$\begin{aligned} \nabla \cdot \mathbf{D} &= 0, & \nabla \cdot \mathbf{B} &= 0, \\ \nabla \times \mathbf{E} &= -\partial_t \mathbf{B}, & \nabla \times \mathbf{B} &= \mu_0 \partial_t \mathbf{D}, \end{aligned} \tag{2.1}$$

where we have already assumed, that no free charges exist in the cavity and, thus no fluxes are present in (2.1).
The relation between the electrical field and the displacement field is given in terms of the polarisation $\mathbf{P}$ by [60, (6.25)]

$$\mathbf{D} = \varepsilon_0 \mathbf{E} + \mathbf{P}. \tag{2.2}$$

We assume the polarisation to react immediately upon the perturbative incident electrical field and that the dye molecules are distributed homogeneously and aligned isotropically. Therefore, we obtain up to third order in the incident field the following relation between $\mathbf{E}$ and $\mathbf{P}$ [61, (1.1.2)]

$$\mathbf{P} = \varepsilon_0 \left(\chi^{(1)} + \chi^{(3)} |\mathbf{E}|^2 \right) \mathbf{E}. \tag{2.3}$$

Here $\chi^{(1)}$ describes the linear influence of the medium on the electrical field and $\chi^{(3)}$ models the nonlinear influence that will later on lead to the so called Kerr effect. Due to the assumed isotropy the term proportional to $\chi^{(2)}$ is not present. Therefore, relation (2.2) acquires under usage of (2.3) the well-known form

$$\mathbf{D} = \varepsilon_0 \epsilon \mathbf{E}, \tag{2.4}$$

with the dielectric function

$$\epsilon = \left(1 + \chi^{(1)} + \chi^{(3)}|\mathbf{E}|^2\right). \tag{2.5}$$

Details on the dielectric function are worked out in Appendix A.
Note, that we are dealing with a dissipative and absorptive material, which finds its expression in ϵ being complex. The real part of the dielectric function is given by the square of the refractive index of the solvent, whereas the imaginary part is given by the absorption properties of the dye, because the wavelength of the intracavity light is far from any absorption line of the solvent.
Thus, we write in the following $\epsilon = \epsilon' + i\epsilon''$, where according to the experimental data [35] we can assume $\epsilon'' \ll \epsilon'$ and the non-linearity to be small, i.e. $|\chi^{(3)}| \ll |\chi^{(1)}|$. To catch up with the notation used in experimental circumstances, see e.g. [35], we write down the equations using the refractive index n and the extinction coefficient γ rather than the dielectric function ϵ. Those quantities are connected via the complex refractive index, see [60, 61],

$$n + i\gamma = \sqrt{\epsilon}. \tag{2.6}$$

Using $\epsilon'' \ll \epsilon'$, that implies $\gamma \ll n$, we find

$$n \approx \sqrt{\epsilon'} \approx n_0 \left(1 + \frac{\Delta n}{n_0}\right), \tag{2.7a}$$

$$\gamma = \frac{\epsilon''}{2n} \approx \gamma_0 \left(1 + \frac{\Delta\gamma}{\gamma_0}\right). \tag{2.7b}$$

Here we have introduced both the linear index of refraction

$$n_0 = \sqrt{1 + \mathrm{Re}\left(\chi^{(1)}\right)} \tag{2.8}$$

and the linear coefficient of absorption

$$\gamma_0 = \mathrm{Im}\left(\chi^{(1)}\right)/n_0 \tag{2.9}$$

as well as their perturbative counterparts arising from the non-linear susceptibility

$$\Delta n = \frac{\mathrm{Re}\left(\chi^{(3)}\right)|\mathbf{E}|^2}{2n_0} \tag{2.10}$$

and the absorption

$$\Delta\gamma = \frac{\mathrm{Im}\left(\chi^{(3)}\right)|\mathbf{E}|^2}{2n_0} - \gamma_0\frac{\Delta n}{n_0}. \tag{2.11}$$

Since the absorption as well as the non-linearity are small, we conclude the perturbation of γ to be negligible, i.e. $\Delta\gamma \approx 0$.
We can now combine (2.1), (2.4), and (2.6) to derive the wave equation in dispersive and dissipative matter

$$\mathbf{0} \approx \nabla^2\mathbf{E} - \frac{n^2 + 2in\gamma}{c^2}\partial_t^2\mathbf{E}, \tag{2.12}$$

with the light velocity $c = 1/\sqrt{\varepsilon_0\mu_0}$.

2.2. Temperature Influence

So far, we are just able to describe the evolution of the photon BEC under influence of the Kerr nonlinearity. However, as already explained in Section 1.5, the photon BEC experiments [35,44] show that this nonlinearity turns out to be negligibly small and cannot be the dominant interaction mechanism. Instead a thermo-optic effect is claimed to introduce the effective interaction, that governs the temporal development. The latter effect is already well studied in the literature [55,61–63] and it is clearly shown that it leads to an additional perturbation of the refractive index induced by the change of the dye-solution temperature. Thus, (2.10) is modified by taking into account the change of temperature linearly [61, 62]

$$\Delta n = \frac{\partial n}{\partial T}\Delta T + \frac{\mathrm{Re}\left(\chi^{(3)}\right)|\mathbf{E}|^2}{2n_0}. \tag{2.13}$$

Here $\Delta T = T - T_0$ describes the temperature difference that arises due to the absorption of photons by the dye with respect to the environmental temperature T_0. Observe, that the notation ΔT will not lead to a confusion since we denote the Laplacian always with ∇^2.
The temperature difference also has its own dynamics that is described by a thermal diffusion equation

$$\partial_t \Delta T = \mathcal{D}\nabla^2 \Delta T + \tilde{B}|\mathbf{E}|^2, \tag{2.14}$$

where the electrical field appears as a source. Here $\mathcal{D} = \kappa/(c_p\rho) = 9.16 \times 10^{-8}\,\mathrm{m}^2/\mathrm{s}$ represents the thermal diffusion coefficient [64, (50,3)] that is determined by the thermal conductivity κ, the specific, isobaric heat c_p as well as the dye-solution density ρ. The numeric values of those constants for Rhodamine 6G solved in Ethylene Glycol are given in Appendix D.
As already mentioned, the photons are the intrinsic source of heating with rate $\tilde{B}$ that is determined by the energy density $u = n_0^2\varepsilon_0|\mathbf{E}|^2/2$ of the electric field, the photon (absorptive) loss rate Γ_{eff}, that is given by the quantum efficiency $\eta = 0.95$ [52], and the frequency dependent absorption rate Γ_{abs}

$$\Gamma_{\mathrm{eff}} = (1-\eta)\Gamma_{\mathrm{abs}}, \tag{2.15}$$

as well as a conversion factor to temperature. With this we find

$$\tilde{B} = \frac{\varepsilon_0 n_0^2}{2c_p\rho}\Gamma_{\mathrm{eff}}. \tag{2.16}$$

2.3. Paraxial Approximation

In this Section the influence of the cavity geometry upon the temperature and the light field is worked out. For this purpose we take into account the dispersion relations of both the wave equation (2.12) and the diffusion equation (2.14) and perform the so-called paraxial approximation [44,60,65]. With this we are able to peal out the different time scales arising in our system. In Figure 2.1(a) the geometry of the cavity is shown. Within the paraxial approximation we assume that the angle between the travel direction of the light and the optical axis is small. In

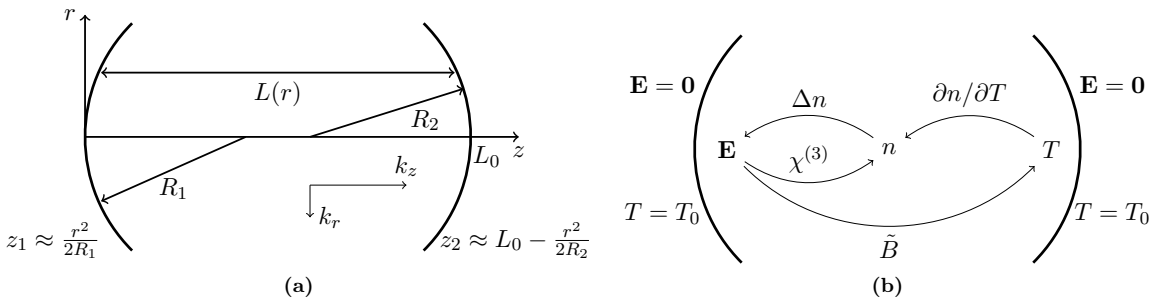

FIG. 2.1: Setup of the cavity. In **(a)** its geometry is shown. The spherically curved mirrors have maximally a distance of L_0 and, due to the curvature R, this holds just at the optical axis. For light beams close to the optical axis the paraxial assumption (2.17) is applicable. For those rays the boundary curvature can be approximated by $z_1 = r^2/(2R)$ at the origin and by $z_2 = L_0 - r^2/(2R)$ at the other cavity end. Note, that in the real cavity we have $L_0 \ll R_i$, contrary to the suggestion of the picture.
In **(b)** the boundary conditions at the cavity mirrors and the interactions inside the cavity are sketched. The electrical field $\mathbf{E}$ changes the refractive index in two ways. On the one hand there is a change directly via the Kerr nonlinearity $\chi^{(3)}$ and on the other hand indirectly via a heating of the dye solution with rate $\tilde{B}$. The temperature difference $\Delta T = T - T_0$ then changes the refractive index by an amount $\frac{\partial n}{\partial T}\Delta T$. Since the refractive index represents an effective potential for the photons, its change Δn acts back on the electrical field $\mathbf{E}$ and imposes in that way an effective photon-photon interaction. Moreover, the mirrors yield Dirichlet boundary conditions for both fields.

other words, we assume the light to propagate close to the optical axis. This yields directly that the transversal part of the wave vector $\mathbf{k}_r$ is much smaller than its longitudinal component k_z. Consequently, the paraxial approximation consists of assuming

$$\mathbf{k}_r^2 \ll k_z^2. \tag{2.17}$$

Moreover, we work with a *micro*cavity, meaning the length of the cavity L is much smaller than the curvature radii R_i, $i = 1, 2$, of the spherically curved mirrors. For the following geometric considerations, the origin of the coordinate system is set to the left end of the cavity as shown in 2.1(a). From geometrical reasoning, we can conclude that the left boundary is given via the Pythagoras' theorem as

$$z_1(r) = R_1 \left(1 - \sqrt{1 - \frac{r^2}{R_1^2}} \right), \tag{2.18}$$

where R_1 is the radius of the left mirror. As we are working in the paraxial limit, the restriction $r \leq R_1$ holds and (2.18) can be approximated to

$$z_1(r) \approx \frac{r^2}{2R_1}. \tag{2.19}$$

The analogue reasoning yields for the right boundary condition

$$z_2(r) \approx L_0 - \frac{r^2}{2R_2}, \tag{2.20}$$

with the corresponding mirror curvature R_2. Therefore, by taking the difference $z_2(r) - z_1(r)$ the cavity length $L(r)$ in dependency on the distance from the optical axis r is given by

$$L(r) \approx L_0 \left[1 - \frac{r^2}{L_0} \left(\frac{1}{R_1} + \frac{1}{R_2}\right)\right]. \tag{2.21}$$

In the following we stick to the experimental case of identical mirrors with radius $R_1 = R_2 = R$, so that (2.21) simplifies to

$$L(r) \approx L_0 \left(1 - \frac{r^2}{L_0 R}\right). \tag{2.22}$$

The mirrors impose Dirichlet boundary conditions for both fields as it is illustrated in Figure 2.1(b). Thus, the longitudinal wave-vector component is given by

$$k_z \equiv k_\mu^z = \approx k_{0\mu} \left(1 + \Delta k_z\right), \quad \mu \in \mathbb{N}, \tag{2.23}$$

where we introduced $k_{0\mu} = \mu\pi/L_0$ and $\Delta k_z = r^2/(L_0 R)$.

2.3.1. Photon Condensate Wave Function

The plane wave dispersion relation of the wave equation (2.12) reads with the frequency ω_μ of the μth mode

$$\omega_\mu = \frac{c}{n} k_\mu. \tag{2.24}$$

Taking into account the small extinction coefficient γ and the small nonlinearity Δn from (2.7) modifies (2.24) to

$$\omega_\mu = \frac{c}{n_0} \left(1 - \frac{\Delta n}{n_0} - i\frac{\gamma_\mu}{n_0}\right) k_\mu. \tag{2.25}$$

Ascribed to the boundary conditions, we take throughout this thesis the wave vector $\mathbf{k}$ to be real and describe the absorption processes by a (small) imaginary part of the mode frequency ω_μ.
The total absolute value of the wave vector is per definition given by

$$k_\mu = \sqrt{k_z^2 + k_r^2}. \tag{2.26}$$

Using (2.17) implies for the absolute value

$$k_\mu \approx k_\mu^z + \frac{{\mathbf{k}_r}^2}{2k_\mu^z}. \tag{2.27}$$

Inserting the z-component from (2.23) we find

$$k_\mu \approx k_{0\mu} + \Delta k_z k_{0\mu} + \frac{{\mathbf{k}_r}^2}{2k_{0\mu}}. \tag{2.28}$$

Thus, combining (2.24) and (2.28) yields

$$\omega_\mu = \frac{c}{n_0} k_{0\mu} \left(1 + \frac{\mathbf{k}_\mu^{r\,2}}{2k_{0\mu}^2} + \Delta k_z\right)\left(1 - \frac{\Delta n}{n_0} - i\frac{\gamma_\mu}{n_0}\right). \tag{2.29}$$

Ergo, in leading order we obtain

$$\omega_\mu \approx \frac{ck_{0\mu}}{n_0}\left[1 + \frac{\mathbf{k}_\mu^{r\,2}}{2k_{0\mu}^2} + \frac{r^2}{L_0 R} - \frac{\Delta n}{n_0} - i\frac{\gamma_\mu}{n_0}\right]. \tag{2.30}$$

Thus, due to those perturbative considerations, we get several modifications of the dispersion relation. The first one stems from the photon movement in the transversal plane and corresponds to their effective kinetic energy. The second one is proportional to the square of the distance from the resonator axis and can, therefore, be interpreted as a harmonic confinement of the photons in the transversal plane. From these two observations we can already deduce that the photons behave like massive particles trapped in a two-dimensional harmonic oscillator potential. Therefore, we can define their mass m_μ and the oscillator frequency Ω from the corresponding prefactors as

$$\frac{\hbar}{m_\mu} = \frac{c}{k_{0\mu} n_0} \quad \Leftrightarrow \quad m_\mu = \frac{\hbar k_{0\mu} n_0}{c} = 1.08 \times 10^{-36} \mu \text{ kg}, \tag{2.31a}$$

$$\frac{m_\mu \Omega^2}{2\hbar} = \frac{ck_{0\mu}}{n_0}\frac{1}{L_0 R} \quad \Leftrightarrow \quad \Omega = \frac{c}{n_0}\sqrt{\frac{2}{L_0 R}} = 2.37 \times 10^{11} \text{ Hz}. \tag{2.31b}$$

The concrete values used here are listed in Appendix D.
The first condition simply follows from the kinetic energy of a free massive particle $\hbar^2 \mathbf{k}_r^2/(2m_\mu)$ and the second one comes from the potential energy of a harmonic oscillator $m_\mu \Omega^2 r^2/2$. Thus, we have an explicit mapping between photons trapped in a microcavity with spherically curved mirrors and massive bosons in a two-dimensional harmonic oscillator at hand. But note, the mass depends on the mode index μ, which is due to the Einstein relation $\hbar\omega_{0\mu} = m_\mu c^2/n_0^2$, that is here given by the zeroth order of (2.30).
The third modification in (2.30) being proportional to Δn takes into account the thermo-optic and the nonlinear index of refraction, due to (2.13). The last term in (2.30) has the particularity of being purely imaginary, meaning this term introduces a decay of the electrical field, which is interpreted as absorptive losses. Therefore, the photon absorption rate is given by

$$\Gamma_\mu = \frac{m_\mu c^2 \gamma_\mu}{\hbar n_0^3} \tag{2.32}$$

that we identify with Γ_{eff} from (2.15). Note here the large differences in the respective time scales that we have introduced so far. Whereas the mode frequency is given in multiples of $\omega_{01} = 4.3 \times 10^{14}$ Hz, the photon trap frequency $\Omega = 2.37 \times 10^{11}$ Hz is several orders of magnitude below. The thermo-optic interaction takes place at the scale $-\omega_{01}\frac{\partial n}{\partial T}\Delta T \sim 10^{10}$ Hz, since the temperature difference is of the order $\Delta T \sim 10^{-1}$ K [44]. Thus, the fastest time scale is given by the mode frequency.

2.3.2. Temperature Field

The diffusive dispersion relation for a plane wave has the form

$$\omega_\nu = -i\mathcal{D}k_\nu^2 \approx -i\mathcal{D}k_{0\nu}^2\left(1+\frac{\mathbf{k}_\nu^{r\,2}}{k_{0\nu}^2}+\Delta k_z\right), \tag{2.33}$$

where we used (2.28). Note that the full plane-wave ansatz for the temperature reads $T = Ae^{i(\mathbf{k}\cdot\mathbf{r}-\omega t)} + A^*e^{-i(\mathbf{k}\cdot\mathbf{r}-\omega^* t)}$ with a complex frequency ω as is suggested by the above equation and common in the literature of open dissipative systems, see e.g. [34]. Accordingly, the complex frequency here contains a damping rate.
Thus, we can also define for the temperature an effective mass m_T and find also a harmonic confinement for a fixed temperature mode with frequency $\Omega_{T\nu}$. With the same reasoning as at the end of Subsection 2.3.1 we find

$$m_T = \frac{\hbar}{2\mathcal{D}} = 5.75\times10^{-28}\ \text{kg}, \tag{2.34a}$$

$$\Omega_{T\nu} = 2\mathcal{D}k_{0\nu}\sqrt{\frac{1}{L_0R}} = 313.43\ \nu\ \text{Hz}. \tag{2.34b}$$

The corresponding numerical values can be found in Appendix D.
Note, that in contrast to Section 2.3.1, instead of the effective mass the effective trap frequency depends on the mode index ν as can be seen by comparing (2.31a) and (2.31b) with (2.34a) and (2.34b), respectively. This results from the fact that the mode frequency depends quadratically on the absolute value of the wave vector and not linearly as in case of the wave equation.
Moreover we have in (2.33) the term $-\mathcal{D}k_{0\nu}^2$. According to the sign and the fact that we consider here a diffusion equation, this term describes an effective loss coming from the reduction of dimensions from three to two by separating the z-dynamics. The corresponding decay time is given by

$$\tau_\nu = \frac{1}{\mathcal{D}k_{0\nu}^2} = \frac{2.49\times10^{-6}}{\nu^2}\ \text{s}. \tag{2.35}$$

Note, that the time scale which is set by τ turns out to be much faster than the one set by $1/\Omega_T$. This suggests to neglect the temperature trap at all. This is also verified by comparing the imposed energy scales

$$\frac{E_{\text{HO}}}{E_\tau} \sim \frac{m\Omega^2 l_{\text{osc}}^2}{\hbar/\tau}, \tag{2.36}$$

where $l_{\text{osc}} = \sqrt{\hbar/m\Omega}$ is the harmonic oscillator length. After simplification we find

$$\frac{E_{\text{HO}}}{E_\tau} \sim \tau\Omega. \tag{2.37}$$

This ratio is of the order 1×10^{-4} and is, thus, negligible.
Furtheron, we see that the time scales for the temperature are generically much slower than those for the photons.

2.4. Mode Expansion and Slowly-Varying Envelope Approximation

Based on the paraxial approximation performed in Section 2.3 we derive now from the full three-dimensional evolution equations for the electric field (2.12) and the temperature (2.14) the corresponding equations describing the evolution of the transversal degrees of freedom. The respective Dirichlet boundary conditions, see Figure 2.1(b), imply for both the electrical field and the temperature difference the following expansions in longitudinal modes

$$\mathbf{E}(\mathbf{r}, z, t) = \sum_{\mu \in \mathbb{N}} \mathbf{E}_\mu(\mathbf{r}, t) e^{-i\omega_{0\mu} t} \sin k_\mu^z \tilde{z}, \tag{2.38a}$$

$$\Delta T(\mathbf{r}, z, t) = \sum_{\nu \in \mathbb{N}} \Delta T_\nu(\mathbf{r}, t) \sin k_\nu^z \tilde{z}, \tag{2.38b}$$

where $k_\mu^z = \mu\pi/L,\ \mu \in \mathbb{N}$, as in (2.23). Note, that the shift $\tilde{z} = z - r^2/(2R)$ in the sin arguments is introduced to meet the boundary conditions, see Figure 2.1(a). Moreover, in (2.38a) we separate the fast oscillating cavity frequency $\omega_{0\mu}$, see end of Subsection 2.3.1, and assume accordingly

$$\left|\partial_t^2 \mathbf{E}_\mu\right| \ll \left|\omega_{0\mu} \partial_t \mathbf{E}_\mu\right|, \tag{2.39}$$

which represents the so-called slowly varying envelope approximation [66–69].

2.4.1. Temperature Diffusion Equation

Let us first, for the sake of simplicity, work on the diffusion equation (2.14), where we insert (2.38b). With this we obtain at first

$$\sum_{\nu \in \mathbb{N}} \partial_t \Delta T_\nu \approx \sum_{\nu \in \mathbb{N}} \mathcal{D}\left[\nabla_r^2 - (k_\nu^z)^2\right] \Delta T_\nu \sin k_\nu^z \tilde{z} + \tilde{B} \sum_{\nu,\mu \in \mathbb{N}} \mathbf{E}_\nu \cdot \mathbf{E}_\mu^* e^{-i\omega_{\nu\mu} t} \sin k_\nu^z \tilde{z} \sin k_\mu^z \tilde{z}, \tag{2.40}$$

where we defined the mode frequency difference $\omega_{\mu\nu} = \omega_{0\mu} - \omega_{0\nu}$ and neglected the terms $\nabla_r^2 k_\mu^z \tilde{z}$ due to the small curvature of the wave front caused by the paraxial approximation.
Since we are interested in the evolution of a single mode T_σ, we project (2.40) to this very mode by using the orthonormality relation of the longitudinal modes

$$\frac{2}{L} \int_0^L d\tilde{z}\ \sin k_\nu^z \tilde{z} \sin k_\sigma^z \tilde{z} = \delta_{\nu\sigma}. \tag{2.41}$$

Thus, multiplying (2.40) with $2\sin(k_\sigma^z)\tilde{z}/L$ and performing the $\tilde{z}$-integral over the cavity length L yields

$$\partial_t \Delta T_\sigma = \mathcal{D}\left[\nabla_r^2 - (k_\sigma^z)^2\right] \Delta T_\sigma + \tilde{B} \sum_{\mu,\nu \in \mathbb{N}} a_{\mu\nu\sigma} \mathbf{E}_\nu \cdot \mathbf{E}_\mu^* e^{-i\omega_{\nu\mu} t}, \tag{2.42}$$

where we defined the coupling constants

$$a_{\mu\nu\sigma} = \frac{2}{L}\int_0^L d\tilde{z}\ \ \sin k_\mu^z \tilde{z} \sin k_\nu^z \tilde{z} \sin k_\sigma^z \tilde{z}. \tag{2.43}$$

Evaluating the integral yields

$$a_{\mu\nu\sigma} = \frac{4\mu\nu\sigma}{\pi} \frac{(-1)^{\mu+\nu+\sigma} - 1}{(\mu+\nu+\sigma)(\mu-\nu-\sigma)(\mu+\nu-\sigma)(\mu-\nu+\sigma)}, \tag{2.44}$$

thus, we only get a non-vanishing coupling $a_{\mu\nu\sigma}$ if the sum of the mode indices $\mu+\nu+\sigma$ is odd. With this (2.44) reads

$$a_{\mu\nu\sigma} = \sum_{n,m,l\in\mathbb{N}} \frac{8\mu\nu\sigma}{\pi} \frac{\delta_{\sigma,2l+1}\left(\delta_{\mu,2n+1}\delta_{\nu,2m+1} + \delta_{\mu,2n}\delta_{\nu,2m}\right) + \delta_{\sigma,2l}\left(\delta_{\mu,2n}\delta_{\nu,2m+1} + \delta_{\mu,2n+1}\delta_{\nu,2m}\right)}{(\mu+\nu+\sigma)(\mu-\nu-\sigma)(\mu+\nu-\sigma)(\mu-\nu+\sigma)}. \tag{2.45}$$

With the corrections (2.22), the newly introduced two-dimensional heating coefficient $\tilde{B}_{\mu\nu\sigma} = \tilde{B} a_{\mu\nu\sigma}$ and the decay time τ_μ (2.35) the temperature equation in (2.42) reduces to

$$\partial_t \Delta T_\sigma = \left(\mathcal{D}\nabla_r^2 - \frac{1}{\tau_\sigma}\right)\Delta T_\sigma + \sum_{\mu,\nu\in\mathbb{N}} \tilde{B}_{\mu\nu\sigma} \mathbf{E}_\mu \cdot \mathbf{E}_\nu^* e^{-i\omega_{\mu\nu}t}. \tag{2.46}$$

Note, that we have now an effective two-dimensional diffusion equation and that in the source term we neglect the correction arising due to the mirror curvature. To incorporate the results of Subsection 2.3.2 we rewrite the diffusion equation according to

$$\hbar\partial_t \Delta T_\sigma = \left(\frac{\hbar^2}{2m_T}\nabla_r^2 - \frac{\hbar}{\tau_\sigma}\right)\Delta T_\sigma + \hbar \sum_{\mu,\nu\in\mathbb{N}} \tilde{B}_{\mu\nu\sigma} \mathbf{E}_\mu \cdot \mathbf{E}_\nu^* e^{-i\omega_{\mu\nu}t}. \tag{2.47}$$

Here, we recognise, that this corresponds to a Schrödinger-like equation in imaginary time. Thus, after imposing a Wick rotation, i.e. rotating the time into the imaginary plane by $t = -i\tau$, the two-dimensional Schrödinger equation with an external pump is obtained.

2.4.2. Photon Condensate Wave Function Equation

We focus now on the derivation of the condensate-wave equation. As the first step, we insert the ansatzes (2.38) into the wave equation (2.12). The corresponding derivatives read

$$\nabla^2 \mathbf{E} \approx \sum_{\mu\in\mathbb{N}} \left[\nabla_r^2 - (k_\mu^z)^2\right] \mathbf{E}_\mu \sin k_\mu^z \tilde{z}, \tag{2.48}$$

where we neglected again the $\nabla_r^2 k_\mu^z \tilde{z}$ terms describing the wave-front curvature due to the paraxial approximation, and

$$\partial_t^2 \mathbf{E} = \sum_{\mu\in\mathbb{N}} \left(\partial_t^2 - 2i\omega_{0\mu}\partial_t - \omega_{0\mu}^2\right) \mathbf{E}_\mu e^{-i\omega_{0\mu}t} \sin k_\mu^z \tilde{z}. \tag{2.49}$$

We apply now the slowly-varying envelope approximation (2.39), so the temporal derivative simplifies to

$$\partial_t^2 \mathbf{E} \approx \sum_{\mu\in\mathbb{N}} \left(-2i\omega_{0\mu}\partial_t - \omega_{0\mu}^2\right) \mathbf{E}_\mu e^{-i\omega_{0\mu}t} \sin k_\mu^z \tilde{z}. \tag{2.50}$$

Thus, inserting the above two derivatives (2.48) and (2.50) into (2.12) leads to

$$\sum_{\mu\in\mathbb{N}} e^{-i\omega_{0\mu}t} \sin k_\mu^z \tilde{z} \left[\nabla_r^2 - (k_\mu^z)^2 + \frac{n^2}{c^2}\left(1 + i\frac{\gamma_\mu}{n}\right)\left(2i\omega_{0\mu}\partial_t + \omega_{0\mu}^2\right)\right] \mathbf{E}_\mu = \mathbf{0}. \tag{2.51}$$

The expression in brackets can be further processed by taking into account (2.13)

$$\nabla_r^2 - (k_\mu^z)^2 + \frac{n_0^2}{c^2}\left[1 + i\frac{\gamma_\mu}{n_0}\left(1 - \frac{\Delta n}{n_0}\right) + \frac{2\Delta n}{n_0}\right]\left(2i\omega_{0\mu}\partial_t + \omega_{0\mu}^2\right). \tag{2.52}$$

Since we aim for an equation up to first order in Δn, we can restrict ourselves to only use the zeroth order of the dispersion relation (2.30) and obtain

$$\nabla_r^2 - 2k_{\mu 0}\Delta k_\mu + 2i\frac{n_0^2}{c^2}\omega_{0\mu}\left[1 + i\frac{\gamma_\mu}{n_0}\left(1 - \frac{\Delta n}{n_0}\right) + 2\frac{\Delta n}{n_0}\right]\partial_t + \frac{n_0^2\omega_{0\mu}^2}{c^2}\left[i\frac{\gamma_\mu}{n_0}\left(1 - \frac{\Delta n}{n_0}\right) + 2\frac{\Delta n}{n_0}\right]. \tag{2.53}$$

Neglecting the small terms yields

$$\nabla_r^2 - 2k_{\mu 0}\Delta k_\mu + 2i\frac{n_0^2}{c^2}\omega_{0\mu}\partial_t + \frac{n_0^2\omega_{0\mu}^2}{c^2}\left[i\frac{\gamma_\mu}{n_0}\left(1 - \frac{\Delta n}{n_0}\right) + 2\frac{\Delta n}{n_0}\right]. \tag{2.54}$$

As our aim is to derive a Schrödinger equation, we divide the whole equation by the prefactor of $i\partial_t$ and multiply by $\hbar$. Then, the very same term acquires the form

$$\frac{\hbar c^2}{2n_0^2\omega_{0\mu}}\left(\nabla_r^2 - 2k_{\mu 0}\Delta k_\mu\right) + i\hbar\partial_t + \frac{\hbar\omega_{0\mu}}{2}\left[i\frac{\gamma_\mu}{n_0}\left(1 - \frac{\Delta n}{n_0}\right) + 2\frac{\Delta n}{n_0}\right]. \tag{2.55}$$

With the notation from the end of Subsection 2.3.1 this reduces to

$$\left(\frac{\hbar^2}{2m_\mu}\nabla_r^2 - \frac{m_\mu\Omega^2}{2}r^2\right) + i\hbar\partial_t + \frac{m_\mu c^2}{2n_0^2}\left[i\frac{\gamma_\mu}{n_0}\left(1 - \frac{\Delta n}{n_0}\right) + 2\frac{\Delta n}{n_0}\right]. \tag{2.56}$$

Therefore, by reinserting the evaluated bracket into the equation (2.51) we find

$$\mathbf{0} \approx \sum_{\mu\in\mathbb{N}} e^{-i\omega_{0\mu}t} \sin k_\mu^z \tilde{z} \left\{i\hbar\partial_t + \frac{\hbar^2}{2m_\mu}\nabla_r^2 - \frac{m_\mu\Omega^2}{2}r^2 + \frac{m_\mu c^2}{2n_0^2}\left[i\frac{\gamma_\mu}{n_0}\left(1 - \frac{\Delta n}{n_0}\right) + 2\frac{\Delta n}{n_0}\right]\right\} \mathbf{E}_\mu. \tag{2.57}$$

As in Subsection 2.4.1 we are interested in the temporal evolution of one specific longitudinal mode $\mathbf{E}_\kappa$. To achieve this we will also project down to this mode via (2.41). By doing this we recall $\Delta n = \Delta n(\Delta T, |\mathbf{E}|^2)$ from (2.13). Before projecting the complete equation let us investigate

the projection of Δn separately:

$$\frac{2}{L}\int_0^L d\tilde{z}\ \sin k_\kappa^z \tilde{z} \sin k_\mu^z \tilde{z} \Delta n = \frac{\partial n}{\partial T}\sum_{\nu\in\mathbb{N}} a_{\mu\nu\kappa}\Delta T_\nu + K\sum_{\nu,\lambda\in\mathbb{N}} b_{\mu\nu\lambda\kappa}\mathbf{E}_\nu \cdot \mathbf{E}_\lambda^* e^{-i\omega_{\nu\lambda}t}, \tag{2.58}$$

where we defined $K = \mathrm{Re}\left(\chi^{(3)}\right)/(2n_0^2)$ and the coupling coefficients

$$b_{\mu\nu\lambda\kappa} = \frac{2}{L}\int_0^L d\tilde{z} \sin k_\mu^z \tilde{z} \sin k_\nu^z \tilde{z} \sin k_\lambda^z \tilde{z} \sin k_\kappa^z \tilde{z}. \tag{2.59}$$

Those coefficients $b_{\mu\nu\lambda\sigma}$ turn out to be related to the previously defined coefficients $a_{\mu\nu\sigma}$ in (2.43). This can be seen by expanding the product $\sin k_\mu^z \tilde{z} \sin k_\nu^z \tilde{z} \sin k_\lambda^z \tilde{z}$ once via the a coefficients

$$\sin k_\mu^z \tilde{z} \sin k_\nu^z \tilde{z} \sin k_\lambda^z \tilde{z} = \sum_{\kappa\in\mathbb{N}} a_{\mu\nu\kappa} \sin k_\kappa^z \tilde{z} \sin_\lambda k^z \tilde{z} = \sum_{\kappa,\sigma\in\mathbb{N}} a_{\mu\nu\kappa} a_{\kappa\lambda\sigma} \sin k_\sigma^z \tilde{z} \tag{2.60}$$

and once by using (2.59) directly

$$\sin k_\mu^z \tilde{z} \sin k_\nu^z \tilde{z} \sin k_\lambda^z \tilde{z} = \sum_{\sigma\in\mathbb{N}} b_{\mu\nu\lambda\sigma} \sin k_\sigma^z \tilde{z}. \tag{2.61}$$

A comparison between (2.60) and (2.61) yields

$$b_{\mu\nu\lambda\sigma} = \sum_{\kappa\in\mathbb{N}} a_{\mu\nu\kappa} a_{\kappa\lambda\sigma}. \tag{2.62}$$

Thus, with definition (2.32) we obtain for the projection of (2.57) upon the mode κ

$$\begin{aligned} i\hbar\partial_t \mathbf{E}_\kappa = &\left(-\frac{\hbar^2}{2m_\kappa}\nabla_r^2 + \frac{m_\kappa \Omega^2}{2} r^2 - \frac{i}{2}\hbar\Gamma_\kappa\right)\mathbf{E}_\kappa \\ &- \sum_{\mu,\nu\in\mathbb{N}} \left(\frac{\partial n}{\partial T} a_{\mu\nu\kappa} T_\nu + K\sum_{\lambda\in\mathbb{N}} b_{\mu\nu\lambda\kappa}\mathbf{E}_\nu \cdot \mathbf{E}_\lambda^* e^{-i\omega_{\nu\lambda}t}\right)\left(\frac{m_\mu c^2}{n_0^2} - \frac{i}{2}\hbar\Gamma_\mu\right)\mathbf{E}_\mu e^{-i\omega_{\mu\kappa}t}. \end{aligned} \tag{2.63}$$

Thus, every longitudinal mode interacts in a two-fold way with the mode κ. The first one is the interaction between the light field and the temperature with the coupling constant

$$\mathfrak{g}_{\mu\nu\kappa}^{\mathrm{thermo}} = -\frac{m_\mu c^2}{n_0^2}\frac{\partial n}{\partial T} a_{\mu\nu\kappa}. \tag{2.64}$$

The interaction constant due to the Kerr-effect on the other hand is given by

$$\mathfrak{g}_{\mu\nu\lambda\kappa}^{\mathrm{Kerr}} = -\frac{m_\mu c^2}{n_0^2} K b_{\mu\nu\lambda\kappa}. \tag{2.65}$$

Note, that in those two definitions (2.64) and (2.65) the inequalities $\frac{\partial n}{\partial T} < 0$ and $K < 0$ are valid [35], respectively.

Inserting the definitions (2.64) and (2.65) into the electrical field equation (2.63) yields

$$i\hbar\partial_t \mathbf{E}_\kappa = \left(-\frac{\hbar^2}{2m_\kappa}\nabla_r^2 + \frac{m_\kappa\Omega^2}{2}r^2 - \frac{i}{2}\hbar\Gamma_\kappa\right)\mathbf{E}_\kappa \tag{2.66}$$
$$+ \sum_{\mu,\nu\in\mathbb{N}} \left(\mathfrak{g}^{\text{thermo}}_{\mu\nu\kappa}T_\nu + \sum_{\lambda\in\mathbb{N}}\mathfrak{g}^{\text{Kerr}}_{\mu\nu\lambda\kappa}\mathbf{E}_\nu\cdot\mathbf{E}^*_\lambda e^{-i\omega_{\nu\lambda}t}\right)\mathbf{E}_\mu e^{-i\omega_{\mu\kappa}t} - \frac{i\hbar}{2}\frac{\partial n}{n_0\partial T}\sum_{\mu,\nu\in\mathbb{N}}\Gamma_\mu a_{\mu\nu\kappa}T_\nu\mathbf{E}_\mu e^{-i\omega_{\mu\kappa}t}.$$

This equation now represents a Gross-Pitaevskii like equation for the longitudinal mode $\mathbf{E}_\kappa$. The first part is basically a harmonic oscillator in the transversal plane underlying dissipation. The second part introduces both the thermo-optic and the Kerr interaction between all the modes.

2.5. Rotating Wave Approximation and Mode Selection

In equation (2.47) as well as in equation (2.66) we have terms that are of the form $e^{-i\omega_{\mu\nu}t}$, i.e. they describe oscillations with a frequency that is an integer multiple of the mode spacing ω_{01}. In Section 2.3 we have shown that the remaining frequencies are several orders of magnitude less than this spacing. Thus, we can perform a rotating wave approximation (RWA) by integrating out the fast time scale. That yields effectively $e^{-i\omega_{\mu\nu}t} \approx \delta_{\mu\nu}$. Consequently, the temperature equation (2.47) simplifies to

$$\partial_t \Delta T_\sigma \approx \left(\mathcal{D}\nabla_r^2 - \frac{1}{\tau_\sigma} - \frac{m_T\Omega_{T\sigma}}{2}r^2\right)\Delta T_\sigma + \sum_{\mu\in\mathbb{N}}\tilde{B}_{\mu\mu\sigma}|\mathbf{E}_\mu|^2. \tag{2.67}$$

The electric field equation (2.66) simplifies correspondingly to

$$i\hbar\partial_t \mathbf{E}_\kappa = \left\{-\frac{\hbar^2}{2m_\kappa}\nabla_r^2 + \frac{m_\kappa\Omega^2}{2}r^2 - \frac{i}{2}\hbar\Gamma_\kappa\left(1 - \frac{\partial n}{n_0\partial T}\sum_{\nu\in\mathbb{N}}a_{\mu\nu\mu}T_\nu\right)\right\}\mathbf{E}_\kappa$$
$$+ \sum_{\nu\in\mathbb{N}}\left(\mathfrak{g}^{\text{thermo}}_{\kappa\nu\kappa}T_\nu + \mathfrak{g}^{\text{Kerr}}_{\kappa\nu\nu\kappa}|\mathbf{E}_\nu|^2\right)\mathbf{E}_\kappa. \tag{2.68}$$

Now the question is left, which modes are the relevant ones in the experimental situation. We know from [35,44] that the emission and absorption spectrum of the dye fits between the spacing of two subsequent longitudinal modes, recall Figure 1.2. Therefore, only one electrical field mode is relevant. The pertinent experimental cases are $\kappa = 7$ [35] and $\kappa = 8$ [49].
The appropriate temperature mode is found by weighting the gain that is given by the heating coefficient $B_{\mu\mu\sigma}$ against the losses τ_σ. Since $\tau_1 > \tau_\sigma$, $\forall\sigma > 1$, the T_1 mode is the longest surviving one. Moreover, we find from (2.44)

$$a_{\mu\mu\sigma} = \frac{4}{\pi^2\sigma}\frac{1}{\sigma^2/(4\mu^2) - 1}, \tag{2.69}$$

that tends to 0 as $\sigma \to \infty$. Together with Figure 2.2(a) we conclude that the $\sigma = 1$ mode is the one that is pumped strongest for both electrical field modes $\mathbf{E}_{7,8}$. Thus, we can restrict ourselves to this mode, as it is also suggested by Figure 2.2(b).

Thus we are from now on dealing with exactly one longitudinal electrical field mode. Moreover,

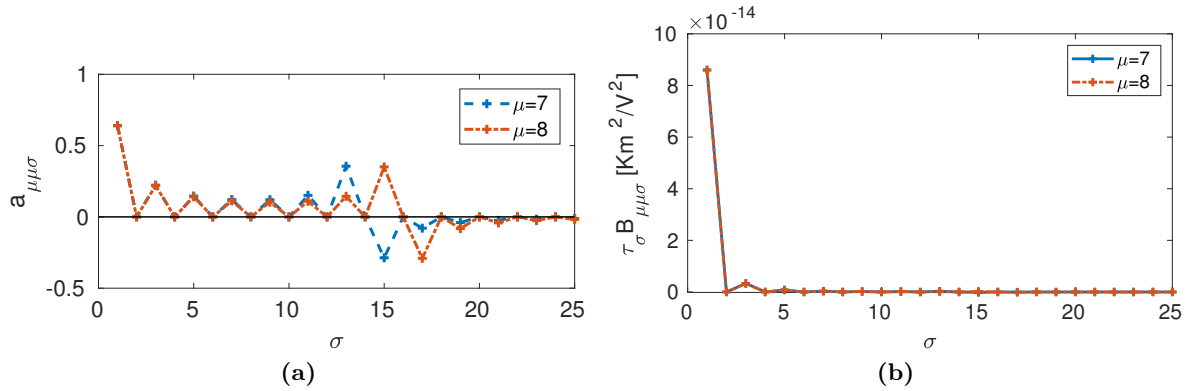

FIG. 2.2: Temperature mode coupling. In **(a)** the coupling constant $a_{\mu\mu\sigma}$ is evaluated for the relevant modes. Observe, that the coupling to the temperature ground mode is the largest. In **(b)** we see the steady state solutions of the homogeneous counterpart to (2.67), i.e. $\Delta T_\sigma = \tau_\sigma \tilde{B}_{\mu\mu\sigma}|\mathbf{E}_\mu|^2$. The $\sigma = 1$ mode is by far the strongest excited mode.

in order to have a scalar wave function, we restrict ourselves to one degree of polarisation, meaning that the vectorial charactor of the electrical field plays no role anymore. Thus, we are also able to define a wave function ψ that is normalized to the mode occupation number N, because there is just one effective photon mass (2.31a) left. We will map from the remaining mode E_κ to the wave function by comparing the energy U stored in the electrical field once expressed by the field E_κ itself and once expressed by the number of photons N. Thus, we find (compare to [70])

$$U = \frac{L}{4}\varepsilon_0 n_0^2 \int d^2x\ |E_\kappa|^2 = \frac{m_\kappa c^2}{n_0^2} \int d^2x\ |\psi|^2 \tag{2.70}$$

yielding

$$\psi = \sqrt{\frac{L\varepsilon_0 n_0^4}{4m_\kappa c^2}}\, E_\kappa. \tag{2.71}$$

Consequently, our final equations read by using (2.71) and leaving out the mode indices to simplify the notation

$$\partial_t \Delta T = \left(\mathcal{D}\nabla_r^2 - \frac{1}{\tau} - \frac{m_T \Omega_T}{2} r^2\right) \Delta T + B|\psi|^2, \tag{2.72a}$$

$$i\hbar\partial_t \psi = \left[-\frac{\hbar^2}{2m}\nabla_r^2 + \frac{m\Omega^2}{2} r^2 - \frac{i}{2}\hbar\Gamma\left(1 - \frac{\partial n}{n_0 \partial T} a\Delta T\right) + g_T \Delta T + g_K |\psi|^2\right] \psi. \tag{2.72b}$$

By replacing the electric field E with the wave function ψ, the heating rate is modified to

$$B = \frac{4\tilde{B}mc^2}{L\varepsilon_0 n_0^4} = \frac{2amc^2}{Ln_0 c_p \rho} \tag{2.73}$$

and the Kerr-interaction constant to

$$g_K = \frac{4\mathfrak{g}^{\mathrm{Kerr}} mc^2}{L\varepsilon_0 n_0^4} = -\frac{2\mathrm{Re}\left(\chi^{(3)}\right) mc^4}{\varepsilon_0 n_0^8}. \tag{2.74}$$

The photon-temperature coupling is not affected by the exchange $E \leftrightarrow \psi$, but the notation is adapted to (2.74):

$$g_T = -\frac{m_\mu c^2}{n_0^2}\frac{\partial n}{\partial T}a. \tag{2.75}$$

2.6. Pumping

Up to now, we have not considered a pump term, since it is not possible to get such a term out of Maxwell's equations, but due to experimental reasons we need to include even such a term. To find the appropriate pump term, consider the energy rate equation

$$\dot{E}_{\mathrm{Ph}} = \left(P_{\mathrm{Pump}} - P_{\mathrm{abs}}\right) N. \tag{2.76}$$

Here, P_{Pump} is the energy that is pumped into the system during a time step. Note, that we only take stimulated emission into account. Since the photon energy is given by

$$E_{\mathrm{Ph}} = \frac{mc^2}{n^2} N, \tag{2.77}$$

we can write down (2.76) as an equation for the photon number

$$\dot{N} = \frac{n_0^2}{mc^2}\left(1 + 2\frac{\partial n}{n_0 \partial T}\Delta T\right)\left(P_{\mathrm{Pump}} - P_{\mathrm{abs}}\right) N, \tag{2.78}$$

where we already take the temperature dependency into account. This equation describes now loss and gain of the intracavity photons at an abstract level and the question arises how to quantify the pump and loss powers. To this purpose we have in mind to treat the pump power as the control parameter, that we denote with p, and is therefore not further processed. The only modification arises due to the change of the refractive index.
In order to find the absorption rate, we take into account the continuity equation following from (2.72b), integrate it over the whole space and find

$$\dot{N} = -\Gamma N, \tag{2.79}$$

that only describes the absorption losses as also P_{abs} does. Therefore, we can identify

$$\Gamma = \frac{n_0^2}{mc^2} P_{\mathrm{abs}}. \tag{2.80}$$

Bringing things together, we can modify (2.72b) by writing down a photon equation that now includes also a pump term

$$i\hbar\partial_t\psi = \left(-\frac{\hbar^2}{2m}\nabla_r^2 + \frac{m\Omega^2}{2}r^2 + g_T\Delta T + g_K|\psi|^2\right)\psi \\ + \frac{i}{2}\hbar\left[\aleph p\left(1 + 2a\frac{\partial n}{n_0\partial T}\Delta T\right) - \Gamma\left(1 - 2a\frac{\partial n}{n_0\partial T}\Delta T\right)\right]\psi. \tag{2.81}$$

Here we have introduced the unit conversion factor $\aleph = n_0^2/(mc^2)$.
Since the pump p also effects the temperature difference we include a corresponding term that is also provided by (2.76) in (2.72a) and find

$$\partial_t\Delta T = \left(\mathcal{D}\nabla_r^2 - \frac{1}{\tau}\right)\Delta T + B|\psi|^2 + \alpha p, \tag{2.82}$$

where $\alpha = (1-\eta)/(V\rho c_p)$ is a factor that converts the pump power to a heating rate. Here V describes the mode volume that is considered to be the relevant volume of the cavity. The final system of mean-field equations is now provided by (2.81) and (2.82).

2.7. Comparison to Polariton-Exciton BEC

Note, that the developed mean-field model for the photon BEC turns out to be formally analogous to similar models of incoherently pumped polariton-exciton condensates, see Figure 2 and [34]. There, a reservoir of particles is coupled to a condensate. The reservoir inhibits a diffusive behaviour and is directly interacting with the condensate. Thus, we can compare this reservoir to the temperature in our system. Moreover, also the polariton condensate obeys an open-dissipative Gross-Pitaevskii equation as the photons do in our case. The equations used in reference [34] are the following. The reservoir equation is given by

$$\frac{\partial n_R}{\partial t} = P - \gamma_R n_R - R\left(n_R\right)|\phi|^2 + D\nabla^2 n_R, \tag{2.83}$$

here n_R denotes the density of the reservoir, D its diffusion coefficient and γ_R the relaxation constant. Furthermore, P denotes the external pump and ϕ the condensate wave function. This equation can be compared to the temperature equation (2.82) in our case. Note, that the major difference lies in the sign of the term proportional to the condensate density. In the exciton-polariton case this is negative, as the reservoir polaritons are scattered on the condensate density. Therefore, the reservoir density gets smaller, where the condensate density is finite. In our case of a photon BEC the sign is positive, as the temperature can only be produced, where photons are present.
The exciton-polariton condensate wave function is described by

$$i\hbar\frac{\partial\phi}{\partial t} = \left\{-\frac{\hbar^2\nabla^2}{2m_{\mathrm{LP}}} + \frac{i\hbar}{2}\big[R(n_R) - \gamma\big] + g\,|\phi|^2 + 2\tilde{g}_R\,n_R\right\}\phi, \tag{2.84}$$

where m_{LP} denotes the mass of the lower branch polaritons and γ stands for the damping of the polariton condensate. The intra condensate interaction is described by the factor g,

Table 2.1.: Table of correspondences between incoherently pumped exciton-polariton and photon BEC. The most important difference is the different sign of the reservoir scattering on the condensate.

Exciton-Polariton BEC	**Photon BEC**
reservoir n_R	temperature T
pump of reservoir P	temperature pump αp
reservoir loss γ_R	temperature relaxation $1/\tau$
scattering on condensate $-R(n_R)$	heating due to condensate B
reservoir scattering $2\tilde{g}_R$	thermo-optic nonlinearity g_T
intracondensate scattering g	Kerr nonlinearity g_K
condensate loss γ	absorption loss Γ
pump due to reservoir scattering $R(n_R)$	pump saturation $2a\frac{\partial n}{n_0 \partial T}\Delta T\left(\aleph p + \Gamma\right)$

whereas the interaction with the reservoir is described by $\tilde{g}_R$. We can compare this equation to the corresponding one for the photon BEC in (2.81). Here we can identify that the shift of the refractive index is the analogon to the interaction with the reservoir in the exciton-polariton case. Moreover, also the loss terms can be identified. The cavity loss of the polariton condensate γ corresponds to the absorption loss Γ in the photon BEC. Moreover, the pump nonlinearity, that is kept general in the exciton-polariton condensate case and denoted by $R(n_R)$ also occurs in (2.81) by identifying $R(n_R)$ by $2a\frac{\partial n}{n_0 \partial T}\Delta T\left(\aleph p + \Gamma\right)$. Note, that the nonlinearity in this expression is small as it is proportional to the thermo-optic coefficient $\frac{\partial n}{\partial T}$ and, therefore, does not occur in (2.82). Our findings are summarised in Table 2.1.

Part II.

Analysis of the two Equations

3. Homogeneous Model

Gallia est omnis divisa in partes tres [...]

G. Iulius Caesar, De Bello Gallico

All Gaul is divided into three parts [...]

We start the analysis of the mean-field model (2.81) and (2.82) with the homogeneous case, i.e. we neglect the harmonic trap in the photon equation and deal instead with the coupled set of equations of motion

$$i\hbar\partial_t\psi = \left\{-\frac{\hbar^2}{2m}\nabla^2 + g_T T + g_K|\psi|^2 + \frac{i}{2}\hbar\left[\aleph p\left(1+2\frac{\partial n}{n_0\partial T}T\right) - \Gamma\left(1-2\frac{\partial n}{n_0\partial T}T\right)\right]\right\}\psi, \tag{3.1a}$$

$$\partial_t T = \left(\mathcal{D}\nabla^2 - \frac{1}{\tau}\right)T + B|\psi|^2 + \alpha p. \tag{3.1b}$$

Here, we simplify the notation by setting $T = \Delta T$, which will also be used throughout the remainder of this thesis. Furthermore, note, that we aim to analyse a free BEC in two dimensions which is usually not possible due to the Mermin-Wagner-Hohenberg theorem [71–73] stating that a continuous symmetry cannot be broken spontaneously in two dimensions. This means that a free BEC, which relies on the breaking of the continuous U(1) symmetry, is not possible at finite temperature in two dimensions. However, this only holds for closed systems and does not apply to our case of an open-dissipative condensation, as the condensation occurs here due to an interplay of thermalisation as well as pump and loss processes.
In Section 3.1 we start by linearising the system (3.1). The resulting linear equations are analysed in the rest of the Chapter. To this end, we examine in Section 3.2 the possible steady states. In fact we will encounter that two steady states exist. The stability of those two is then analysed in detail in Section 3.3. Finally, we specify to the experimental relevant case and discuss the appearing excitations together with their spectrum in Section 3.4.

3.1. Linearisation

In this Section we linearise the system (3.1). For this purpose we perform the ansatz [34]

$$\psi(\mathbf{r},t) = e^{-i\mu t/\hbar}\left[\sqrt{\mathfrak{n}_0} + \delta\psi(\mathbf{r},t)\right], \tag{3.2a}$$

$$T(\mathbf{r},t) = T_0 + \delta T(\mathbf{r},t) \tag{3.2b}$$

Here μ denotes the photon chemical potential and $\delta\psi$ as well as δT represent small perturbations around the steady states $\mathfrak{n}_0$ and T_0, respectively.
After inserting (3.2) into (3.1) and keeping only terms up to first order in the perturbations we find the linear system

$$\begin{aligned} i\hbar\partial_t\delta\psi =& -\mu(\sqrt{\mathfrak{n}_0}+\delta\psi) - \frac{\hbar^2}{2m}\nabla^2\delta\psi + g_T(T_0\sqrt{\mathfrak{n}_0}+T_0\delta\psi+\sqrt{\mathfrak{n}_0}\delta T) + g_K\left[\mathfrak{n}_0\sqrt{\mathfrak{n}_0}+\mathfrak{n}_0\left(2\delta\psi+\delta\psi^*\right)\right] \\ &+ i\frac{\hbar}{2}\left[(\aleph p-\Gamma)(\sqrt{\mathfrak{n}_0}+\delta\psi)+2P\left(T_0\sqrt{\mathfrak{n}_0}+T_0\delta\psi+\sqrt{\mathfrak{n}_0}\delta T\right)\right], \end{aligned} \tag{3.3a}$$

$$\partial_t\delta T = \left(\mathcal{D}\nabla^2-\frac{1}{\tau}\right)\delta T - \frac{T_0}{\tau} + B\left[\mathfrak{n}_0+\sqrt{\mathfrak{n}_0}(\delta\psi+\delta\psi^*)\right]+\alpha p. \tag{3.3b}$$

In the photon equation we defined the abbreviation

$$P = 2\frac{\partial n}{n_0\partial T}(\aleph p+\Gamma). \tag{3.4}$$

To get further insight, we are going to discuss in the next Section the possible steady states.

3.2. Steady State

The steady state is described by the zeroth order in the perturbations of (3.3). Thus, it is described by the coupled algebraic equations

$$\mu\sqrt{\mathfrak{n}_0} = \left[g_T T_0 + g_K\mathfrak{n}_0 + \frac{i\hbar}{2}\left(\aleph p-\Gamma+2PT_0\right)\right]\sqrt{\mathfrak{n}_0}, \tag{3.5a}$$

$$T_0 = \tau B\mathfrak{n}_0+\alpha p\tau. \tag{3.5b}$$

From (3.5) we deduce that two steady states exist. The trivial steady state is defined by

$$\mathfrak{n}_{0\mathrm{triv}} = 0 \tag{3.6}$$

and according to (3.5b)

$$T_{\mathrm{triv}} = \alpha\tau p. \tag{3.7}$$

In order to determine the second steady state, that has a finite photon number, we separate (3.5) into imaginary and real part. This yields two equations determining the chemical potential as well as the temperature, respectively. From the imaginary part we find how the temperature

$$T_0 = \frac{\Gamma-\aleph p}{2P} \tag{3.8}$$

depends of the pump parameter p and the absorption loss rate Γ. Inserting (3.8) into (3.5b) fixes the photon number

$$\mathfrak{n}_0 = \frac{\Gamma-\aleph p}{2\tau BP} - \frac{\alpha p}{B}. \tag{3.9}$$

As the photon density is nonnegativ, (3.9) yields the criticality condition

$$2P\alpha p_{\text{crit}} = \Gamma - \aleph p_{\text{crit}}. \tag{3.10}$$

Inserting the definition (3.4) leads to the critical pump value

$$p^{\pm}_{\text{crit}} = -\frac{\Gamma}{2\aleph} - \frac{1}{4\alpha\frac{\partial n}{n_0\partial T}} \pm \sqrt{\left(\frac{\Gamma}{2\aleph} + \frac{1}{4\alpha\frac{\partial n}{n_0\partial T}}\right)^2 + \frac{\Gamma}{2\alpha\frac{\partial n}{n_0\partial T}\aleph}}\,. \tag{3.11}$$

In order to select the physical branch in (3.11), we consider the limit $\alpha \to 0$. Then (3.11) reads

$$p^{\pm}_{\text{crit}} \approx -\frac{\Gamma}{2\aleph} - \frac{1}{4\alpha\frac{\partial n}{n_0\partial T}} \pm \left(\frac{1}{4\alpha\frac{\partial n}{n_0\partial T}} + \frac{2\frac{\partial n}{n_0\partial T}\alpha\Gamma^2}{\aleph^2} + \frac{3\Gamma}{2\aleph}\right). \tag{3.12}$$

As this needs to be finite even in the case $\alpha = 0$, we conclude, that the +-branch is the relevant branch and finally find

$$p_{\text{crit}}(\alpha = 0) = \frac{\Gamma}{\aleph}. \tag{3.13}$$

The real part of (3.5) on the other hand yields the equation of state

$$\mu = g_T T_0 + g_K \mathfrak{n}_0 \tag{3.14}$$

which consists of two components. The first part stems from the thermo-optic effect and pumping, whereas the second part is due to the Kerr interaction. Using (3.5b) we can write the chemical potential even in three parts

$$\mu = \mu_p + \mu_T + \mu_K \tag{3.15}$$

with the chemical potential that arises through the pump

$$\mu_p = g_T \tau \alpha p, \tag{3.16}$$

and the ones being due to the termo-optic effect

$$\mu_T = g_T \tau B \mathfrak{n}_0 \tag{3.17}$$

and due to the Kerr effect

$$\mu_K = g_K \mathfrak{n}_0. \tag{3.18}$$

Since μ_K and μ_T depend both on the photon density $\mathfrak{n}_0$, like it is the case in [57], we can deduce from the equation of state (3.15) that the total dimensionless interaction strength $\tilde{g}$ consists of two parts reflecting the competition between the spatio-temporally retarded thermo-optic and the spatially local, instantaneous Kerr interaction

$$\tilde{g} = \tilde{g}_T + \tilde{g}_K. \tag{3.19}$$

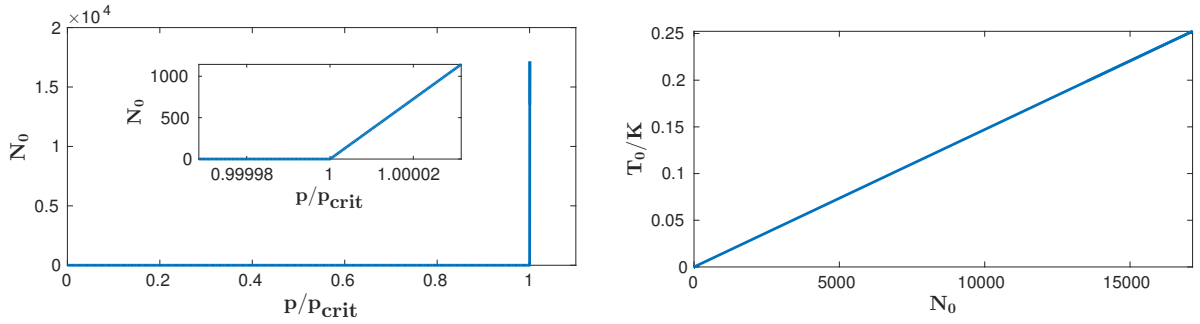

FIG. 3.1: Steady state of system (3.1) as described by (3.5b) and (3.9) for the experimental parameters that are listed in D. In **(a)** the photon number N_0 depends on the pump parameter p according to (3.6), (3.9) as well as (3.22). In **(b)** the temperature T depends on the photon number N_0. In both cases the plotted quantities show a linear behaviour.

The strength of the thermo-optic interaction is defined by

$$\tilde{g}_T = \frac{m}{\hbar^2} g_T \tau B \tag{3.20}$$

and the interaction strength of the Kerr effect by

$$\tilde{g}_K = \frac{m}{\hbar^2} g_K. \tag{3.21}$$

In both cases the factor $m/\hbar^2$ has been inserted in order to obtain a dimensionless interaction strength [54, 74]. From (3.20) we see that the strength of the thermo-optic interaction $\tilde{g}_T$ itself depends upon three parameters. It is directly proportional to the photon-temperature coupling g_T from (2.75), the temperature relaxation time τ, cf. (2.35), and the heating rate B, according to (2.73).

Figure 3.1 shows this steady state. At the transition $p = p_{\mathrm{crit}}$ a rapid increase of the photon number happens. This is related to the smallness of the thermo-optic coefficient $\frac{\partial n}{\partial T} = -4.86 \times 10^{-4}$ that enters the photon steady state (3.9) in the denominator via P in T_0, see (3.4). For the plot we assume that the trapped BEC is nearly homogeneous in the trap centre. Then we can estimate the number N_0 of photons in the condensate by multiplying the photon density $\mathfrak{n}_0$ with the mode volume πl_{osc}^2, where $l_{\mathrm{osc}} = \sqrt{\hbar/(m\Omega)}$ is the harmonic oscillator length and we find

$$N_0 = \pi l_{\mathrm{osc}}^2 \mathfrak{n}_0. \tag{3.22}$$

As one can read off from Figure 3.1, the photon number and, thus, the photon density depend in the experimental regime linearly on the pump parameter.

Now the question arises how the trivial steady state (3.6) and (3.7) is connected with the nontrivial steady state (3.8) and (3.9). For this purpose consider the limit $p \to p_{\mathrm{crit}}$. In this case per definition it holds

$$\mathfrak{n}_0 = 0 = \mathfrak{n}_{0\mathrm{triv}} \tag{3.23}$$

and thus we obtain

$$T_0 = \alpha\tau p_{\text{crit}} = T_{\text{triv}}(p = p_{\text{crit}}). \tag{3.24}$$

Therefore, we can conclude that the phase transition is continuous and that the chemical potential in the trivial steady state is fixed according to

$$\mu_{\text{triv}} = g_T \tau \alpha p. \tag{3.25}$$

3.3. Dynamical Stability

In order to examine the stability of the homogeneous condensate, we come now to the terms of first order in the perturbation in (3.3). By using (3.5) the linear perturbations (3.3) reduce to

$$\begin{aligned} i\hbar\partial_t\delta\psi + \mu\delta\psi = &-\frac{\hbar^2}{2m}\nabla^2\delta\psi + g_T(T_0\delta\psi + \sqrt{\mathfrak{n}_0}\delta T) + g_K\mathfrak{n}_0(2\delta\psi + \delta\psi^*) \\ &+ \frac{i\hbar}{2}\left(\aleph p - \Gamma + 2PT_0\right)\delta\psi + i\hbar P\sqrt{\mathfrak{n}_0}\delta T, \end{aligned} \tag{3.26a}$$

$$\partial_t\delta T = \mathcal{D}\nabla^2\delta T - \frac{\delta T}{\tau} + B\sqrt{\mathfrak{n}_0}\left(\delta\psi + \delta\psi^*\right). \tag{3.26b}$$

To proceed further we perform a Fourier ansatz, similar to [34], for the perturbation $\delta\psi$ and δT

$$\delta\psi(\mathbf{r}, t) = \sum_{\mathbf{k}} \left[u_{\mathbf{k}} e^{i(\mathbf{k}\cdot\mathbf{r} - \omega_{\mathbf{k}}t)} + v^*_{\mathbf{k}} e^{-i(\mathbf{k}\cdot\mathbf{r} - \omega^*_{\mathbf{k}}t)}\right], \tag{3.27a}$$

$$\delta T(\mathbf{r}, t) = \sum_{\mathbf{k}} \left[t_{\mathbf{k}} e^{i(\mathbf{k}\cdot\mathbf{r} - \omega_{\mathbf{k}}t)} + t^*_{\mathbf{k}} e^{-i(\mathbf{k}\cdot\mathbf{r} - \omega^*_{\mathbf{k}}t)}\right]. \tag{3.27b}$$

In this ansatz we consider the frequency ω to be a complex quantity, as we have a system that also involves damping. This damping leads to a stable steady state, iff $\text{Im}\,(\omega_{\mathbf{k}}) < 0$. Moreover, (3.27b) ensures a real temperature perturbation. Note, that in reference [34] there is a typo where the conjugation of the frequency in Equations (3) and (4) is not denoted.
Inserting now the ansatzes (3.27) into (3.26a) yields for the BEC wave function

$$\begin{aligned} &(\hbar\omega_{\mathbf{k}} + \mu)u_{\mathbf{k}} e^{i(\mathbf{k}\cdot\mathbf{r} - \omega_{\mathbf{k}}t)} - (\hbar\omega^*_{\mathbf{k}} + \mu)v^*_{\mathbf{k}} e^{-i(\mathbf{k}\cdot\mathbf{r} - \omega^*_{\mathbf{k}}t)} \\ =&\epsilon_{\mathbf{k}}\left[u_{\mathbf{k}} e^{i(\mathbf{k}\cdot\mathbf{r} - \omega_{\mathbf{k}}t)} + v^*_{\mathbf{k}} e^{-i(\mathbf{k}\cdot\mathbf{r} - \omega^*_{\mathbf{k}}t)}\right] + (g_T + iP)\sqrt{\mathfrak{n}_0}\left[t_{\mathbf{k}} e^{i(\mathbf{k}\cdot\mathbf{r} - \omega_{\mathbf{k}}t)} + t^*_{\mathbf{k}} e^{-i(\mathbf{k}\cdot\mathbf{r} - \omega^*_{\mathbf{k}}t)}\right] \\ &+ g_K\mathfrak{n}_0\left[\left(2u_{\mathbf{k}} + v_{\mathbf{k}}\right)e^{i(\mathbf{k}\cdot\mathbf{r} - \omega_{\mathbf{k}}t)} + \left(u^*_{\mathbf{k}} + 2v^*_{\mathbf{k}}\right)e^{-i(\mathbf{k}\cdot\mathbf{r} - \omega^*_{\mathbf{k}}t)}\right] \\ &+ \frac{i\hbar}{2}\left(\aleph p - \Gamma + 2PT_0\right)\left(u_{\mathbf{k}} e^{i(\mathbf{k}\cdot\mathbf{r} - \omega_{\mathbf{k}}t)} + v^*_{\mathbf{k}} e^{-i(\mathbf{k}\cdot\mathbf{r} - \omega^*_{\mathbf{k}}t)}\right). \end{aligned} \tag{3.28}$$

Here, we introduced the free particle dispersion

$$\epsilon_{\mathbf{k}} = \frac{\hbar^2 k^2}{2m}. \tag{3.29}$$

In order to find the equations for $u_{\mathbf{k}}$ and $v_{\mathbf{k}}$ we compare the coefficients of corresponding exponentials

$$\hbar\omega_{\mathbf{k}} u_{\mathbf{k}} + \mu u_{\mathbf{k}} = \epsilon_{\mathbf{k}} u_{\mathbf{k}} + (g_T + iP)\sqrt{\mathfrak{n}_0}\, t_{\mathbf{k}} + g_K \mathfrak{n}_0 (2u_{\mathbf{k}} + v_{\mathbf{k}}) + \frac{i\hbar}{2}\left(\aleph p - \Gamma + 2PT_0\right) u_{\mathbf{k}}, \quad (3.30a)$$

$$\hbar\omega_{\mathbf{k}} v_{\mathbf{k}} - \mu v_{\mathbf{k}} = -\epsilon_{\mathbf{k}} u_{\mathbf{k}} + (-g_T + iP)\sqrt{\mathfrak{n}_0}\, t_{\mathbf{k}} - g_K \mathfrak{n}_0 (u_{\mathbf{k}} + 2v_{\mathbf{k}}) + \frac{i\hbar}{2}\left(\aleph p - \Gamma + 2PT_0\right) v_{\mathbf{k}}, \quad (3.30b)$$

where we additionally complex conjugate the second equation. Inserting the ansatz (3.27) into the remaining temperature equation (3.26b) yields

$$\begin{aligned} &- i\omega_{\mathbf{k}} t_{\mathbf{k}} e^{i(\mathbf{k}\cdot\mathbf{r} - \omega_{\mathbf{k}} t)} + i\omega_{\mathbf{k}}^* t_{\mathbf{k}}^* e^{-i(\mathbf{k}\cdot\mathbf{r} - \omega_{\mathbf{k}}^* t)} \\ =& - \mathcal{D}k^2 \left[t_{\mathbf{k}} e^{i(\mathbf{k}\cdot\mathbf{r} - \omega_{\mathbf{k}} t)} + t_{\mathbf{k}}^* e^{-i(\mathbf{k}\cdot\mathbf{r} - \omega_{\mathbf{k}}^* t)} \right] - \frac{1}{\tau}\left[t_{\mathbf{k}} e^{i(\mathbf{k}\cdot\mathbf{r} - \omega_{\mathbf{k}} t)} + t_{\mathbf{k}}^* e^{-i(\mathbf{k}\cdot\mathbf{r} - \omega_{\mathbf{k}}^* t)} \right] \\ &+ B\sqrt{\mathfrak{n}_0}\left[(u_{\mathbf{k}} + v_{\mathbf{k}})\, e^{i(\mathbf{k}\cdot\mathbf{r} - \omega_{\mathbf{k}} t)} + (u_{\mathbf{k}}^* + v_{\mathbf{k}}^*)\, e^{-i(\mathbf{k}\cdot\mathbf{r} - \omega_{\mathbf{k}}^* t)} \right]. \end{aligned} \quad (3.31)$$

As above the equation for $t_{\mathbf{k}}$ and $t_{\mathbf{k}}^*$ is deduced by collecting the prefactors of corresponding exponentials

$$\omega_{\mathbf{k}} t_{\mathbf{k}} = -i\mathcal{D}\mathbf{k}^2 t_{\mathbf{k}} - \frac{i}{\tau} t_{\mathbf{k}} + B\sqrt{\mathfrak{n}_0}\,(u_{\mathbf{k}} + v_{\mathbf{k}}). \quad (3.32)$$

We proceed now by investigating the stability of both the trivial steady state and the finite photon number steady state.

3.3.1. Trivial Steady State

First we insert the trivial steady state (3.6) and (3.7) into the equations (3.30) and (3.32). From (3.30) we obtain the equations

$$\left[\hbar\omega_{\mathbf{k}} - \epsilon_{\mathbf{k}} + \frac{i\hbar}{2}\left(\aleph p - \Gamma + 2P\alpha p\right)\right] u_{\mathbf{k}} = 0, \quad (3.33a)$$

$$\left[\hbar\omega_{\mathbf{k}} - \epsilon_{\mathbf{k}} + \frac{i\hbar}{2}\left(\aleph p - \Gamma + 2P\alpha p\right)\right] v_{\mathbf{k}} = 0. \quad (3.33b)$$

The corresponding spectrum is yielded by the zeros of the brackets. Note, that the vanishing of their imaginary part matches exactly to the criticality condition (3.10). Therefore, this state is stable for $p < p_{\text{crit}}$ and unstable for $p > p_{\text{crit}}$. The temperature perturbation is described by the equation

$$\left(\omega_{\mathbf{k}} - i\mathcal{D}\mathbf{k}^2 - \frac{i}{\tau}\right) t_{\mathbf{k}} = 0. \quad (3.34)$$

Thus, the temperature perturbations are purely imaginary with a negative sign. This means, that the temperature fluctuations always decay. To sum up, the stability of the trivial steady state is described by the stability of the photon dispersion, which becomes unstable as soon as the nontrivial steady state starts to exist.
We turn now our attention to the stability of the nontrivial steady state.

3.3.2. Nontrivial Steady State

In order to keep the notation as simple and meaningful as possible, we redefine the perturbation coefficients $u_{\mathbf{k}}$, $v_{\mathbf{k}}$ and $t_{\mathbf{k}}$ to dimensionless quantities, by pulling the amplitudes of the non-trivial steady state (3.30) and (3.32) out of those perturbations. This means that for the remainder of this Section the new quantities $\tilde{u}_{\mathbf{k}} = u_{\mathbf{k}}/\sqrt{\mathfrak{n}_0}$, $\tilde{v}_{\mathbf{k}} = v_{\mathbf{k}}/\sqrt{\mathfrak{n}_0}$ as well as $\tilde{t}_{\mathbf{k}} = t_{\mathbf{k}}/T_0$ are considered. By doing so, the stability of the steady state will then be fully described by only considering the chemical potentials (3.16), (3.17) and (3.18). In the following we will drop the tildes again. In this case (3.30) yields together with (3.32) a linear system of equations determining the stability of the nontrivial steady state that we write for further investigations in vector-matrix form as

$$\hbar\omega_{\mathbf{k}} \begin{pmatrix} u_{\mathbf{k}} \\ v_{\mathbf{k}} \\ t_{\mathbf{k}} \end{pmatrix} = \begin{pmatrix} \epsilon_{\mathbf{k}} + \mu_K & \mu_K & \mu_p + \mu_T + i\hbar P \\ -\mu_K & -\epsilon_{\mathbf{k}} - \mu_K & -\mu_p - \mu_T + i\hbar P \\ i\kappa & i\kappa & -i\left(D_{\mathbf{k}} + \sigma\right) \end{pmatrix} \begin{pmatrix} u_{\mathbf{k}} \\ v_{\mathbf{k}} \\ t_{\mathbf{k}} \end{pmatrix}. \tag{3.35}$$

By writing down the line corresponding to the temperature equation, we introduce also here an energy notation as it is done for the photon equations that are stated in terms of the one-particle energy $\epsilon_{\mathbf{k}}$ and the chemical potentials. Thus, for the temperature we introduce the heating energy

$$\kappa = \frac{\hbar}{\tau} - \frac{\hbar\alpha\tau p}{T_0}, \tag{3.36}$$

the diffusion energy $D_{\mathbf{k}} = \hbar\mathcal{D}\mathbf{k}^2$ as well as the relaxation energy $\sigma = \hbar/\tau$.
In the following, we will refer to the system matrix in (3.35) with S. The characteristic polynomial p_S of S is given by

$$\begin{aligned} p_S(\omega_{\mathbf{k}}) = &- (\hbar\omega_{\mathbf{k}})^3 - i(\hbar\omega_{\mathbf{k}})^2 \left(\mathcal{D}_{\mathbf{k}} + \sigma\right) + \hbar\omega_{\mathbf{k}} \left(\epsilon_{\mathbf{k}}^2 + 2\epsilon_{\mathbf{k}}\mu_K - 2\kappa P\right) \\ &+ i(\epsilon_{\mathbf{k}}^2 + 2\epsilon_{\mathbf{k}}\mu_{\mathbf{k}}) \left(\mathcal{D}_{\mathbf{k}} + \sigma\right) - 2i\kappa\epsilon_{\mathbf{k}}(\mu_p + \mu_T). \end{aligned} \tag{3.37}$$

In case of a vanishing thermo-optic coefficient, i.e. $\frac{\partial n}{\partial T} = 0$ and, thus, according to (3.17) $\mu_T = 0$, as well as in case of vanishing pump, we recover as eigenvalues of S the usual Bogoliubov dispersion relation [21]

$$\left(\hbar\omega_{\mathbf{k}}^{\mathrm{Bog}}\right)^2 = \epsilon_{\mathbf{k}}^2 + 2\epsilon_{\mathbf{k}}\mu_K \tag{3.38}$$

and the previous $\mathbf{k}$-dependent damping from (3.34) of the temperature

$$\omega_{\mathbf{k}} = -i\left(\mathcal{D}\mathbf{k}^2 + \frac{1}{\tau}\right) \tag{3.39}$$

showing again that the diffusion acts as a damping of the temperature.

In the long wavelength limit, the characteristic polynomial (3.37) simplifies to

$$p_S(\omega_{\mathbf{0}}) = -(\hbar\omega_{\mathbf{0}})^3 - i(\hbar\omega_{\mathbf{0}})^2\sigma - 2\hbar\omega_{\mathbf{0}}P\kappa. \tag{3.40}$$

As one can see, in that limit the eigenvalues do not depend upon the photon-photon interaction. Moreover, we have always the eigenvalue $\hbar\omega^1_{\mathbf{0}} = 0$ present. This is nothing but the signature of the Goldstone theorem [75], which states that breaking a continuous U(1)-symmetry yields a vanishing energy gap at $\mathbf{k} = \mathbf{0}$. Interestingly, the Goldstone theorem is not only valid for a closed quantum system, but also for an open-dissipative one like the photon BEC or the exciton-polariton condensate [34]. By evaluating the remaining second-order equation we find from (3.40) for the next two eigenvalues

$$\hbar\omega^{\pm}_{\mathbf{0}} = -\frac{i\sigma}{2} \pm i\sqrt{\frac{\sigma^2}{4} + 2P\kappa}\,. \tag{3.41}$$

Bear in mind that according to definition (3.4) we have $P < 0$. Thus, the real part of the eigenvalues $\omega^{\pm}_{\mathbf{0}}$ vanishes iff $\sigma^2 > 8P\kappa$. Furtheron, $P < 0$ yields $\sqrt{\sigma^2/4 + 2P\kappa} < \sigma/2$ which means that the imaginary part of $\omega_{\mathbf{0}}$ is always negative and, therefore, the condensate turns out to be stable in this limit.

In the short wavelength limit $|\mathbf{k}| \to \infty$ the characteristic polynomial (3.37) acquires the form

$$p_S(\omega_{\mathbf{k}}) = -(\hbar\omega_{\mathbf{k}})^3 - i(\hbar\omega_{\mathbf{k}})^2\mathcal{D}_{\mathbf{k}} + \hbar\omega_{\mathbf{k}}\epsilon^2_{\mathbf{k}} + i\epsilon^2_{\mathbf{k}}\mathcal{D}_{\mathbf{k}}, \tag{3.42}$$

where the lower powers of $\mathbf{k}$ have been neglected. Two solutions are provided by the free particle dispersion

$$\hbar\omega_{\mathbf{k}\pm} \pm = \epsilon_{\mathbf{k}}, \tag{3.43}$$

whereas the third solution is given by the free diffusion dispersion

$$\hbar\omega_{\mathbf{k}} = -i\mathcal{D}_{\mathbf{k}}. \tag{3.44}$$

Thus, neither the interactions nor the pump influence these three solutions and the condensate is always stable in the short wavelength limit.

The remaining question of concern is after the stability of the condensate in between the extremal cases $|\mathbf{k}| = 0$ and $|\mathbf{k}| \to \infty$. Here, this is discussed in the full generality, whereas in the next Section it will be specified to the experimental case. In order to examine this stability, we investigate the zeros of

$$\begin{aligned} -ip_S(i\omega_{\mathbf{k}}) =& (\hbar\omega_{\mathbf{k}})^3 + (\hbar\omega_{\mathbf{k}})^2\left(\mathcal{D}_{\mathbf{k}} + \sigma\right) + \hbar\omega_{\mathbf{k}}\left[\left(\hbar\omega^{\mathrm{Bog}}_{\mathbf{k}}\right)^2 - 2\kappa P\right] \\ &+ \left(\hbar\omega^{\mathrm{Bog}}_{\mathbf{k}}\right)^2\left(\mathcal{D}_{\mathbf{k}} + \sigma\right) - 2\kappa\epsilon_{\mathbf{k}}(\mu_p + \mu_T) \end{aligned} \tag{3.45}$$

as this is now a polynomial with real-valued coefficients. Because of real valuedness, the Routh-Hurwitz criterion [76] is now applicable. This states, that a third order polynomial $p(x) = x^3 + a_2x^2 + a_1x + a_0$, is stable, i.e. the roots have negative real parts, iff the following three

conditions hold

$$a_2 > 0, \tag{3.46a}$$
$$a_0 > 0, \tag{3.46b}$$
$$a_2 a_1 > a_0. \tag{3.46c}$$

In our case, the first condition amounts to the inequality

$$\hbar \left(\mathcal{D}\mathbf{k}^2 + \frac{1}{\tau} \right) > 0, \tag{3.47}$$

that is trivially fulfilled. The second inequality (3.46b) is in our case given by

$$\left(\hbar\omega_{\mathbf{k}}^{\mathrm{Bog}} \right)^2 (\mathcal{D}_{\mathbf{k}} + \sigma) > 2\kappa\epsilon_{\mathbf{k}}(\mu_p + \mu_T), \tag{3.48}$$

which simplifies by using (3.38) to

$$|\mathbf{k}| > k_{\mathrm{crit}} \tag{3.49}$$

with the associated critical k value

$$k_{\mathrm{crit}} = \sqrt{-\frac{1}{2}\left(\frac{\sigma}{\mathcal{D}\hbar} + \frac{4m\mu_K}{\hbar^2} \right) + \sqrt{\frac{1}{4}\left(\frac{\sigma}{\mathcal{D}\hbar} - \frac{4m\mu_K}{\hbar^2} \right)^2 + \frac{4m\kappa(\mu_P + \mu_T)}{\mathcal{D}\hbar^3}}}. \tag{3.50}$$

As k_{crit} must be a real-valued quantity, this stability criterion only plays a role, if

$$\frac{\sigma}{\mathcal{D}\hbar} + \frac{4m\mu_K}{\hbar^2} < \sqrt{\left(\frac{\sigma}{\mathcal{D}\hbar} - \frac{4m\mu_K}{\hbar^2} \right)^2 + \frac{4m\kappa(\mu_P + \mu_T)}{\mathcal{D}\hbar^3}}, \tag{3.51}$$

which can be simplified to

$$\sigma\mu_K < \kappa(\mu_P + \mu_T). \tag{3.52}$$

Thus, if (3.52) is valid, the stability criterion (3.49) restricts the allowed wave vectors $\mathbf{k}$. Conversely, if the Kerr interaction outweighs the thermo-optic and pump interaction, the condensate is stable for any $\mathbf{k}$, as k_{crit} is formally imaginary.
The third inequality (3.46c) reads after simplification with (3.29)

$$\mathbf{k}^2 > \frac{P\sigma}{\frac{\hbar^2(\mu_p + \mu_T)}{2m} - \hbar\mathcal{D}P}. \tag{3.53}$$

To sum up, the nontrivial steady state is stable, iff (3.49) is fulfilled. As due to (3.4) we have $P < 0$ in the nontrivial steady state, this condition is always valid.

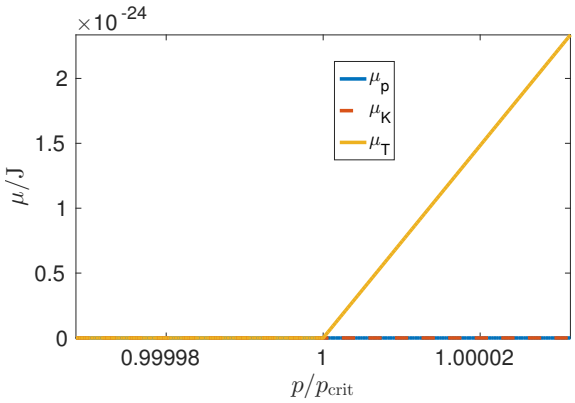

FIG. 3.2: Plot of the different parts of the chemical potential (3.15), together with (3.16)-(3.18). The chemical potential that arises due to the thermo-optic interaction is the most influential among the different chemical potentials. The plot parameters can be found in Appendix D.

3.4. Experimental Case

We specify now our findings to the experimental case. We start our investigation by comparing the different parts of the chemical potential (3.15), together with (3.16)-(3.18), in order to find out whether one of the ingredients dominates. Those different parts are plotted in Figure 3.2. There one can clearly see, that the thermo-optic chemical potential μ_T dominates the chemical potential by far. From this we can deduce for the numerical value of the dimensionless thermo-optic interaction constant (3.20)

$$\tilde{g}_T = 2.56 \times 10^{-4}. \tag{3.54}$$

This is close to the experimental value of $(7 \pm 3) \times 10^{-4}$ reported in [35].

Thus, in the experimental case the photons only interact via the thermo-optic mechanism and we can assume the Kerr interaction to vanish, i.e. $\mu_K \approx 0$. Since we are working slightly above the critical pump power p_{crit}, only small pump powers are involved. Thus, we can also neglect the pump chemical potential μ_p and the pump influence on κ, i.e. we have $\mu_p \approx 0$ and $\kappa \approx \sigma$, see (3.36). Therefore, the experimental case is the antipode to the case that is described directly beneath (3.37), where the thermo-optic and pump influences were neglected in comparison to the Kerr interaction.
As a consequence, we can simplify the characteristic polynomial p_S (3.37) of the system matrix S to

$$p_S(\omega_{\mathbf{k}}) \approx -(\hbar\omega_{\mathbf{k}})^3 - i(\hbar\omega_{\mathbf{k}})^2(\mathcal{D}_{\mathbf{k}} + \sigma) + \hbar\omega_{\mathbf{k}}\left(\epsilon_{\mathbf{k}}^2 - 2\sigma P\right) + i\epsilon_{\mathbf{k}}^2(\mathcal{D}_{\mathbf{k}} + \sigma) - 2i\sigma\epsilon_{\mathbf{k}}\mu_T. \tag{3.55}$$

Also the stability criterion (3.50) simplifies to

$$k_{\text{crit}} \approx \sqrt{-\frac{\sigma}{2\mathcal{D}\hbar} + \sqrt{\left(\frac{\sigma}{2\mathcal{D}\hbar}\right)^2 + \frac{\sigma}{\xi^2\mathcal{D}\hbar}}} \tag{3.56}$$

with the coherence length $\xi = \sqrt{\hbar^2/(2m\mu_T)}$ [21, (6.62)]. As we see in (3.56), for increasing diffusion $\mathcal{D}$ we have that k_{crit} decreases, whereas it rises with growing photon number and

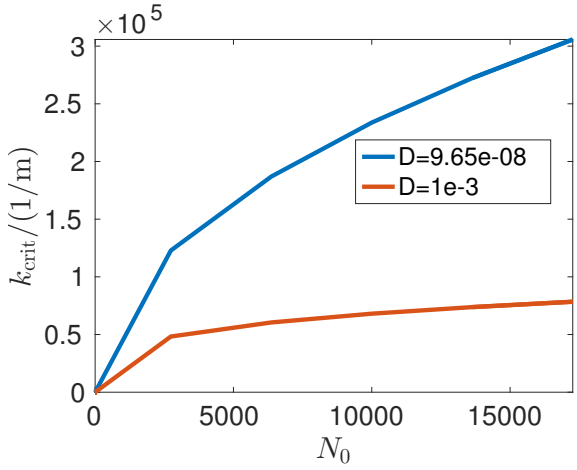

FIG. 3.3: Plot of critical wave number k_{crit} from (3.56). The diffusion constant D is given in units of m^2/s. The current experiment possesses $D = 9.65 \times 10^{-8}\,\mathrm{m}^2/\mathrm{s}$.

thus growing pump. This means that on the one hand the thermo-optic interaction somehow destabilises the condensate, but on the other hand the diffusion has a stabilising influence. For small diffusion we can simplify (3.56) to

$$k_{\mathrm{crit}} \approx \frac{1}{\xi}. \tag{3.57}$$

In Figure 3.3 the critical wave number according to (3.56) is visualised. Therefore, for reasonable photon numbers, the critical wave number is of the order of $k_{\mathrm{crit}} \sim 1 \times 10^5\,\mathrm{m}$. Hence, in an experiment the homogeneous condensate would be stable, if the modes with wave number smaller than k_{crit} are not allowed. This can be achieved, if the mirror diameter is smaller than the length scale that is set by $1/k_{\mathrm{crit}}$.

The dispersion relation for a condensate with $N_0 = 10,000$ photons is shown in Figure 3.4. The corresponding eigenvectors can be found in Figure 3.5. For small wave numbers the condensate is unstable as can be followed by the large positive imaginary part of the eigenvalue shown in red in Figure 3.4(b). On the other hand the remaining two modes are stable. Compared to Figure 3.4(a) we see, that the unstable eigenmode corresponds to a vanishing eigenfrequency, meaning that the condensate shows a diffusive behaviour. This holds true for $\mathbf{k} \to \mathbf{0}$, as can be seen in the inlet, so this eigenmode corresponds to the Goldstone mode. This means, that although the Mermin-Wagner-Hohenberg theorem does not hold in the present case of an open-dissipative system, the Goldstone theorem still applies. The corresponding eigenvector is $\nu_2(\mathbf{k} = \mathbf{0}) = (1, -1, 0)/\sqrt{2}$, i.e. a rotation of the condensate, analogue to the findings of Wouters and Carusotto in [34]. This mode gets stable as the temperature amplitude $t_{\mathbf{k}}$ becomes of the order of $u_{\mathbf{k}}$ and $v_{\mathbf{k}}$.
Contrarily, the residual modes always have nonzero eigenfrequencies. This means that, in correspondence to (3.43), they behave as free photons in the microcavity in the short wavelength limit. Therefore, in the stable regime only one-particle excitations are possible. For $\mathbf{k} = \mathbf{0}$ their frequencies are given according to (3.41) by $\mathrm{Re}\,(\omega_{\mathbf{0}\pm}) = \pm 7.34 \times 10^5\,\mathrm{Hz}$ with the damping $\mathrm{Im}\,(\omega_{\mathbf{0}\pm}) = -2.12 \times 10^5\,\mathrm{Hz}$. From the corresponding eigenvectors, whose elements are plotted in panels **(a)** and **(c)** we can conclude that those two modes correspond to pure excitations of $u_{\mathbf{k}}$ and $v_{\mathbf{k}}$, respectively, in the limit $|\mathbf{k}| \to \infty$. In the limit $\mathbf{k} \to \mathbf{0}$ these modes get also mixed.

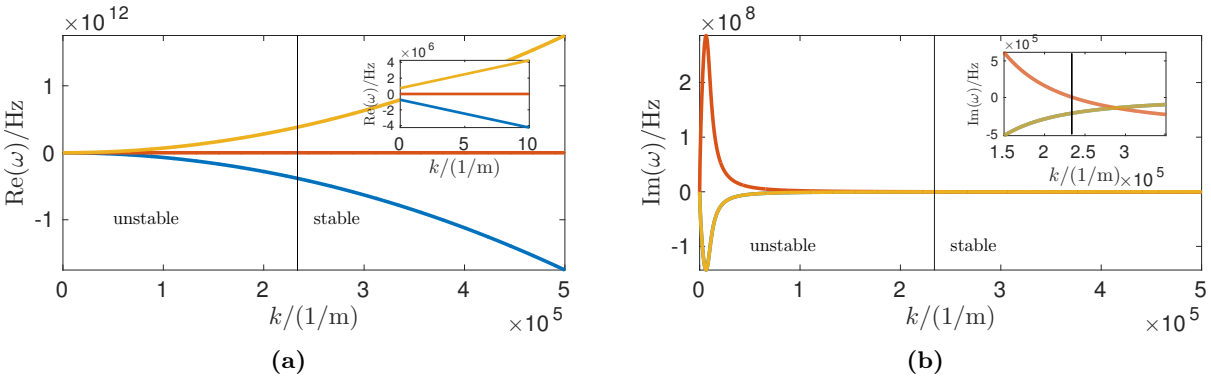

FIG. 3.4: Typical dispersion with **(a)** the oscillation frequency and **(b)** the damping rate as described by the roots of (3.55). The used parameters can be found in Appendix D. The pump is adjusted to $N_0 = 10,000$ photons. In both drawings the vertical line indicates the critical wave number k_{crit} at which the homogeneous condensate gets stable as shown in the inlet in **(b)**.

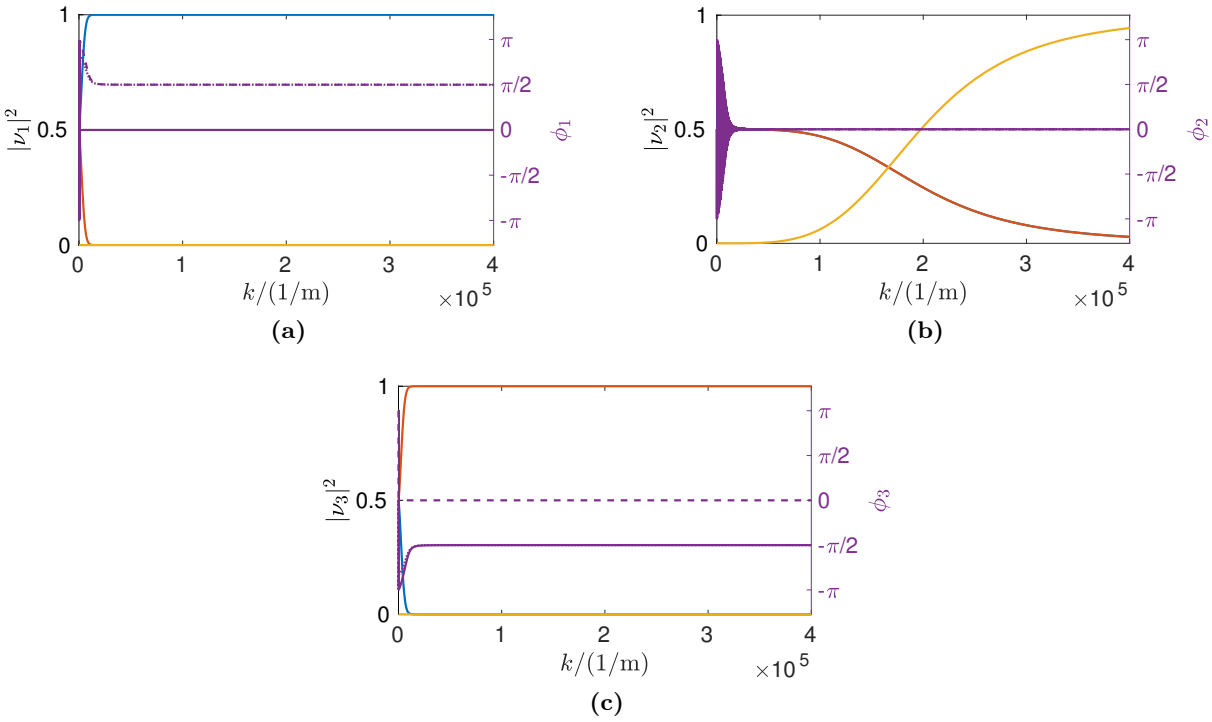

FIG. 3.5: Eigenvectors to the eigenvalues of (3.55) with $u_{\mathbf{k}}$ (blue), $v_{\mathbf{k}}$ (yellow) and $t_{\mathbf{k}}$ (red) corresponding to the eigenvalue in **(a)** yellow, **(b)** red and **(c)** blue in Figure 3.4. On the left y axis are the squared absolute values of the coordinates $|\nu_i|^2$, whereas on the right y-axis the corresponding phase ϕ_i is plotted.

4. Photon BEC in a Harmonic Trap

PUCK: How now, spirit! whither wander you?
Fairy: Over hill, over dale,
Thorough bush, thorough brier,
Over park, over pale,
Thorough flood, thorough fire,
I do wander everywhere,
Swifter than the moon's sphere;

William Shakespeare, A Midsummer Night's Dream, Act II, Scene 1

In this Chapter we ought to describe the photon Bose-Einstein condensate in a harmonic trap, as this is currently the most relevant experimental case. For this purpose the full equations (2.81) and (2.82) are considered:

$$\partial_t T = \nabla^2 T - \frac{1}{\tau} T + B|\psi|^2, \tag{4.1a}$$

$$\begin{aligned} i\hbar\partial_t \psi = &\left(-\frac{\hbar^2}{2m}\nabla^2 + \frac{m\Omega^2}{2} r^2 + g_T T + g_K |\psi|^2 \right) \psi \\ &+ \frac{i\hbar}{2} \left[p\aleph \left(1 + 2\frac{\partial n}{\partial T} T \right) - \Gamma \left(1 - 2\frac{\partial n}{\partial T} T \right) \right] \psi, \end{aligned} \tag{4.1b}$$

where $r = \sqrt{x^2 + y^2}$ denotes the distance from the optical axis. To simplify our notation we denote in the following the two involved coordinate directions x and y by x_1 and x_2, respectively. Correspondingly, the position vector is from now on written as $\mathbf{x} = (x_1, x_2)^T$. Moreover, according to the results from the preceding chapter, we neglect the pump of the temperature, as this almost no contribution.

From the analysis of a usual Gross-Pitaevskii equation it is well known that the interaction between condensate particles has an influence on the frequencies of the lowest-lying collective modes [77–79], see also Appendix C. Dynamical measurements of those frequencies turn out to be very precise [80]. Therefore, measuring these collective oscillations reveals reliable information about the underlying nature of the interaction.

In this Chapter we derive the frequencies of the dipole, the quadrupole and the breathing mode for the photon BEC. Usually one uses a variational approach to calculate these frequencies [21, 77], that relies on the action and the accompanying Hamilton's principle. However, this technique cannot be used in our setting of an open-dissipative system, as the energy is not a conserved quantity. Instead we derive the cumulants equations of motion that carry the same information, but no action is needed to calculate them. Details of this technique can be found in [81] and in Appendix C. In order to apply this method, we show in Section 4.1 the ansatzes that we use for the shapes of the condensate wave function and the temperature distribution. As

in our setting pump and loss processes are an explicit part of the dynamics, also the amplitude of these two functions is determined by the pump and loss processes. The corresponding evolution equations are derived in Section 4.2. After that we extract the cumulants equations of motion in Section 4.3. These equations are then analysed by means of a linear stability analysis. For this purpose in Section 4.4 the steady state is determined. In the following sections we investigate the stability of this steady state. On the one hand we examine in Section 4.5 the stability under perturbations where the centre-of-mass of the condensate oscillates, i.e. we analyse the dipole mode. On the other hand we also look into a perturbation of the widths in the second last Section 4.6. This leads us to the quadrupole and the breathing mode. Finally, in Section 4.7 we discuss possible experimental realisations.

4.1. Ansatz

In this Section the ansatz for solving the system (4.1) is introduced and discussed. At first, the pump spot p is assumed to be of Gaussian shape and to be radially symmetric with width s as well as centred around the origin:

$$p(\mathbf{x}) = \frac{P_0}{\pi s^2} \exp\left[-\frac{\mathbf{x}^2}{s^2}\right]. \tag{4.2}$$

The unperturbed photon equation represents a Schrödinger equation with a harmonic potential. Thus, we presume the ansatz of the BEC mean-field wave function to be a Gaussian, as it is the ground state solution of the harmonic oscillator. This approach is also used in references [77, 79, 82]. Thus, we write

$$\psi(\mathbf{x},t) = \sqrt{\frac{N(t)}{\pi q_1(t) q_2(t)}} \exp\left\{ \sum_{j=1,2} -\left[\frac{1}{2q_j(t)^2} + iA_j(t)\right] [x_j - x_{0j}(t)]^2 + i x_j C_j(t) \right\}. \tag{4.3}$$

Here $N(t)$ describes the time dependent photon number, $q_j(t)$ stands for the widths in the x_1, x_2 directions, respectively, and $A_j(t)$ denotes their corresponding phases. With these parameters we are already able to describe two oscillatory eigenstates, namely the quadrupole and the breathing mode, i.e. width oscillations in or out of phase, see panels **(a), (b)** in Figure 4.1. As we also want to describe the centre-of-mass motion, that is called dipole mode, see panel **(c)** in Figure 4.1, we allow for a time dependency of the centre-of-mass coordinates x_{0j} and their corresponding phases C_j.

We perform a similar ansatz for the temperature diffusion equation as a Gaussian function by its own is a solution of the unperturbed diffusion equation and it is pumped by a Gaussian function. Therefore, we assume the temperature profile to be given by

$$T(\mathbf{x},t) = \frac{T_0(t)}{\pi r_1(t) r_2(t)} \exp\left\{ \sum_{i=1,2} -\frac{[x_i - y_{0i}(t)]^2}{r_i(t)^2} \right\}. \tag{4.4}$$

Here we also allow for a time-dependence of the amplitude $T_0(t)$ as well as the widths $r_i(t)$ and the centre-of-mass coordinates $y_{0i}(t)$. As the temperature is a real function no phases as in the

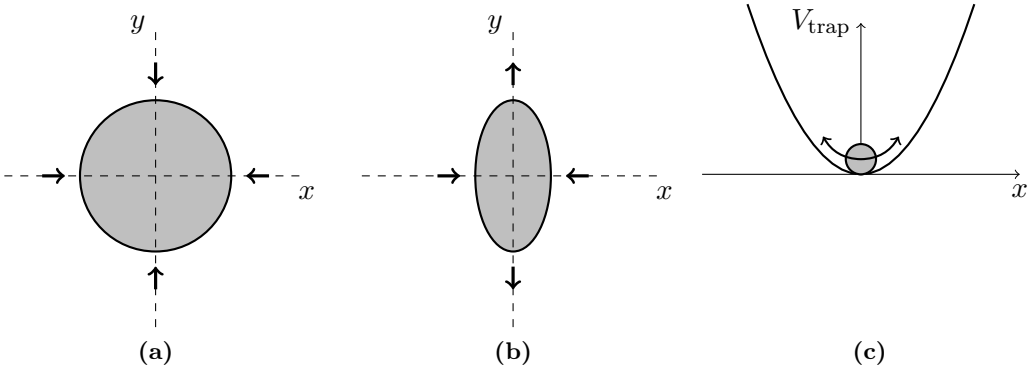

FIG. 4.1: Eigenmodes that are described by ansatz (4.3). In **(a)** the breathing mode is characterised by the widths oscillating in phase making the condensate look as if it would breath. Panel **(b)** displays the quadrupole mode that is described by the widths oscillation with 90° out of phase. A sketch of the dipole mode can be seen in Panel **(c)**, where the centre-of-mass of the condensate moves classically in the harmonic trapping potential.

ansatz for the photon wave function (4.3) are included here.
In the following we will treat the amplitudes $N(t)$ and $T_0(t)$, the widths $q_j(t)$ and $r_j(t)$ as well as the centre-of-mass coordinates x_{0j} and y_{0j} as variational parameters. The aim is then to derive the evolution equations for these variational parameters.

4.2. Normalisation

As we are dealing with an open system, the temperature amplitude T_0 and the photon number N_0 are not constant in time, but they depend on the pump strength P_0 and, as we consider a spatial extension of the involved quantities, also on the widths and centres-of-masses of the respective Gaussian shaped functions. For this purpose we calculate the continuity equations belonging to both equations (4.1). The respective equation for (4.1a) is found by by inserting the ansatzes (4.3) and (4.4) and by integrating over the whole cavity subsequently

$$\partial_t T_0 = -\frac{T_0}{\tau} + BN, \tag{4.5}$$

where we assume no fluxes through the mirrors. For the photon equation (4.1b) we find by multiplying this equation by the complex conjugated wave function ψ^* and adding the conjugated equation after integrating the result

$$\partial_t N = \aleph P_0 N G_{\mathrm{P}\psi} + 2\aleph \frac{\partial n}{\partial T} T_0 N P_0 G_{\mathrm{TP}\psi} - \Gamma N + 2\Gamma \frac{\partial n}{\partial T} T_0 N G_{\mathrm{T}\psi}, \tag{4.6}$$

where we defined the three Gaussian integrals

$$G_{\mathrm{P}\psi} = \int d^2x\ p(\mathbf{x})|\psi(\mathbf{x},t)|^2, \tag{4.7a}$$

$$G_{\mathrm{T}\psi} = \int d^2x\ T(\mathbf{x},t)|\psi(\mathbf{x},t)|^2, \tag{4.7b}$$

$$G_{\mathrm{TP}\psi} = \int d^2x\ T(\mathbf{x},t)p(\mathbf{x})|\psi(\mathbf{x},t)|^2. \tag{4.7c}$$

By using the ansatzes (4.2)–(4.4) those integrals gather again a Gaussian form and can be solved by using the method described in Appendix B

$$G_{\mathrm{P}\psi} = \frac{1}{\pi\sqrt{(q_1^2+s^2)(q_2^2+s^2)}}\exp\left[-\sum_{j=1,2}\frac{x_{0j}^2}{s^2+q_j^2}\right], \tag{4.8a}$$

$$G_{\mathrm{T}\psi} = \frac{1}{\pi\sqrt{(q_1^2+s^2)(q_2^2+s^2)}}\exp\left[-\sum_{j=1,2}\frac{(x_{0j}-y_{0j})^2}{r_j^2+q_j^2}\right], \tag{4.8b}$$

$$G_{\mathrm{TP}\psi} = \frac{1}{\pi^2\prod_{j=1,2}\sqrt{r_j^2q_j^2+q_j^2s^2+r_j^2s^2}}\exp\left[-\sum_{j=1,2}\frac{(x_{0j}-y_{0j})^2s^2+x_{0j}^2r_j^2+y_{0j}^2q_j^2}{r_j^2q_j^2+q_j^2s^2+r_j^2s^2}\right], \tag{4.8c}$$

where we left out the explicit time dependencies as it will be done in the following. Thus the photon number and the temperature amplitude depend not only on the pump strength, as it is suspected, but also on the widths of all the involved functions in a nonlinear way.

4.3. Cumulants Equations

The usual variational approach to calculate the evolution of a Gaussian shaped mean-field BEC wave function uses the action functional and Hamilton's principle [78]. As we are dealing with an open system such quantities do not longer exist since they rely on energy conservation. Nevertheless, we still stay with the Gaussian ansatzes, but instead of considering an action we directly determine the evolution equations for the respective first and second cumulants of those Gaussian ansatzes and derive the corresponding evolution equations describing the full dynamics. For an overview on this method consult Appendix C.

4.3.1. Temperature Equations

In order to obtain the equation governing the centre-of-mass dynamics of the temperature we multiply (4.1a) by the spatial variable $x_k,\ k=1,2$, and integrate subsequently over the whole cavity

$$\partial_t\int d^2x\ x_kT = \mathcal{D}\int d^2x\ x_k\nabla^2T - \frac{1}{\tau}\int d^2x\ x_kT + B\int d^2x\ x_k|\psi|^2. \tag{4.9}$$

Taking into account the ansatzes (4.2)–(4.4) and performing the integrals yields

$$\partial_t y_{0k} = \frac{BN}{T_0}(x_{0k} - y_{0k}). \tag{4.10}$$

This equation shows that the temperature centre-of-mass y_{0k} always follows the photon centre-of-mass x_{0k} in a diffusive, i.e. nonoscillatory, way.

The dynamics of the temperature width can be calculated analogously by considering the second central moment

$$\begin{aligned}\partial_t \int d^2x\ (x_k - y_{0k})^2 T =& \mathcal{D} \int d^2x\ (x_k - y_{0k})^2 \nabla^2 T - \frac{1}{\tau}\int d^2x\ (x_k - y_{0k})^2 T \\ &+ B \int d^2x\ (x_k - y_{0k})^2 |\psi|^2.\end{aligned} \tag{4.11}$$

Therefore, the temperature width is governed by the equation

$$\partial_t r_k^2 = 4\mathcal{D} + \frac{BN}{T_0}(q_k^2 - r_k^2) + 2\frac{BN}{T_0}(y_{0k} - x_{0k})^2. \tag{4.12}$$

Also here we find that the temperature width follows the photon width in a diffusive manner. On top of that we have the influence of the regular diffusion of the temperature represented by the term $4\mathcal{D}$.

Without a coupling to the photons, i.e. $B = 0$, we conclude from (4.5), that the resulting temperature Gaussian function is described by a decaying amplitude with decay time τ:

$$T_0(t) = T_0(t_0) \exp\left(-\frac{t - t_0}{\tau}\right), \tag{4.13}$$

whereas from (4.12) it follows that the width increases with the diffusion constant according to the Einstein law

$$r_k(t)^2 = 4\mathcal{D}(t - t_0),\ k = 1, 2. \tag{4.14}$$

We compare the analytical results to the numerical solution of the plain diffusion equation. The used numerical procedure is explained in Appendix C.3. Those numerical results are shown in Figure 4.2. As one sees, the results match in a reasonable way showing that both methods, the analytical method presented in this Section and the numerical method, are appropriate ways to solve the diffusion equation. Even in the case that an external source of Gaussian shape is present the numerical solution of the ODEs (4.5) and (4.12) agrees with the numerical solution of the full diffusion equation, as it is shown in Figure 4.3.

4.3.2. Photon Wave Function Equations

In this Section we aim for the corresponding equations for the photon wave function. The procedure relies again on calculating the evolution equation of the first and second cumulant

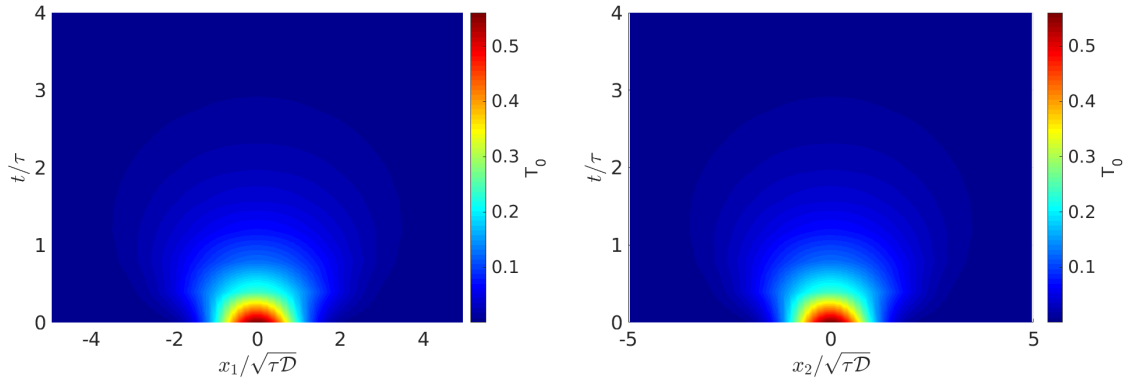

(a)

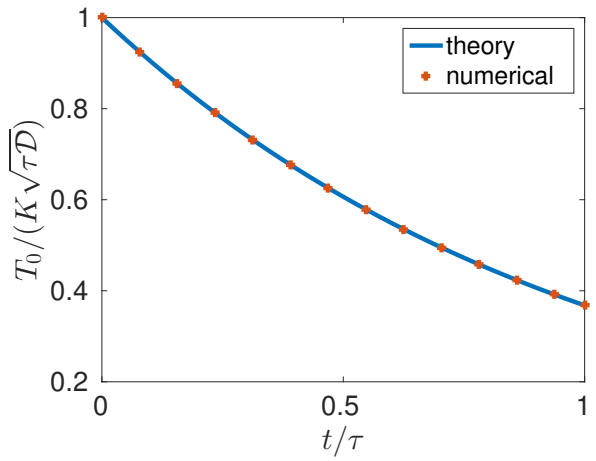

(b)

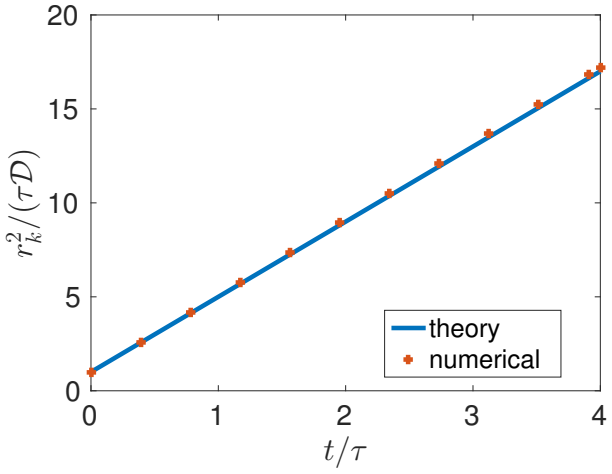

(c)

FIG. 4.2: Numerical solution of simple diffusion equation. In **(a)** the projection of the numerical solution to the x_1 and x_2 axis are shown, respectively. The corresponding integral T_0 is presented in Panel **(b)**, whereas the width is plotted in Panel **(c)**. Note, that due to the isotropy the widths in both directions coincide. As one can see, the agreement between theory and numerics is reasonable.

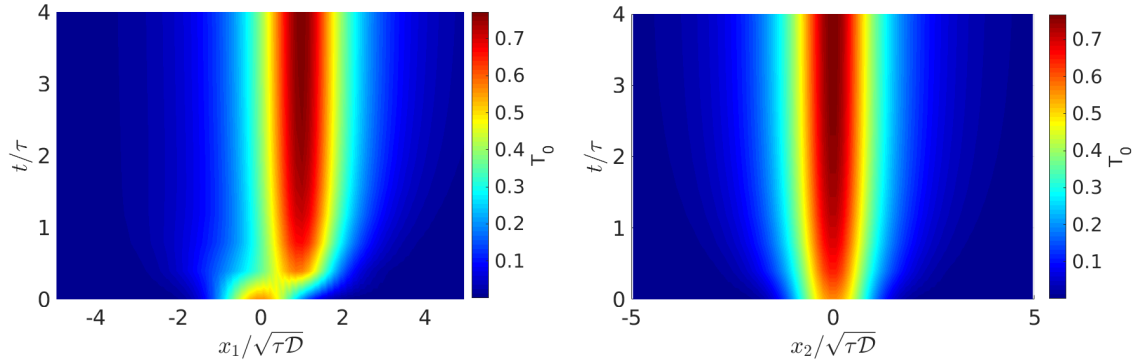

(a)

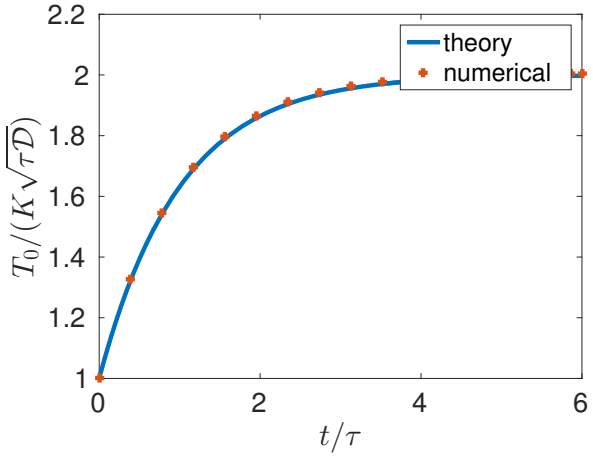

(b)

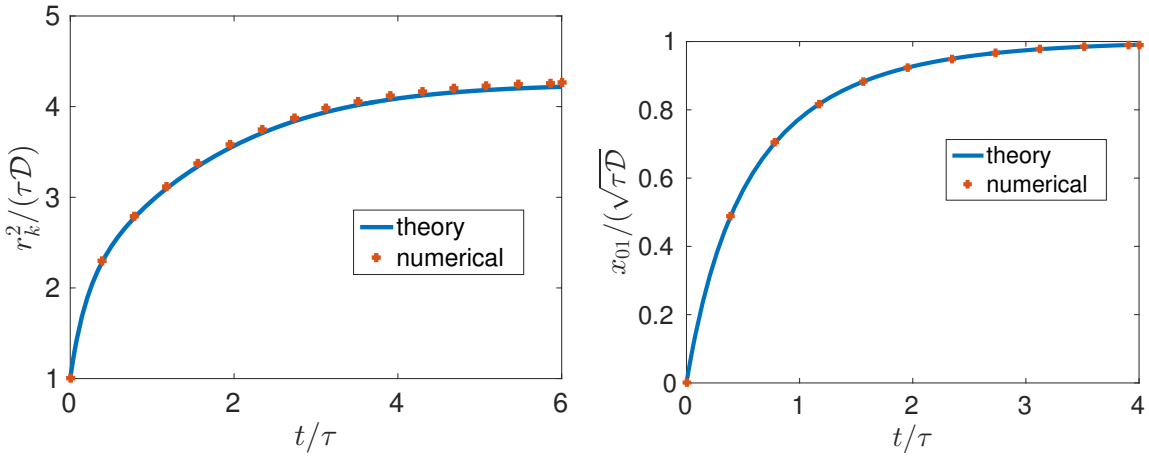

(c)

FIG. 4.3: Numerical solution of diffusion equation with external source that is located at $(x_{01}, x_{02}) = (1, 0)$ with amplitude $N = 2$ and with $q_{01} = q_{02} = 0.5$. In **(a)** the projection of the numerical solution to the x_1 and x_2 axis are shown, respectively. The corresponding integral T_0 is presented in panel **(b)**, whereas the square of the width r_k^2 and the centre-of-mass coordinate x_{01} are plotted in Panel **(c)**. As one can see, the agreement between theory and numerics is reasonable. In Panels **(b)** and **(c)** the crosses mark the numerical solution of the system.

by averaging the open-dissipative Gross-Pitaevskii equation (4.1b) with certain weights. How this procedure works for a closed Gross-Pitaevskii equation is developed in Appendix C in detail. There, it is also shown that our analytic approach, which is also applicable to open-dissipative systems, is equivalent to the usual variational approach, that can only be used for closed systems.

We start by calculating the centre-of-mass equation. For this purpose we multiply (4.1b) by $x_k - x_{0k}$ and integrate:

$$\begin{aligned} i\hbar \int d^2x\ (x_k - x_{0k})\psi^* \partial_t \psi = &-\frac{\hbar^2}{2m}\int d^2x\ (x_k - x_{0k})\psi^* \nabla\psi + \frac{m\Omega^2}{2}\int d^2x\ (x_k - x_{0k})\mathbf{x}^2|\psi|^2 \\ &+ g_T \int d^2x\ (x_k - x_{0k})T|\psi|^2 + g_k \int d^2x\ (x_k - x_{0k})|\psi|^4 + \frac{i\hbar}{2}\left[\aleph \int d^2x\ (x_k - x_{0k})p|\psi|^2 \right. \\ &\left. +2\aleph\frac{\partial n}{n_0 \partial T}\int d^2x\ (x_k - x_{0k})pT|\psi|^2 + 2\frac{\partial n}{n_0 \partial T}\Gamma \int d^2x\ (x_k - x_{0k})T|\psi|^2\right]. \end{aligned} \tag{4.15}$$

Performing the integrals yields the following complex differential equation for x_{0k} and C_{0k}

$$\begin{aligned} i\hbar\frac{\partial_t x_{0k}}{2} + \hbar A_k q_k^2 \partial_t x_{0k} - \frac{\hbar q_k^2}{2}\partial_t C_k =& \frac{\hbar^2}{2m}\left(iC_k + 2A_k C_k q_k^2\right) + \frac{m\Omega^2}{2}x_{0k}q_k^2 \\ &+ g_T T_0 G_{\mathrm{T}\psi}\frac{(x_{0k} - y_{0k})q_k^2}{q_k^2 + r_k^2} + \frac{i\hbar}{2}R_k q_k^2, \end{aligned} \tag{4.16}$$

where we defined

$$\begin{aligned} R_k = &-\aleph P_0 G_{\mathrm{P}\psi}\frac{x_{0k}}{q_k^2 + r_k^2} + 2\aleph\frac{\partial n}{n_0 \partial T}P_0 T_0 G_{\mathrm{TP}\psi}\frac{(y_{0k} - x_{0k})s^2 - x_{0k}r_k^2}{r_k^2 q_k^2 + q_k^2 s^2 + s^2 r_k^2} \\ &+ 2\frac{\partial n}{n_0 \partial T}\Gamma T_0 G_{\mathrm{T}\psi}\frac{(y_{0k} - x_{0k})}{r_k^2 + q_k^2}. \end{aligned} \tag{4.17}$$

The momentum C_k of the ansatz (4.3) is determined by the imaginary part of (4.16) to

$$C_k = \frac{m}{\hbar}\left(\partial_t x_{0k} + R_k q_k^2\right). \tag{4.18}$$

Finally, by inserting (4.18) into (4.16) we arrive at a second order differential equation for the centre-of-mass coordinate:

$$\partial_t^2 x_{0k} = \partial_t(R_k q_k^2) - \frac{2\hbar}{m}A_k R_k - \Omega^2 x_{0k} - 2\frac{g_T}{m}T_0 G_{\mathrm{T}\psi}\frac{y_{0k} - x_{0k}}{q_k^2 + r_k^2}. \tag{4.19}$$

In comparison to a particle-particle interaction that is local in space and time we find here an interaction dependent contribution to the oscillation frequency violating the Kohn theorem, compare to (C.11) in Appendix C.1.3. Moreover, compared to a closed system we observe the pump terms, here collected under the notation R_k, occurring in the result for C_k yielding an additional damping and also a frequency shift.

The equation governing the evolution of the width is calculated in the same manner. Equation

(4.1b) gets weighted by $(x_k - x_{0k})^2 - q_k^2/2$ and afterwards integrated:

$$\begin{aligned} i\hbar \int d^2x \ \left[(x_k - x_{0k})^2 - \frac{q_k^2}{2}\right] \psi^* \partial_t \psi &= -\frac{\hbar^2}{2m} \int d^2x \ \left[(x_k - x_{0k})^2 - \frac{q_k^2}{2}\right] \psi^* \nabla \psi \\ &+ \frac{m\Omega^2}{2} \int d^2x \ \left[(x_k - x_{0k})^2 - \frac{q_k^2}{2}\right] \mathbf{x}^2 |\psi|^2 + g_T \int d^2x \ \left[(x_k - x_{0k})^2 - \frac{q_k^2}{2}\right] T|\psi|^2 \\ &+ g_k \int d^2x \ \left[(x_k - x_{0k})^2 - \frac{q_k^2}{2}\right] |\psi|^4 \\ &+ \frac{i\hbar}{2} \left\{ \aleph \int d^2x \ \left[(x_k - x_{0k})^2 - \frac{q_k^2}{2}\right] p|\psi|^2 + 2\aleph \frac{\partial n}{\partial T} \int d^2x \ \left[(x_k - x_{0k})^2 - \frac{q_k^2}{2}\right] pT|\psi|^2 \right. \\ &\left. + 2\frac{\partial n}{n_0 \partial T} \Gamma \int d^2x \ \left[(x_k - x_{0k})^2 - \frac{q_k^2}{2}\right] T|\psi|^2 \right\}. \end{aligned} \tag{4.20}$$

After performing the integrals (4.20) takes the form

$$\begin{aligned} i\hbar \frac{q_k \partial_t q_k}{2} + \hbar \frac{q_k^4 \partial_t A_k}{2} &= \frac{\hbar^2}{2m} \left(-\frac{1}{2} - 2iA_k q_k^2 + 2A_k^2 q_k^4 \right) + \frac{m\Omega^2}{4} q_k^4 \\ &+ g_T T_0 G_{\mathrm{T}\psi} \left[\frac{(y_{0k} - x_{0k})^2 q_k^4}{(p_k^2 + q_k^2)^2} - \frac{q_k^4}{2(q_k^2 + p_k^2)} \right] - g_K \frac{N q_k^2}{8\pi q_1 q_2} + \frac{i\hbar}{2} I_k q_k^4. \end{aligned} \tag{4.21}$$

Here, the pump influence is given by

$$\begin{aligned} I_k =& \aleph P_0 G_{\mathrm{P}\psi} \left[\frac{x_{0k}^2}{(s_k^2 + q_k^2)^2} - \frac{1}{2(s_k^2 + q_k^2)} \right] + 2\frac{\partial n}{n_0 \partial T} \Gamma T_0 G_{\mathrm{T}\psi} \left[\frac{(y_{0k} - x_{0k})^2}{(r_k^2 + q_k^2)^2} - \frac{1}{2(r_k^2 + q_k^2)} \right] \\ &+ 2\aleph \frac{\partial n}{n_0 \partial T} P_0 T_0 G_{\mathrm{TP}\psi} \left[\left(\frac{(x_{0k} - y_{0k}) s^2 + x_{0k} r_k^2}{q_k^2 r_k^2 + r_k^2 s^2 + q_k^2 s^2} \right)^2 - \frac{(r_k^2 + s^2)}{2(q_k^2 r_k^2 + r_k^2 s_k^2 + q_k^2 s^2)} \right]. \end{aligned} \tag{4.22}$$

The imaginary part of (4.21) yields

$$A_k = -\frac{m}{2\hbar} \left(\frac{\partial_t q_k}{q_k} - I_k q_k^2 \right). \tag{4.23}$$

Inserting (4.23) into the real part of (4.21) leads to an equation of motion for the widths q_k

$$\begin{aligned} \partial_t^2 q_k =& q_k \partial_t (I q_k^2) + \frac{\hbar^2}{m^2 q_k^3} - I^2 q_k^5 + 2\dot{q}_k q_k^2 I - \Omega^2 q_k \\ &- \frac{4g_T}{m} T_0 G_{\mathrm{T}\psi} \left[\frac{(y_{0k} - x_{0k})^2 q_k}{(r_k^2 + q_k^2)^2} - \frac{q_k}{2(q_k^2 + r_k^2)} \right] + \frac{g_K N}{2\pi m} \frac{1}{q_1 q_2 q_k}. \end{aligned} \tag{4.24}$$

We have now all the equations together that determine the dynamics of the two Gaussian functions (4.3) and (4.4). In order to gain an overview we collect the equations that describe

the evolution of the variational parameters in the following

$$\partial_t T_0 = -\frac{T_0}{\tau} + BN, \tag{4.25a}$$

$$\partial_t y_{0k} = \frac{BN}{T_0}(x_{0k} - y_{0k}), \tag{4.25b}$$

$$\partial_t r_k^2 = 4\mathcal{D} + \frac{BN}{T_0}(q_k^2 - r_k^2) + 2\frac{BN}{T_0}(y_{0k} - x_{0k})^2, \tag{4.25c}$$

$$\partial_t N = \aleph P_0 N G_{\mathrm{P}\psi} + 2\aleph \frac{\partial n}{\partial T} T_0 N P_0 G_{\mathrm{TP}\psi} - \Gamma N + 2\Gamma \frac{\partial n}{\partial T} T_0 N G_{\mathrm{T}\psi}, \tag{4.25d}$$

$$\partial_t^2 x_{0k} = \partial_t(R_k q_k^2) - \frac{2\hbar}{m} A_k R_k - \Omega^2 x_{0k} - 2\frac{g_T}{m} T_0 G_{\mathrm{T}\psi} \frac{y_{0k} - x_{0k}}{q_k^2 + r_k^2}, \tag{4.25e}$$

$$\begin{aligned}\partial_t^2 q_k =& q_k \partial_t(I_k q_k^2) + \frac{\hbar^2}{m^2 q_k^3} - I_k^2 q_k^5 + 2\dot{q}_k q_k^2 I - \Omega^2 q_k \\ &- \frac{4g_T}{m} T_0 G_{\mathrm{T}\psi} \left[\frac{(y_{0k} - x_{0k})^2 q_k}{(r_k^2 + q_k^2)^2} - \frac{q_k}{2(q_k^2 + r_k^2)} \right] + \frac{g_K N}{2\pi m} \frac{1}{q_1 q_2 q_k},\end{aligned} \tag{4.25f}$$

together with the pump influences (4.17) and (4.22). Note that, whereas the equations governing the evolution of the temperature are differential equations of first order, the corresponding equations for the photon wave function are of second order. This relates to the difference between diffusive and quantum dynamics, i.e. the first one cannot oscillate, while the latter is intrinsically oscillating. In the following we are interested in the stability of the steady state of the condensate described by the set of equations (4.25).

4.4. Steady State

At first the steady state is studied in detail. According to (4.25b) the centre-of-mass coordinates of the temperature and the photon wave function coincide in the steady state, i.e.

$$y_{0k} = x_{0k}, \ k = 1, 2. \tag{4.26}$$

Inserting this in (4.25e) yields these equilibria to be centred around the origin

$$x_{0k} = 0 = y_{0k}, \ k = 1, 2. \tag{4.27}$$

Subsequently, we obtain from (4.25d) the steady state temperature amplitude

$$T_0^0 = \frac{\Gamma - \aleph P_0 G_{\mathrm{P}\psi}^0}{2\frac{\partial n}{n_0 \partial T}(\aleph G_{\mathrm{TP}\psi}^0 + \Gamma G_{\mathrm{T}\psi}^0)} \tag{4.28}$$

determining via (4.25a) the photon number

$$N_0 = \frac{T_0^0}{\tau B}. \tag{4.29}$$

Here we denoted the steady state values of the Gaussian weights with the upper index 0. From (4.8) together with (4.27) those weights are calculated to be

$$G^0_{\mathrm{P}\psi} = \frac{1}{\pi(q_0^2 + s^2)}, \tag{4.30}$$

$$G^0_{\mathrm{T}\psi} = \frac{1}{\pi(q_0^2 + r_0^2)}, \tag{4.31}$$

$$G^0_{\mathrm{TP}\psi} = \frac{1}{\pi^2(r_0^2 q_0^2 + q_0^2 s^2 + s^2 r_0^2)}. \tag{4.32}$$

Combining (4.28) with (4.29) yields the equilibrium photon number

$$N_0 = \frac{\Gamma - \aleph P_0 G^0_{\mathrm{P}\psi}}{2\tau B \frac{\partial n}{n_0 \partial T}(\aleph G^0_{\mathrm{TP}\psi} + \Gamma G^0_{\mathrm{T}\psi})}. \tag{4.33}$$

Thus, the critical pump power P_0^{crit} is given by

$$P_0^{\mathrm{crit}} = \frac{\Gamma}{\aleph G^0_{\mathrm{P}\psi}}. \tag{4.34}$$

From (4.25c) we read off

$$r_0^2 = 4\mathcal{D}\tau + q_0^2. \tag{4.35}$$

Thus, the equilibrium temperature width is determined on the one hand by the photon width q_0 and on the other hand by the diffusion process that happens during the relaxation time τ. The steady state equation for the photon width q_0 is, thus, described by

$$0 = \frac{\hbar^2}{m^2 q_0^4} - q_0^4 I_0^2 - \Omega^2 + \frac{g_T \tau B N_0}{\pi m} \frac{1}{(2q_0^2 + 4\mathcal{D}\tau)^2} + \frac{g_K N_0}{2\pi m} \frac{1}{q_0^4}, \tag{4.36}$$

as can be seen from (4.25f). Here the pumping influence is described by the term $-q_0^4 I_0^2$, where

$$I_0 = -\frac{\aleph P_0}{\pi(s^2 + q_0^2)^2} - \frac{\frac{\partial n}{n_0 \partial T}\Gamma T_0^0}{\pi(2q_0^2 + 4\mathcal{D}\tau)^2} - \frac{\aleph \frac{\partial n}{n_0 \partial T} P_0 T_0^0 (q_0^2 + 4\mathcal{D}\tau + s^2)}{\pi^2[(q_0^2 + s^2)(q_0^2 + 4\mathcal{D}\tau) + q_0^2 s^2]^2} \tag{4.37}$$

following from (4.22). The length scale of this equation is set by the harmonic oscillator length $l_{\mathrm{osc}} = \sqrt{\hbar/(m\Omega)} = 7.69\,\mu\mathrm{m}$, as can bee seen by dividing by the trap frequency. In the course of this, we obtain

$$0 = \frac{l_{\mathrm{osc}}}{q_0^4} - \frac{q_0^4 I_0^2}{\Omega^2} - 1 + \frac{2\tilde{g}_T N_0 l_{\mathrm{osc}}^4}{\pi(2q_0^2 + 4\mathcal{D}\tau)^2} + \frac{\tilde{g}_K N_0 l_{\mathrm{osc}}^4}{2\pi \tilde{q}_0^4}, \tag{4.38}$$

with the dimensionless interaction constants according to (3.20) and (3.21).

4.4.1. Small Pumping

As the pump enters the steady state equation (4.36) and (4.38) quadratically, we will at first neglect this influence on the BEC width. Therefore, we consider the photon number as an externally fixed parameter. In this case (4.38) simplifies to

$$0 = \frac{1}{q_0^4} - \frac{1}{l_{\mathrm{osc}}^4} + \frac{2\tilde{g}_T N_0}{\pi(2q_0^2 + 4\mathcal{D}\tau)^2} + \frac{\tilde{g}_K N_0}{2\pi q_0^4}. \tag{4.39}$$

In case of vanishing diffusion, i.e. $\mathcal{D} = 0$, equation (4.36) is analytically solvable

$$q_0 = l_{\mathrm{osc}} \left(1 + \frac{\tilde{g} N_0}{2\pi}\right)^{1/4}, \tag{4.40}$$

where $\tilde{g} = \tilde{g}_T + \tilde{g}_K$ is the total photon-photon interaction strength.
Formula (4.40) is exactly what one suspects if only an instantaneous and local interaction acts between the photons, as a temporal retardation can not have any influence on a steady state in time.

For small diffusion constants we can expand the thermo-optic term up to first order in the diffusion constant and obtain

$$\frac{\tilde{g}_T N_0}{\pi(2q_0^2 + 4\mathcal{D}\tau)^2} \approx \frac{\tilde{g}_T N_0}{2\pi q_0^4} \left(1 - \frac{2\mathcal{D}\tau}{q_0^2}\right). \tag{4.41}$$

Thus, the thermo-optic interaction decreases as the diffusion constant increases. But this has now an influence upon the measurement. According to [53] Equation (4.40) is used to obtain the effective photon-photon interaction strength from the measurement of the condensate width in dependence on the photon number. Therefore, (4.41) shows that a systematic error of the order

$$\frac{\mathcal{D}\tau}{l_{\mathrm{osc}}^2} = 3.9 \times 10^{-3} \tag{4.42}$$

is involved in the analysis of the experimental data. However, in the current experiments done with Ethylene Glycol as a solvent, this error is only of the order of a per mille.

This behaviour can also be seen in the limit $\mathcal{D} \to \infty$ that corresponds according to (4.35) to the limit $r_0 \to \infty$. In this case the part of equation (4.36), that incorporates the thermo-optic interaction vanishes and, thus, no such interaction is present any more. The physical origin is that with increasing diffusion constant the temperature produced by the photons is directly carried away and cannot contribute to a local change of the index of refraction. Conclusively, the diffusion has a suppressing influence on the thermo-optic interaction. Thus, the case of vanishing diffusion has the largest interaction, whereas the case of dominating diffusion has the smallest interaction.

The numerical solution of (4.39) for arbitrary diffusion is shown in Figure 4.4. As the width of the BEC is an indicator for the interaction influence, one can conclude that for increasing diffusion constant the interaction gets, indeed, smaller as described above, since the BEC width at given photon number decreases with increasing diffusion constant. On the other hand, the

temperature width r_0 grows for increasing diffusion constant, meaning the absorbed photon energy is carried away. In order to quantify this further, the data for the larger diffusion values are fitted to the function

$$\left(\frac{q_0}{l_{\mathrm{osc}}}\right)^{\mathrm{fit}} = \left(1 + \frac{N\tilde{g}}{2\pi}\right)^{b}, \tag{4.43}$$

where $\tilde{g}$ and b are treated as fit parameters. The resulting parameters are shown in Figure 4.5. In panel (a) of this Figure the deviation from the fit to the numerical data is plotted. The agreement between data and fit is still reasonable, as the deviation is in the order 10^{-5}. The corresponding fit parameters are illustrated in panel (b). For growing diffusion the fitted interaction constant $\tilde{g}$ tends to decrease, whereas the exponent b gets larger. Thus, those findings support the explanation, that for rising diffusion constant the thermo-optic interaction reduces as the spread of the interaction energy enlarges in this scenario.

4.4.2. Homogeneous Pumping

We specify now to the case of homogeneous pumping. To this end the pump width s is considered to be of the order of the cavity radius, thus, it outweighs all the other length scales. In particular $s \gg q_k$ as well as $s \gg r_k$ hold. The pump strength is in this case stated in terms of the corresponding density

$$\mathcal{P} = \frac{P_0}{A_{\mathrm{cav}}}, \tag{4.44}$$

where $A_{\mathrm{cav}} = \pi s^2$ is the cavity surface. Within this limit the Gaussian weights (4.8) simplify to

$$G_{\mathrm{P}\psi} \approx \frac{1}{\pi s^2}, \tag{4.45a}$$

$$G_{\mathrm{T}\psi} = \frac{\exp\left[-\sum\limits_{j=1,2} \frac{(x_{0j}-y_{0j})^2}{r_j^2+q_j^2}\right]}{\pi\sqrt{(q_1^2+r_1^2)(q_2^2+r_2^2)}}, \tag{4.45b}$$

$$G_{\mathrm{TP}\psi} \approx \frac{1}{\pi s^2} G_{\mathrm{T}\psi}. \tag{4.45c}$$

Thus, the photon number (4.33) is in this limit given by

$$N_0 \approx \frac{\Gamma - \aleph\mathcal{P}}{\tau B \frac{\partial n}{n_0 \partial T}\left(2\aleph\mathcal{P} + \Gamma\right) G^0_{\mathrm{T}\psi}} \tag{4.46}$$

and by using (4.31) thus can be written as

$$N_0 = \frac{(\Gamma - \aleph\mathcal{P})\pi(2q_0^2 + 4\mathcal{D}\tau)}{\tau B \frac{\partial n}{n_0 \partial T}\left(2\aleph\mathcal{P} + \Gamma\right)}. \tag{4.47}$$

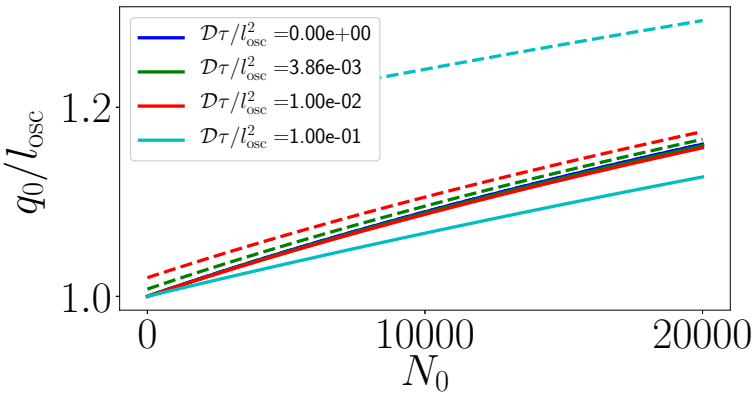

FIG. 4.4: Steady state width according to (4.39) and (4.25c). The parameters are taken from Appendix D. The diffusion parameter $\mathcal{D}\tau/l^2_{\rm osc}$ is varied and the value $\mathcal{D}\tau/l^2_{\rm osc} = 3.86 \times 10^{-3}$ corresponds to the experimental case. The solid lines indicate the width of the BEC, whereas the dashed lines indicate the temperature width.

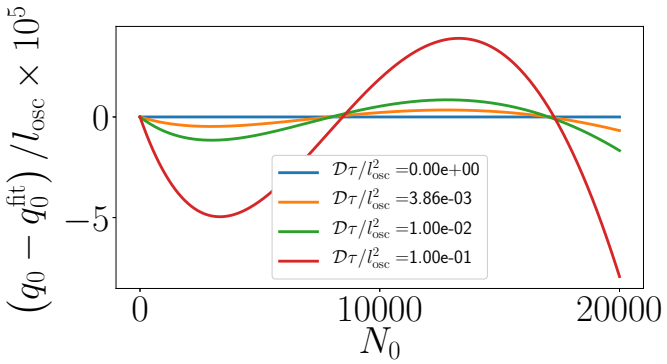

(a)

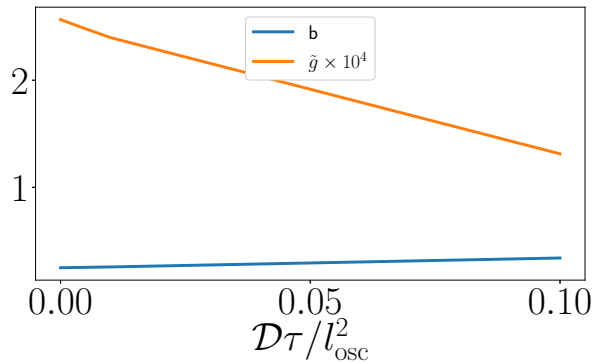

(b)

FIG. 4.5: Results of fits of the data shown in Figure 4.4 to the formula $q_0^{\rm fit} = [1 + \tilde{g}N_0/(2\pi)]^b$, where $\tilde{g}$ and b are treated as fit parameters, for different diffusion constants. In **(a)** the deviation from the numerically calculated data q_0 to the fitted values $q_0^{\rm fit}$ is plotted. Panel **(b)** shows the corresponding fit parameters in dependence on the diffusion constant $\mathcal{D}\tau/l^2_{\rm osc}$.

Therefore, the critical pump power (4.34) is given by

$$\mathcal{P}_{\mathrm{crit}} = \frac{\Gamma}{\aleph}. \tag{4.48}$$

Moreover, the photon number does explicitly depend on both the BEC width q_0 and the temperature width r_0. Thus, in case of dominating diffusion, i.e. $\mathcal{D} \to \infty$ also the photon number grows to infinite large values as in this case, as in the Subsection above, $q_0 \to l_{\mathrm{osc}}$ and $r_0 \to \infty$. Therefore, it follows already from here, that in the case of homogeneous pump the temperature diffusion has a higher influence in comparison to the case of vanishing pump.
The influence of the pump upon the width I_k, see (4.22), simplifies to

$$I_k \approx 2\frac{\partial n}{n_0 \partial T} T_0 G_{\mathrm{T}\psi} \left[\frac{(y_{0k} - x_{0k})^2}{(r_k^2 + q_k^2)^2} - \frac{1}{2(r_k^2 + q_k^2)} \right] (\Gamma + 2\aleph\mathcal{P}) \tag{4.49}$$

amounting to the equilibrium value

$$I_0 \approx -\frac{\partial n}{n_0 \partial T} \tau B N_0 \frac{G^0_{\mathrm{T}\psi}}{2(q_0^2 + 2\mathcal{D}\tau)} (\Gamma + 2\aleph\mathcal{P}), \tag{4.50}$$

where (4.29) is used. As the term proportional to I_0^2 contributes via a minus sign to the condensate width, we see that the pump leads to a focusing of the condensate. Moreover, this influence is small, since I_0 is proportional to $\frac{\partial n}{\partial T}$. Since this pump term contributes quadratically to the condensate width, it can be neglected. Thus, (4.38) can be simplified to

$$0 = \frac{1}{q_0^4} - \frac{1}{l_{\mathrm{osc}}^4} + \frac{2\tilde{g}_T N_0}{\pi(2q_0^2 + \mathcal{D}\tau)^2} + \frac{\tilde{g}_K N_0}{2\pi q_0^4}. \tag{4.51}$$

Therefore, the steady state is described by equations (4.47) and (4.51). In case of vanishing diffusion, this system can be solved perturbatively. In this case the widths of the condensate and the temperature coincide. Therefore, the condensate width is given by

$$q_0 = \left(1 + \frac{N_0 \tilde{g}}{2\pi}\right)^{1/4}, \tag{4.52}$$

where $\tilde{g} = \tilde{g}_T + \tilde{g}_K$ is the total interaction strength. As the interaction in the system is small, this can be approximated by

$$q_0 \approx 1 + \frac{N_0 \tilde{g}}{8\pi}. \tag{4.53}$$

Inserting this into (4.47) yields

$$N_0 \approx N_0^0 \left(1 + \frac{N_0^0 \tilde{g}}{8\pi}\right), \tag{4.54}$$

where the photon number in the noninteracting case is given by

$$N_0^0 = \frac{2\pi l_{\mathrm{osc}}^2 (\Gamma - \aleph\mathcal{P})}{\left[\tau B \frac{\partial n}{n_0 \partial T} (2\aleph\mathcal{P} + \Gamma)\right]}. \tag{4.55}$$

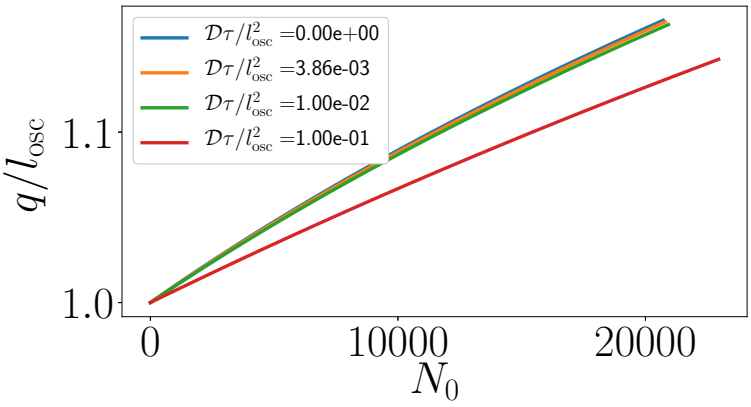

FIG. 4.6: Steady state of the homogeneously pumped system as described by (4.47) and (4.38) for different diffusion strengths $\mathcal{D}\tau$. The remaining parameters are taken from Appendix D. The value $\mathcal{D}\tau/l^2_{\rm osc} = 3.86 \times 10^{-3}$ corresponds to the experimental case.

Thus, the photon number increases with increasing interaction strength $\tilde{g}$.
The numerical solution of this system for arbitrary diffusion constants is shown in Figure 4.6. It can be seen, that, indeed, with increasing diffusion the photon number increases, whereas the effective interaction decreases, as it is discussed above.

4.4.3. Focused Pumping

In the following we consider the opposite extremal case. The pump spot width is now assumed to be smaller than the remaining length scales. It holds now especially $s \ll q_0$. Therefore, the Gaussian weights (4.8) simplify to

$$G^0_{\mathrm{P}\psi} \approx \frac{1}{\pi q_0^2}, \tag{4.56}$$

$$G^0_{\mathrm{T}\psi} \approx \frac{1}{\pi(2q_0^2 + 4\mathcal{D}\tau)}, \tag{4.57}$$

$$G^0_{\mathrm{TP}\psi} \approx \frac{1}{\pi(q_0^2 + 4\mathcal{D}\tau)} G^0_{\mathrm{P}\psi}. \tag{4.58}$$

Thus, as in the preceding Section the scale of the pump width determined the system parameters, q_0 determines them in the present case. Accordingly, the photon number is in this extremal case given by

$$N_0 \approx \frac{\Gamma - \aleph P_0/(\pi q_0^2)}{\tau B \frac{\partial n}{n_0 \partial T}\left(2\frac{\aleph P_0}{\pi^2 q_0^4} - \frac{\Gamma}{2\pi q_0^2}\right)}, \tag{4.59}$$

where the criticality condition takes now the form

$$P_0^{\mathrm{crit}} \approx \frac{\Gamma \pi q_0^2}{\aleph}. \tag{4.60}$$

The pump influence in the steady state is according to (4.22)

$$I_0 \approx -\frac{\aleph P_0}{\pi q_0^4} - \frac{\partial n}{\partial T}\left[\frac{\Gamma}{2\pi(2q_0^2+4\mathcal{D}\tau)^2} - \frac{\aleph P_0 T_0}{2\pi^2 q_0^4(q_0^2+4\mathcal{D}\tau)}\right]. \tag{4.61}$$

In contrast to the case of homogeneous pumping, in (4.61) is now a term that does not incorporate the thermo-optic coefficient $\frac{\partial n}{n_0 \partial T}$. Thus, the square of (4.61) is approximately given by

$$I_0^2 \approx \left(\frac{\aleph P_0}{\pi q_0^4}\right)^2. \tag{4.62}$$

That means that the pump has indeed a reducing influence upon the condensate width q_0 in the case of a very small pump spot, as can be seen from the special case of (4.38):

$$0 = \frac{1}{q_0^4} - \left(\frac{\aleph P_0}{\pi\Omega}\right)^2 \frac{1}{q_0^4} - \frac{1}{l_{\mathrm{osc}}^4} + \frac{2\tilde{g}_T N_0}{\pi(2q_0^2+4\mathcal{D}\tau)^2} + \frac{\tilde{g}_K N_0}{2\pi q_0^4}. \tag{4.63}$$

In case of a vanishing diffusion constant this equation can again be solved for q_0 leading to

$$q_0 = l_{\mathrm{osc}}\left[1 + \frac{\tilde{g}N_0}{2\pi} - \left(\frac{\aleph P_0}{\pi\Omega}\right)^2\right]^{1/4}. \tag{4.64}$$

As the steady state is now studied in great detail, light shall be shed in the following on its stability. For this purpose the modes announced in Figure 4.1 are in the following discussed. As the focus only lies on the intracondensate interaction the experimental relevant case is the one of homogeneous pumping [52]. Otherwise also the pump laser would induce an increase of the condensate width.

4.5. Dipole Mode

At first, attention is paid towards the motion of the centre-of-mass of the condensate in the harmonic trapping potential. As in the steady state the centres-of-mass of the temperature and the photon-wave function are centred around the origin according to (4.26) and (4.27), we consider now small deviations from this equilibrium and write

$$x_{0k}(t) = \delta x_{0k}(t) \tag{4.65a}$$

as well as

$$y_{0k}(t) = \delta y_{0k}(t). \tag{4.65b}$$

As first we find from (4.25b)

$$\partial_t \delta y_{0k} = \frac{\delta x_{0k} - \delta y_{0k}}{\tau}, \tag{4.66}$$

where we used (4.29). The linearised version of (4.25e) is directly given by

$$\partial_t^2 \delta x_{0k} + \Omega^2 \delta x_{0k} = q_0^2 \partial_t(\delta R) - I_0 q_0^2 \delta R - 2\frac{\hbar^2 \tilde{g}_T}{m^2} \frac{\delta y_{0k} - \delta x_{0k}}{\pi (q_0^2 + r_0^2)^2}, \tag{4.67}$$

with the pump influence

$$\delta R \approx K N_0 \left(\delta y_{0k} - \delta x_{0k}\right). \tag{4.68}$$

The prefactor K is defined as

$$K = 2\frac{\partial n}{n_0 \partial T} \frac{\tau B}{\pi (2q_0^2 + 4\mathcal{D}\tau)^2} \left(\aleph \mathcal{P} + \Gamma\right) \tag{4.69}$$

and the time derivative of δR is given by

$$\partial_t \delta R = K \left[\frac{\delta x_{0k} - \delta y_{0k}}{\tau} - \dot{\delta x}_{0k}\right] \tag{4.70}$$

where (4.67) is used.
By introducing the perturbation vector

$$\mathbf{v} = \begin{pmatrix} \delta y_{0k} \\ \delta x_{0k} \\ \dot{\delta x}_{0k} \end{pmatrix} \tag{4.71}$$

the system of linear differential equations reads

$$\partial_t \mathbf{v} = S_{\text{dipol}} \mathbf{v}, \tag{4.72}$$

with the system matrix

$$S_{\text{dipol}} = \begin{pmatrix} -1/\tau & 1/\tau & 0 \\ 0 & 0 & 1 \\ -\frac{q_0^2 K N_0}{\tau} + \left(\frac{K N_0}{2}\right)^2 - L N_0 & \frac{q_0^2 K N_0}{\tau} - \left(\frac{K N_0}{2}\right)^2 + L N_0 - \Omega^2 & -q_0^2 K N_0 \end{pmatrix}. \tag{4.73}$$

Here, the thermo-optic interaction is described by the parameter

$$L = \frac{2\tilde{g}_T \hbar^2}{\pi m^2 (2q_0^2 + 4\mathcal{D}\tau)^2}. \tag{4.74}$$

With the ansatz

$$\mathbf{v}(t) = \mathbf{v}_0 e^{-i\omega t} \tag{4.75}$$

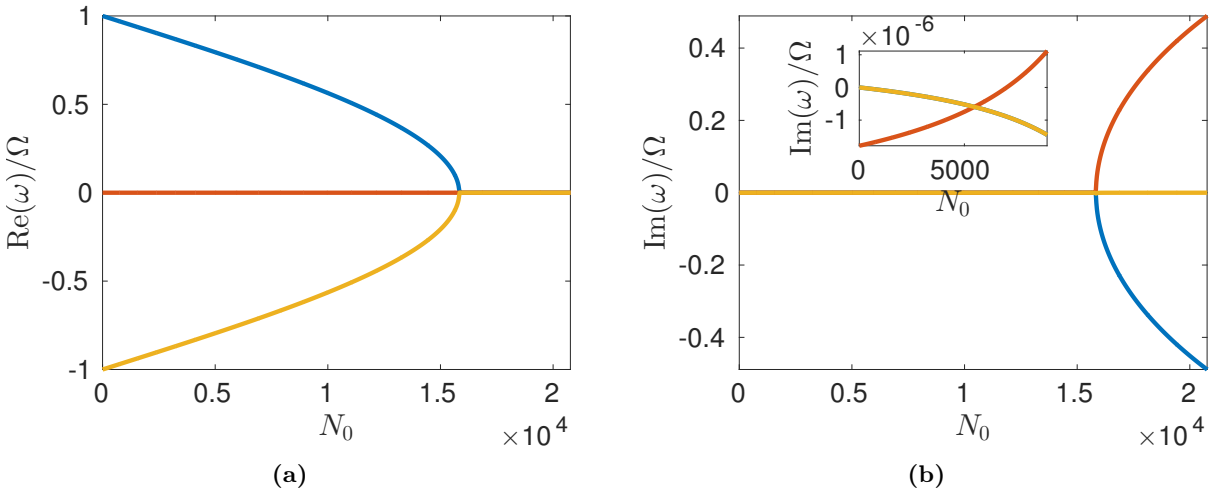

FIG. 4.7: Dipole mode frequencies as described by (4.76) together with (4.73). In **(a)** the oscillation frequencies are shown, whereas in **(b)** the corresponding damping frequencies are plotted. The inlet shows the damping frequencies for smaller photon numbers.

the oscillation frequency is determined by the equation

$$\det\left(S + i\omega \mathbb{1}_{3\times 3}\right) = 0. \tag{4.76}$$

The numerically calculated solutions of (4.76) are shown in Figure 4.7. In panel (a) the oscillation frequencies are plotted. Obviously, the Kohn theorem is broken due to the temporally retarded interaction. Moreover, the Kohn theorem is not only broken, but the dipole mode frequency also vanishes for a certain photon number N_0^{crit}, meaning this mode can only be excited for photon numbers smaller than N_0^{crit}. On the other hand in panel (b) the damping frequencies are shown. For photon numbers smaller than N_0^{stab} the dipole mode is stable and nearly undamped. If the photon number gets larger, the dipole mode is slightly unstable. But the damping rate stays in the order of $1 \times 10^{-6}\Omega \sim 1 \times 10^{-4}\,\mathrm{Hz}$, on the other hand the BEC lifetime is in the order of about $1 \times 10^{-7}\,\mathrm{s}$. Therefore, the instability occurs on a much slower time scale than the lifetime of the condensate. As the photon number exceeds N_0^{crit} the dipole mode gets highly unstable. One can interpret this behaviour as the condensate scatters with the potential that occurs due to the thermo-optic effect and decays only slowly in time. At some point this potential might be large enough to prevent the condensate from oscillating.

4.6. Breathing- and Quadrupole Mode

We focus now on the dynamics of the widths. As one can already see in (4.25c) and (4.25f), these modes couple explicitly to the dynamics of the photon number N and the temperature T_0, since the steady state of the widths q_i and r_i does not vanish according to Section 4.4. Therefore, also equations (4.25a) and (4.25d) need to be taken into account in the following linearisation. Before proceeding it shall be noted, that also here we only consider the case of homogeneous

pumping. Due to this, (4.25d) simplifies to

$$\partial_t N \approx \left[\aleph\mathcal{P} - \Gamma + 2\frac{\partial n}{n_0 \partial T} G_{\mathrm{T}\psi}\left(\aleph\mathcal{P} + \Gamma\right)\right] N. \tag{4.77}$$

In the following small perturbations in the vicinity of the steady state are studied. For this purpose we assume, viz.,

$$T_0 = T_0^0(1 + \delta T), \tag{4.78a}$$
$$N = N_0(1 + \delta N), \tag{4.78b}$$
$$r_k = r_0(1 + \delta r_k), \tag{4.78c}$$
$$y_{0k} = \delta y_k, \tag{4.78d}$$
$$q_k = q_0(1 + \delta q_k), \tag{4.78e}$$
$$x_{0k} = \delta x_k, \tag{4.78f}$$

where the quantities with δ denote small perturbations of the steady state values. At first it is noted, that the temperature equation (4.25a) is already linear and it reads

$$\partial_t \delta T_0 = -\frac{\delta T_0}{\tau} + B\delta N. \tag{4.79}$$

With K from (4.69) the linearisation of the photon number equation (4.25d) reads

$$\partial_t \delta N \approx K\left[\delta T_0 + \delta N_0 - \frac{q_0^2(\delta q_1 + \delta q_2) - r_0^2(\delta r_1 + \delta r_2)}{q_0^2 + r_0^2}\right], \tag{4.80}$$

where r_0 is given by (4.35). The corresponding equation for the temperature width reads

$$\partial_t \delta r_k = -\frac{2\mathcal{D}}{q_0^2}(\delta N - \delta T_0) + \frac{1}{\tau}\left(\frac{1}{1 + 4\mathcal{D}\tau/q_0^2}\delta q_k + \delta r_k\right). \tag{4.81}$$

Finally the equation for the photon width reads

$$\begin{aligned}\partial_t^2 \delta q_k =& q_0^2 \dot{\delta I}_k + 4q_0^2 I_0 \dot{\delta q}_k - I_0 q_0^4(2\delta I_k + 5\delta q_k) - \frac{3\hbar^2}{m^2 q_0^4}\delta q_k \\ &- \Omega^2 \delta q_k + L\left[\delta T_0 + \delta q_k - \frac{q_0^2(\delta q_1 + \delta q_2 + 2\delta q_k) + r_0^2(\delta r_1 + \delta r_2 + 2\delta r_k)}{q_0^2 + r_0^2}\right] \\ &- \frac{\hbar^2 \tilde{g}_K N_0}{2\pi m^2 q_0^4}(\delta q_1 + \delta q_2 + \delta q_k).\end{aligned} \tag{4.82}$$

Here, δI_K is given by

$$\delta I_k = -\delta T_0 + \frac{q_0^2(\delta q_1 + \delta q_2 + 2\delta q_k) + r_0^2(\delta r_1 + \delta r_2 + 2\delta r_k)}{q_0^2 + r_0^2} \tag{4.83}$$

with corresponding time derivative

$$\dot{\delta I}_k = -\dot{\delta T}_0 + \frac{q_0^2(\dot{\delta q}_1 + \dot{\delta q}_2 + 2\dot{\delta q}_k) + r_0^2(\dot{\delta r}_1 + \dot{\delta r}_2 + 2\dot{\delta r}_k)}{q_0^2 + r_0^2}, \tag{4.84}$$

where the time derivatives of the temperature quantities δT_0 and δr_j are given by (4.79) and (4.81). With the notation $\delta\nu_i = (\delta r_i, \delta q_i, \dot{\delta q_i})^T$ these equations are summarised in vector matrix form:

$$\frac{d}{dt}\begin{pmatrix}\begin{pmatrix}\delta T_0\\ \delta N\end{pmatrix}\\ \delta\nu_1\\ \delta\nu_2\end{pmatrix} = \begin{pmatrix} C & E & E\\ F & J & M\\ F & M & J\end{pmatrix}\begin{pmatrix}\begin{pmatrix}\delta T_0\\ \delta N\end{pmatrix}\\ \delta\nu_1\\ \delta\nu_2\end{pmatrix}, \tag{4.85}$$

where the following matrices are defined. At first there are the matrices that couple the temperature and the photon number perturbations to the different degrees of freedom. Among those there is

$$C = \begin{pmatrix} -1/\tau & B\\ K & K\end{pmatrix} \tag{4.86}$$

coupling those two quantities to themselves. The matrix

$$E = \begin{pmatrix} 0 & 0 & 0\\ -K\dfrac{r_0^2}{q_0^2+r_0^2} & -K\dfrac{q_0^2}{q_0^2+r_0^2} & 0\end{pmatrix} \tag{4.87}$$

describes the coupling to the widths and finally

$$F = \begin{pmatrix} 2\mathcal{D}/q_0^2 & -2\mathcal{D}/q_0^2\\ 0 & 0\\ L + \dfrac{q_0^2 K N_0}{2}\left(\dfrac{1}{\tau} + \dfrac{8\mathcal{D}r_0^2}{q_0^2(q_0^2+r_0^2)}\right) + KN_0 & -\dfrac{q_0^2 K N_0}{2}\left(B + \dfrac{8\mathcal{D}r_0^2}{q_0^2(q_0^2+r_0^2)}\right)\end{pmatrix} \tag{4.88}$$

is responsible for the coupling of the widths to the temperature. The nonvanishing entries of the 3×3 matrix J connecting the entries of the vectors $\delta\nu_i$ to themselves are

$$J_{r,r} = \frac{1}{\tau}, \tag{4.89a}$$

$$J_{r,q} = \frac{1/\tau}{1 + 4\mathcal{D}\tau/q_0^2}, \tag{4.89b}$$

$$J_{q,\dot{q}} = 1, \tag{4.89c}$$

$$J_{\dot{q},r} = \frac{3q_0^2 r_0^2 K N_0}{2\tau(q_0^2 + r_0^2)} - \frac{3r_0^2 q_0^4 K N_0}{q_0^2 + r_0^2} - 3\frac{r_0^2 L}{q_0^2 + r_0^2}, \tag{4.89d}$$

$$\begin{aligned} J_{\dot{q},q} = {} & \frac{r_0^2 q_0^4 K N_0}{q_0^2 + r_0^2} \frac{3/\tau}{1 + 4\mathcal{D}\tau/q_0^2} + \frac{K N_0 q_0^4}{2}\left(\frac{6q_0^2}{q_0^2 + r_0^2} + 5\right) - 3\frac{\hbar^2}{m^2 q_0^4} \\ & - \Omega^2 + L\left(1 - \frac{3q_0^2}{q_0^2 + r_0^2}\right) - \frac{\hbar^2 \tilde{g}_K N_0}{2\pi m^2 q_0^4}, \end{aligned} \tag{4.89e}$$

$$J_{\dot{q},\dot{q}} = -2q_0^2 K N_0 + \frac{q_0^4 K N_0}{2(q_0^2 + r_0^2)}. \tag{4.89f}$$

Finally, the matrix M coupling the vectors $\delta\nu_i$ among each other has only three finite entries:

$$M_{\dot{q},r} = \frac{r_0^2}{r_0^2 + q_0^2}\left(\frac{q_0^2 K N_0}{2\tau} - K N_0 q_0^4 - L\right), \tag{4.90}$$

$$M_{\dot{q},q} = \frac{q_0^2 r_0^2 K N_0}{2\tau(q_0^2 + r_0^2)} \frac{1}{1 + 4\mathcal{D}\tau/q_0^2} - \frac{K N_0 q_0^6}{q0^2 + r_0^2} - \frac{\hbar^2 \tilde{g}_K N_0}{\pi q_0^4}, \tag{4.91}$$

$$M_{\dot{q},\dot{q}} = \frac{K N_0 2 q_0^4}{2(q_0^2 + r_0^2)}. \tag{4.92}$$

The eigenvalues of the system matrix are shown in Figure 4.8. From panel (a) we can read off, that due to the thermo-optic interaction the breathing and the quadrupole mode are shifted to smaller frequencies. The dashed lines in the plot are the results from Appendix C.2, where the case of a contact interaction is investigated. Comparing the thermo-optic to the local interaction results reveals, that similar to the dipole mode, also the breathing mode, which is not influenced by a contact interaction, is effected by the nonlocal thermo-optic interaction. panel (b) shows, that all the dampings are positive, meaning, that this mode is unstable. But as in the case of the dipole mode, these instabilities are in the order of $1 \times 10^{-4}\,\mathrm{s}$, which is much larger than the lifetime of the condensate.

4.7. Experimental Realisation

In this Section we give a short overview on potential experimental realisations and measurements of the lowest-lying collective frequencies, that have been calculated in this Chapter. In principle, there are two ways for performing those measurements.

The first one goes back to a suggestion of Martin Weitz and is based on a direct observation of the three modes described in the Sections 4.5 and 4.6. The dipole mode, for instance, could

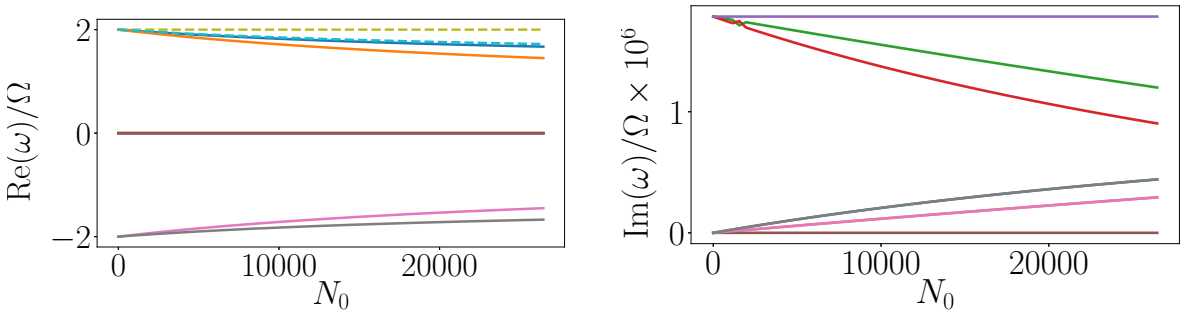

(a) **(b)**

FIG. 4.8: Plot of the (Panel **(a)**) frequencies and (Panel **(b)**) damping rates of the breathing (blue and grey) and the quadrupole (orange and magenta) mode. The other colours show the damping of the diffusive quantities, viz., the photon number, the temperature amplitude and its widths. The dashed curves in Panel **(a)** are the breathing and quadrupole mode frequencies in case of a contact interaction with strength $\tilde{g}_T$, according to (C.24).

be excited by using two lasers. The first one homogeneously pumps the whole cavity, whereas the second one creates a Bose-Einstein condensate via an off-centre pulse. The excited mode can then be observed by measuring spatially resolved the light leaking out the cavity and by calculating the respective moments of the condensate density. But this necessitates also that the oscillations are temporally resolved. As the frequencies are suspected to be of the order of the trap frequency, cf. Figures 4.7 and 4.8, motions that happen at time scales of the order 100 ps need to be analysed. For this purpose a so-called streak camera, which can measure processes taking place on time scales of 100 fs [83], needs to be used.

The second way to measure collective frequencies was brought up by Robert Nymann and is based on the measurement of the eigenenergies of the dye-filled microcavity. Therefore, it uses the expansion of the condensate wave function into harmonic oscillator eigenstates, that are given by

$$\phi_\alpha(\mathbf{x}) = \frac{H_{\alpha_1}(x_1/l_{\mathrm{osc}})H_{\alpha_2}(x_2/l_{\mathrm{osc}})}{\sqrt{2^{\alpha_1+\alpha_2}\alpha_1!\alpha_2!\pi l_{\mathrm{osc}}^2}} \exp\left(-\frac{x_1^2}{2l_{\mathrm{osc}}^2} - \frac{x_2^2}{2l_{\mathrm{osc}}^2}\right), \tag{4.93}$$

where $\alpha = (\alpha_1, \alpha_2) \in \mathbb{N}^2$ is a multiindex, l_{osc} stands for the harmonic oscillator length, and the Hermite polynomial of degree n is denoted by H_n. Consider the Gaussian ansatz (4.3) for the condensate wave function. If we neglect the diffusion, the pump and the interaction, then the time dependent widths are given by

$$q_j(t) \approx l_{\mathrm{osc}}\left[1 + \delta q_j(t)\right]. \tag{4.94}$$

If we further assume the displacement from the trap centre $x_{0j}(t)$ to be small, the expansion of the wave function (4.3) into the Hermite-Gauss modes reads

$$\psi(\mathbf{x}, t) \approx \sqrt{N}\left[\phi_{00}(\mathbf{x}) + \frac{x_{01}(t)}{\sqrt{2}}\phi_{10}(\mathbf{x}) + \frac{x_{02}(t)}{\sqrt{2}}\phi_{01}(\mathbf{x}) + \frac{\delta q_1(t)}{\sqrt{2}}\phi_{20}(\mathbf{x}) + \frac{\delta q_2(t)}{\sqrt{2}}\phi_{02}(\mathbf{x})\right]. \tag{4.95}$$

Thus, for measuring the lowest-lying collective frequencies it is sufficient to take only the first three eigenenergies of the cavity with its degenerated eigenmodes into account. The correspond-

ing photon density reads then

$$|\psi(\mathbf{x},t)|^2 = N\left\{|\phi_{00}(\mathbf{x})|^2 + \sqrt{2}\left[x_{01}(t)\phi_{10}(\mathbf{x}) + x_{02}(t)\phi_{01}(\mathbf{x}) + \delta q_1(t)\phi_{20}(\mathbf{x}) + \delta q_2(t)\phi_{02}(\mathbf{x})\right]\phi_{00}\right\}. \tag{4.96}$$

In general, the expansion into the eigenmodes is given by

$$\psi(\mathbf{x},t) = \sum_\alpha a_\alpha(t)\phi_\alpha(\mathbf{x}), \tag{4.97}$$

with complex time-dependent expansion coefficients

$$a_\alpha(t) = \int d^2x\ \psi(\mathbf{x},t)\phi_\alpha(\mathbf{x}). \tag{4.98}$$

Comparing (4.96) to (4.97) yields that $a_{00} \gg a_\alpha$ for all $\alpha \neq (0,0)$. Accordingly, the photon density $|\psi|^2$ is then given by

$$|\psi|^2 \approx N\left[|a_{00}|^2\phi_{00}^2 + 2\sum_\alpha |a_\alpha a_{00}|\cos(\omega_{0\alpha}t)\phi_\alpha\phi_{00}\right]. \tag{4.99}$$

Here, the sum only includes the first two excited states, cf. to (4.96), and $\omega_{0\alpha} = \omega_{00} - \omega_\alpha$ is the difference between the eigenfrequencies

$$\omega_\alpha = \Omega\left(\alpha_1 + \alpha_2 + 1\right) \tag{4.100}$$

of the ground state ω_{00} and the excited states ω_α.
A comparison of the expansions (4.96) and (4.99) shows that the time dependency of the moments in the ansatz (4.3) is the same as the difference of the eigenfrequencies of the first cavity modes.
Thus, from the knowledge of the eigenfrequencies we can conclude the frequencies of the lowest-lying collective modes. Taking also the interaction into account, one can think of the eigenfunctions ϕ_α as the perturbed eigenfunctions and consequently ω_α represent the perturbed eigenfrequencies. Accordingly, the approach sketched above is also valid in the interacting case. Those eigenfrequencies can be measured by a high-resolution spectroscopy of the light leaking out of the cavity. However, one has to bear in mind that in the current experiments no equilibrium has been reached so far, but the theory presented in this thesis is designed for perturbations of the equilibrium.

Part III.

Reduction to One Equation

5. Green's Function of Temperature

A desert heath. Thunder and lightning.
Enter three Witches.
1st: When shall we three meet again
In thunder, lightning, or in rain?
2nd: When the hurlyburly's done,
When the battle's lost and won.
3rd: That will be ere the set of sun.[...]
ALL: Fair is foul, and foul is fair:
Hover through the fog and filthy air.

William Shakespeare, Macbeth, Act I, Scene 1

In the last two Chapters we have seen, that the temperature can lead to some instabilities of the photon Bose-Einstein condensate in the case of the homogeneous system as well as in the case of the dipole mode in the trapped system. Therefore, we conclude that it is worthwhile to eliminate the temperature from our considerations, in order to work out whether these instabilities are due to the previous Gaussian ansatz for the temperature or due to the model itself. As the equation, that guides the temporal evolution of the temperature, is a linear diffusion equation, we can describe the temperature also by means of a Green's function that is driven by the electric field. Therefore, this Chapter deals with the derivation of this Green's function, where as the tool we use the Laplace transformation. As a consequence the equation, that governs the photons, turns out to be a nonlinear-partial integro differential equation, where the temporal nonlocality stems from a convolution of the temperature propagator and the photon wave function at all times of the system history. This means, that not only a nonlocality in space occurs due to the temperature diffusion but also a nonlocality in time is present. In the forthcoming Chapters we encounter again the Laplace transformation as a method to solve this equation. This is also one of the main differences to the mean-field equations for the exciton-polariton condensates proposed in [34]. There, the reservoir equation is kept as general as possible. Therefore, also some reservoir nonlinearities can occur, which means, that a Green's function formalism is not possible in this case. But, in our case, the temperature equation is kept as simple as possible allowing us to use this formalism.

As we have seen in the last Chapters, the evolution of the temperature field T produced by the photons is determined by the linear diffusion equation

$$\partial_t T = \mathcal{D}\nabla^2 T - \frac{1}{\tau}T + B\mathfrak{n}, \tag{5.1}$$

where $\mathfrak{n} = |\psi|^2$ denotes the condensate density.
In the following the aim is to find the corresponding propagator in order to eliminate the tem-

perature degree of freedom from the mean-field description. For this purpose (5.1) is Fourier transformed in space, but Laplace transformed in time. This very thought will always be the leading principle in the remaining part of the thesis. In the following the Fourier transformed functions are denoted by a tilde:

$$\tilde{f}(\mathbf{k}) = \int_{\mathbb{R}^2} d^2x \; f(\mathbf{x}) e^{-i\mathbf{k}\cdot\mathbf{x}}, \quad \mathbf{k} \in \mathbb{R}^2. \tag{5.2}$$

Correspondingly, the Laplace transformed functions are denoted by a breve sign:

$$\breve{g}(s) = \int_0^\infty dt \; g(t) e^{-st}, \quad s \in \mathbb{C}. \tag{5.3}$$

Note that due to the definition of the Laplace transformation s is a complex frequency, whose real part represents a damping rate and whose imaginary part corresponds to an oscillation frequency. As we will see in the next two Chapters the advantage of the Laplace transformation is that it can deal with the initial condition at $t = 0$ and with the convolutions that arise due to the elimination of the temperature.
The Fourier-Laplace transformed diffusion equation (5.1) reads

$$s\breve{\tilde{T}}(\mathbf{k}, s) - \tilde{T}(\mathbf{k}, 0) = -\mathcal{D}\mathbf{k}^2 \breve{\tilde{T}}(\mathbf{k}, s) + B\breve{\tilde{\mathfrak{n}}}(\mathbf{k}, s). \tag{5.4}$$

Here the initial condition of the temperature appears due to the properties of the Laplace transformation, see e.g. [84, Table 1]. But, as this temperature describes the temperature difference to the environment, that is produced by the photons during the experiment, the initial condition is assumed to vanish, i.e. $\tilde{T}(\mathbf{k}, 0) = 0$. Thus, the transformed temperature is given by

$$\breve{\tilde{T}}(\mathbf{k}, s) = \breve{\tilde{\mathcal{G}}}(\mathbf{k}, s) B \breve{\tilde{\mathfrak{n}}}(\mathbf{k}, s), \tag{5.5}$$

where the Fourier-Laplace transformed Green's function of (5.1) reads

$$\breve{\tilde{G}}(\mathbf{k}, s) = \frac{1}{s + \mathcal{D}\mathbf{k}^2 + 1/\tau}. \tag{5.6}$$

Therefore, the temperature in real space and time is provided by the equation

$$T(\mathbf{x}, t) = B(\mathcal{G} * \mathfrak{n})(\mathbf{x}, t), \tag{5.7}$$

where $*$ denotes the convolution operator

$$(f * g)(\mathbf{x}, t) = \int_{\mathbb{R}^2} d^2x' \int_0^t dt' \; f(\mathbf{x} - \mathbf{x}', t - t') g(\mathbf{x}', t'). \tag{5.8}$$

Now the propagator $\mathcal{G}(\mathbf{x}, t)$ needs to be calculated explicitly. According to [84, Table 6.2] the inverse Laplace transform of (5.6) is given by

$$\tilde{\mathcal{G}}(\mathbf{k}, t) = e^{-\left(\mathcal{D}\mathbf{k}^2 + 1/\tau\right)t}. \tag{5.9}$$

Therefore, the inverse Fourier transform is given by a Gaussian integral that amounts finally

to

$$\mathcal{G}(\mathbf{x},t)=\frac{\exp\left(-\frac{\mathbf{x}^2}{4\mathcal{D}t}-\frac{t}{\tau}\right)}{4\pi\mathcal{D}t}. \tag{5.10}$$

Note that in the limit $\mathcal{D}\to 0$ the propagator gets local in space;

$$\lim_{\mathcal{D}\to 0}\mathcal{G}(\mathbf{x},t)=e^{-t/\tau}\delta(\mathbf{x}). \tag{5.11}$$

Due to the diffusion no such analogy exists for the time. Thus, the propagator is always nonlocal with respect to time.
As the Fourier and the Laplace transformation are always performed upon the spatial and temporal variable, respectively, the corresponding variables are left out in the following, as long as it does not lead to any confusion.
Finally, inserting (5.7) into (2.81) yields a Gross-Pitaevskii equation that is nonlocal in both space and time

$$i\hbar\partial_t\psi=\left\{-\frac{\hbar^2\nabla^2}{2m}+\frac{m\Omega^2}{2}\mathbf{x}^2+g_TB\mathcal{G}*|\psi|^2+\frac{i\hbar}{2}\left[\aleph p-\Gamma+2B\left(\aleph p+\Gamma\right)\mathcal{G}*|\psi|^2\right]\right\}\psi. \tag{5.12}$$

However, in this last part of the thesis we only consider the thermo-optic interaction, as the Kerr interaction is to small in the current experiments and no new information can be obtained regarding the above mentioned instabilities.

As a remark, we mention that spatial nonlocalities are well known from the field of dipolar Bose-Einstein condensates, for an overview see [21].

6. Homogeneous Condensate

All the world's a stage,
And all the men and women merely players;
They have their exits and their entrances,
And one man in his time plays many parts,[...]

William Shakespeare, As You Like It, Act II, Scene 7

In this Chapter we revisit the homogeneous system that was already examined in Chapter 3. The main difference is that we deal in the present Chapter with a partial-integro differential equation for the condensate wave-function instead of a set of two partial-differential equations for the temperature and the condensate wave function. On the one hand this has the advantage that no assumption upon the temperature wave function is needed, but it has on the other hand the disadvantage that we need to deal with the integro-differential equation. In particular this means that some mathematical subtleties occur that are not known from a corresponding analysis of usual differential equations. Those already appear during the linearisation procedure performed in Section 6.1. First, we see that the steady state still has some influence on the perturbations, which is most elegantly dealt with in the Fourier-Laplace transformed picture according to Section 6.2. But as a consequence of these transformations, we find a nonlocality in the frequency as the linearised wave function depends upon higher frequencies. This yields a recursion relation for the perturbations of the homogeneous wave function with respect to frequencies. But before solving this, we first calculate the two steady states in Section 6.3, where it turns out that all the results from Chapter 3 will be reproduced. With those results at hand we then turn towards the stability of the steady states, which is examined in Section 6.4. There we will first work on the stability of the trivial steady state that gets unstable as soon as the nontrivial fixed point starts to exist. In order to determine the stability of the latter we finally solve the recursion relation from Section 6.1. Here it turns out that not only the solution from Chapter 3 is reproduced, but in addition to that we obtain higher modes that come from the recursion relation itself.

6.1. Linearisation

We start our analysis with the homogeneous system, that is described by the equation

$$i\hbar\partial_t\psi = \left[-\frac{\hbar^2\nabla^2}{2m} + g_T B\mathcal{G} * |\psi|^2 + \frac{i\hbar}{2}\left(\aleph p - \Gamma + P\mathcal{G} * |\psi|^2\right)\right]\psi, \tag{6.1}$$

where the thermo-optic pump influence is given by

$$P = 2B\frac{\partial n}{n_0 \partial T}(\aleph p + \Gamma). \tag{6.2}$$

We linearise (6.1) as in Chapter 3 with the ansatz

$$\psi(\mathbf{x},t) = [\sqrt{\mathfrak{n}_0} + \delta\psi(\mathbf{x},t)]\, e^{-i\mu t/\hbar}, \tag{6.3}$$

where $\mathfrak{n}_0$ denotes the homogeneous steady state condensate density, $\delta\psi(\mathbf{x},t)$ stands for a perturbation and μ is the chemical potential. Inserting (6.3) into (6.1) and neglecting all terms of the order $\mathcal{O}(\delta\psi^2)$ yields

$$\begin{aligned}\mu(\sqrt{\mathfrak{n}_0} + \delta\psi) + i\hbar\partial_t\delta\psi = &-\frac{\hbar^2\nabla^2}{2m}\delta\psi + \left(g_T B + i\frac{\hbar P}{2}\right)[(\mathcal{G}*1)\sqrt{\mathfrak{n}_0} + (\mathcal{G}*1)\delta\psi \\ &+\mathcal{G}*\delta\psi^* + \mathcal{G}*\delta\psi]\,\mathfrak{n}_0 + \frac{i\hbar}{2}(\aleph p - \Gamma)(\sqrt{\mathfrak{n}_0} + \delta\psi).\end{aligned} \tag{6.4}$$

Before proceeding with the calculation one subtlety needs to be mentioned. We are dealing in the present case with a nonlocality in time. This means that in the partial integro-differential equation (6.1) also a convolution in time appears. The effect of this temporal convolution upon the linearised equation (6.4) is now as follows. Usually, in the case of an ordinary differential equation one sets the perturbation to zero, i.e. $\delta\psi = 0$, in order to obtain an algebraic equation for the steady state that is then reinserted into the linear equation. As a result of this procedure, one ends up with a homogeneous equation in the perturbation $\delta\psi$. But in the present case the situation is more involved as a steady state is defined as the long time limit of (6.4) for vanishing perturbations $\delta\psi$. Since in our integral equation (6.1) the convolution ranges due to causality from the initial time $t_0 = 0$ up to the present time t, we find an inhomogeneity for the resulting equation of $\delta\psi$ that is due to the leftover of the steady state. Dealing with this is most elegantly done in the framework of the Laplace transformation.

6.2. Laplace Transformation

Therefore, we proceed now by Fourier-Laplace transforming the whole equation (6.4):

$$\begin{aligned}&\mu\left[\frac{\delta(\mathbf{k})}{s}\sqrt{\mathfrak{n}_0} + \delta\breve{\tilde{\psi}}(\mathbf{k},s)\right] + i\hbar\left[s\delta\breve{\tilde{\psi}}(\mathbf{k},s) - \delta\tilde{\psi}(\mathbf{k},0)\right] \\ &= \frac{\hbar^2\mathbf{k}^2}{2m}\delta\breve{\tilde{\psi}}(\mathbf{k},s) + \left(g_T B + \frac{i\hbar P}{2}\right)\left\{\breve{\tilde{\mathcal{G}}}(\mathbf{0},s)\frac{\sqrt{\mathfrak{n}_0}}{s}\delta(\mathbf{k}) + \mathcal{L}\left[\mathcal{F}\left[(\mathcal{G}*1)\delta\psi(\mathbf{x},t)\right]\right]\right. \\ &\left.+\breve{\tilde{\mathcal{G}}}(\mathbf{k},s)\left[\delta\breve{\tilde{\psi}}(\mathbf{k},s) + \delta\breve{\tilde{\psi}}(\mathbf{k},s)^*\right]\right\}\mathfrak{n}_0 + \frac{i\hbar}{2}(\aleph p - \Gamma)\left[\frac{\delta(\mathbf{k})}{s}\sqrt{\mathfrak{n}_0} + \delta\breve{\tilde{\psi}}(\mathbf{k},s)\right].\end{aligned} \tag{6.5}$$

Here we have used that $\int d^2x'\ \mathcal{G}(\mathbf{x}-\mathbf{x}', t-t') = \tilde{\mathcal{G}}(\mathbf{0}, t-t')$ and denoted the operators of the Fourier and the Laplace transform by $\mathcal{F}$ and $\mathcal{L}$, respectively. Moreover, the terms that contain the homogeneous steady state are Fourier transformed to a Dirac-delta function $\delta(\mathbf{k})$, as they can only affect modes with infinite wavelength. Exactly those terms turn out to lead to the inhomogeneity described above.

One Fourier-Laplace transformation is still left to perform. Due to the linearisation, there enters the term $(\mathcal{G} * 1)\delta\psi(\mathbf{x}, t)$ in the second line of (6.5) that almost looks like a convolution but is none. This yields a second subtlety, which is not known from the case of usual partial-differential equations, namely a coupling to higher frequencies, as can be seen by calculating its Fourier-Laplace transformation

$$\mathcal{L}\left[\mathcal{F}\left[(\mathcal{G} * 1)\delta\psi(\mathbf{x}, t)\right]\right] = \mathcal{L}\left[\int_0^t dt'\ \tilde{\mathcal{G}}(\mathbf{0}, t - t')\delta\tilde{\psi}(\mathbf{k}, t)\right]. \tag{6.6}$$

According to (5.9) we have $\tilde{\mathcal{G}}(\mathbf{0}, t - t') = \exp\left[-(t - t')/\tau\right]$, so the integral inside the Laplace transformation (6.6) can be evaluated resulting in

$$\mathcal{L}\left[\mathcal{F}\left[(\mathcal{G} * 1)\delta\psi(\mathbf{x}, t)\right]\right] = \tau\mathcal{L}\left[\left(1 - e^{-t/\tau}\right)\delta\tilde{\psi}(\mathbf{k}, t)\right]. \tag{6.7}$$

Using [84, Table 5.1, (6)] yields finally

$$\mathcal{L}\left[\mathcal{F}\left[(\mathcal{G} * 1)\delta\psi(\mathbf{x}, t)\right]\right] = \tau\left[\delta\breve{\tilde{\psi}}(\mathbf{k}, s) - \delta\breve{\tilde{\psi}}\left(\mathbf{k}, s + \frac{1}{\tau}\right)\right]. \tag{6.8}$$

Thus, the Fourier-Laplace transformation leads to a coupling to higher (damping) frequencies that are given by integer multiples of $1/\tau$. With this (6.5) reduces to the following linear equation in the frequency domain:

$$\begin{aligned}
&\frac{\delta(\mathbf{k})}{s}\sqrt{\mathfrak{n}_0}\left[\mu - \left(g_T B + \frac{i\hbar P}{2}\right)\breve{\tilde{\mathcal{G}}}(\mathbf{0}, s)\mathfrak{n}_0 - \frac{i\hbar}{2}\left(\aleph p - \Gamma\right)\right] - i\hbar\delta\tilde{\psi}(\mathbf{k}, 0) \\
&- \tau\left(g_T B + \frac{i\hbar P}{2}\right)\mathfrak{n}_0\delta\breve{\tilde{\psi}}(\mathbf{k}, s + 1/\tau) \\
&= \left[-\mu - i\hbar s + \frac{\hbar^2\mathbf{k}^2}{2m} + \tau\left(g_T B + \frac{i\hbar P}{2}\right)\mathfrak{n}_0 + \frac{i\hbar}{2}\left(\aleph p - \Gamma\right)\right]\delta\breve{\tilde{\psi}}(\mathbf{k}, s) \\
&+ \left(g_T B + \frac{i\hbar P}{2}\right)\mathfrak{n}_0\breve{\tilde{\mathcal{G}}}(\mathbf{k}, s)\left[\delta\breve{\tilde{\psi}}(\mathbf{k}, s) + \delta\breve{\tilde{\psi}}(\mathbf{k}, s)^*\right]
\end{aligned} \tag{6.9}$$

To sum up, we have the following differences in comparison to the usual differential equation approach. The first term of the left-hand side, that, as we see in the next section, describes the steady state, leads to an inhomogeneity in the equation for the perturbation $\delta\psi$. The second difference is the last term on the left-hand site, since this term couples to higher frequencies. Let us now determine at first the steady states in the next section.

6.3. Steady States

We proceed now by examining the homogeneous steady states. These are already imprinted in (6.9) by performing the limit $|\mathbf{k}| \to 0$ and $s \to 0$. Whereas the first limit is necessary to find a solution, which is homogeneous in space, the latter is required to achieve the steady state in the

long-time limit. In these limits (6.9) takes the form

$$\mu\sqrt{\mathfrak{n}_0} = \left\{ g_T B \breve{\breve{\mathcal{G}}}(\mathbf{0},0)\mathfrak{n}_0 + \frac{i\hbar}{2}\left[(\aleph p - \Gamma) + P\breve{\breve{\mathcal{G}}}(\mathbf{0},0)\mathfrak{n}_0\right]\right\}\sqrt{\mathfrak{n}_0}. \tag{6.10}$$

First, we note from (5.6) that $\breve{\breve{\mathcal{G}}}(\mathbf{0},0) = \tau$. Secondly, we see that (6.10) has two solutions. One of them is the trivial steady state

$$\mathfrak{n}_0{}^{\text{triv}} = 0. \tag{6.11}$$

The second solution involves a finite photon density, which means that in this case we can simplify (6.10) to

$$\mu = \tau g_T B \mathfrak{n}_0 + \frac{i\hbar}{2}\left[(\aleph p - \Gamma) + P\tau\mathfrak{n}_0\right]. \tag{6.12}$$

The imaginary part of (6.12) yields the order parameter $\mathfrak{n}_0$ in terms of the control parameter p:

$$\mathfrak{n}_0 = \frac{\Gamma - \aleph p}{\tau P}. \tag{6.13}$$

Note, that according to (6.2) we have $P < 0$ as $\frac{\partial n}{\partial T} < 0$. Therefore, we read off from (6.13) the constraint

$$p \geq p_{\text{crit}}, \tag{6.14}$$

which is crucial for the existence of this steady state. The critical pump power is defined by

$$p_{\text{crit}} = \frac{\Gamma}{\aleph}. \tag{6.15}$$

The nontrivial state (6.13) gives rise to a finite chemical potential μ_T that is determined by the real part of (6.12):

$$\mu_T = \tau g_T B \mathfrak{n}_0. \tag{6.16}$$

Therefore, the effective photon-photon interaction constant g is given by

$$g = \tau g_T B. \tag{6.17}$$

As we have $\mathfrak{n}_0|_{p=p_{\text{crit}}} = \mathfrak{n}_0{}^{\text{triv}}$, the transition is continuous. As this should also hold for the chemical potential, we can conclude from (6.16), that $\mu_T^{\text{triv}} = 0$. In comparison to the results of Section 3.2 we have reproduced exactly the same steady states, in case of vanishing Kerr interaction and temperature pump, i.e. $g_K = 0$ and $\alpha = 0$.

6.4. Dynamical Stability

As the possible steady states of (6.1) are now known, we aim to determine their stability. Inserting (6.10) into (6.9) yields

$$\begin{aligned}\frac{\sqrt{\mathfrak{n}_0}\delta(\mathbf{k})}{s+1/\tau}\left(\mu_T+i\tilde{\mu}_P\right)-i\hbar\delta\tilde{\psi}(\mathbf{k},0)&=\left(-i\hbar s+\frac{\hbar^2\mathbf{k}^2}{2m}-\mu\right)\delta\breve{\tilde{\psi}}(\mathbf{k},s)\\&+\left(\mu_T+i\tilde{\mu}_P\right)\left\{\delta\breve{\tilde{\psi}}(\mathbf{k},s)-\delta\breve{\tilde{\psi}}(\mathbf{k},s+1/\tau)+\frac{\breve{\tilde{\mathcal{G}}}(\mathbf{k},s)}{\tau}\left[\delta\breve{\tilde{\psi}}(\mathbf{k},s)+\delta\breve{\tilde{\psi}}(\mathbf{k},s)^*\right]\right\}\\&+\frac{i\hbar}{2}\left(\aleph p-\Gamma\right)\delta\breve{\tilde{\psi}}(\mathbf{k},s).\end{aligned}\tag{6.18}$$

To simplify the notation, we define the pump pseudo-chemical potential by

$$\tilde{\mu}_P=\frac{\hbar P\tau}{2}\mathfrak{n}_0\tag{6.19}$$

and use definition (6.16). Note, that we call it a pseudo-chemical potential, as it appears in the imaginary part of (6.18) and, thus, works as a damping.

6.4.1. Trivial Steady State

We are now in the position to determine the stability of the trivial steady state (6.11). In this case (6.18) simplifies by using (6.11) and (6.16)

$$\delta\tilde{\psi}(\mathbf{k},0)=\left(-i\hbar s+\frac{\hbar^2\mathbf{k}^2}{2m}\right)\delta\breve{\tilde{\psi}}(\mathbf{k},s)+\frac{i\hbar}{2}\left(\aleph p-\Gamma\right)\delta\breve{\tilde{\psi}}(\mathbf{k},s).\tag{6.20}$$

Therefore, the Fourier-Laplace transformed solutions to the perturbations in the trivial steady state read

$$\delta\breve{\tilde{\psi}}(\mathbf{k},s)=\frac{\delta\tilde{\psi}(\mathbf{k},0)}{-i\hbar s+\frac{\hbar^2\mathbf{k}^2}{2m}+\frac{i\hbar}{2}\left(\aleph p-\Gamma\right)}.\tag{6.21}$$

The question is now what this solution in the frequency domain reveals about the behaviour of the inverse Laplace transformed pendant. In order to answer this, consider the series

$$f(t)=\sum_l\alpha_l e^{\lambda_l t}\tag{6.22}$$

with coefficients $\alpha_l\in\mathbb{C}$ and frequencies $\lambda_l\in\mathbb{C}$. The Laplace transformation is given by

$$\breve{f}(s)=\sum_l\frac{\alpha_l}{s-\lambda_l}.\tag{6.23}$$

In this procedure the values λ_l are determined as the roots of the denominator of (6.21) and are, thus, the singularities of the Laplace transformed solution. Therefore, our strategy is now

to find exactly those singularities. In case of (6.21) there is only one singularity

$$\lambda = -i\frac{\hbar \mathbf{k}^2}{2m} + \frac{1}{2}\left(\aleph p - \Gamma\right). \tag{6.24}$$

We see, that $\mathrm{Re}\,(\lambda) \geq 0$ for $p \geq p_{\mathrm{crit}}$, indicating that the trivial steady state gets unstable, as the nontrivial steady state starts to exist.

6.4.2. Nontrivial Steady State

We come now to the stability of the nontrivial steady state. Therefore, we insert (6.12) into (6.18) and find

$$\begin{aligned}\frac{\sqrt{\mathfrak{n}_0}\delta(\mathbf{k})}{s+1/\tau}\left(\mu_T + i\tilde{\mu}_P\right) - i\hbar\delta\tilde{\psi}(\mathbf{k},0) &= \left(-i\hbar s + \frac{\hbar^2\mathbf{k}^2}{2m}\right)\delta\breve{\tilde{\psi}}(\mathbf{k},s) \\ + \left(\mu_T + i\tilde{\mu}_P\right)&\left\{-\delta\breve{\tilde{\psi}}(\mathbf{k},s+1/\tau) + \frac{\breve{\tilde{\mathcal{G}}}(\mathbf{k},s)}{\tau}\left[\delta\breve{\tilde{\psi}}(\mathbf{k},s) + \delta\breve{\tilde{\psi}}(\mathbf{k},s)^*\right]\right\}.\end{aligned} \tag{6.25}$$

To proceed further, we split the perturbations into real and imaginary part:

$$\delta\breve{\tilde{\psi}}(\mathbf{k},s) = \breve{\tilde{u}}(\mathbf{k},s) + i\breve{\tilde{v}}(\mathbf{k},s). \tag{6.26}$$

Inserting this into (6.18) and collecting the real and imaginary parts leads to the following recursion relation

$$\begin{pmatrix}\hbar\tilde{v}(\mathbf{k},0)\\ \\ -\hbar\tilde{u}(\mathbf{k},0)\end{pmatrix} + \begin{pmatrix}\mu_T\\ \\ \tilde{\mu}_P\end{pmatrix}\frac{\sqrt{\mathfrak{n}_0}\delta(\mathbf{k})}{s+1/\tau} + M\begin{pmatrix}\breve{\tilde{u}}(\mathbf{k},s+1/\tau)\\ \\ \breve{\tilde{v}}(\mathbf{k},s+1/\tau)\end{pmatrix} = L(\mathbf{k},s)\begin{pmatrix}\breve{\tilde{u}}(\mathbf{k},s)\\ \\ \breve{\tilde{v}}(\mathbf{k},s)\end{pmatrix}, \tag{6.27}$$

where the system matrix $L(\mathbf{k},s)$ is defined by

$$L(\mathbf{k},s) = \begin{pmatrix}\epsilon_{\mathbf{k}} + \frac{\mu_T}{\tau}\breve{\tilde{\mathcal{G}}}(\mathbf{k},s) & \hbar s\\ \\ -\hbar s + \frac{\tilde{\mu}_P}{\tau}\breve{\tilde{\mathcal{G}}}(\mathbf{k},s) & \epsilon_k\end{pmatrix}, \tag{6.28}$$

with the one-particle energy $\epsilon_{\mathbf{k}}$ defined according to (3.29). The matrix M is given by the respective chemical potentials

$$M = \begin{pmatrix}\mu_T & -\tilde{\mu}_P\\ \\ \tilde{\mu}_P & \mu_T\end{pmatrix} \tag{6.29}$$

and, thus, carries the information off the thermo-optics.
Equation (6.18) can be solved iteratively, providing us with the Fourier-Laplace transformed

solution of the linear part of the nonlocal Gross-Pitaevskii equation:

$$\begin{pmatrix} \breve{\tilde{u}}(\mathbf{k},s) \\ \breve{\tilde{v}}(\mathbf{k},s) \end{pmatrix} = \sum_{j=0}^{\infty} M^j \left(\prod_{l=0}^{j} L^{-1}(\mathbf{k}, s+l/\tau) \right) \left[\begin{pmatrix} (-1)^j \hbar \tilde{u}(\mathbf{k},0) \\ \hbar \tilde{v}(\mathbf{k},0) \end{pmatrix} + \begin{pmatrix} \mu_T \\ \tilde{\mu}_P \end{pmatrix} \frac{\sqrt{\mathfrak{n}_0}\,\delta(\mathbf{k})}{s+(j+1)/\tau} \right]. \tag{6.30}$$

We can interpret the result (6.30) as a thermo-optic perturbation series as both the chemical potential μ_T due to the interaction, see (6.16), and the pseudo-chemical potential $\tilde{\mu}_P$ due to the pump, see 6.19, are proportional to $\frac{\partial n}{\partial T}$, see (2.75) and (6.2), respectively. In the following discussion we ignore at first the steady state contribution. Moreover, we consider only the zeroth term in the series, as the results for the higher summands can be found by replacing s by $s+l/\tau$. Along the philosophy that we have already developed when we discussed the trivial steady state, we look also here for the singularities of the solution (6.30). These are obviously determined by the inverse system matrix

$$L^{-1}(\mathbf{k},s) = \frac{1}{\det(L(\mathbf{k},s))} \begin{pmatrix} \epsilon_k & -\hbar s \\ \hbar s - \frac{\tilde{\mu}_P}{\tau} \breve{\tilde{\mathcal{G}}}(\mathbf{k},s) & \epsilon_{\mathbf{k}} + \frac{\mu_T}{\tau} \breve{\tilde{\mathcal{G}}}(\mathbf{k},s) \end{pmatrix}. \tag{6.31}$$

Note, that we also have to deal with the singularities of the matrix entries. By using the definition (5.6), we can write L^{-1} as

$$\begin{aligned} L^{-1}(\mathbf{k},s) =& \frac{1}{(\tau s + \tau \mathcal{D}\mathbf{k}^2 + 1)\det(L(\mathbf{k},s))} \\ & \times \begin{pmatrix} \left(\tau s + \tau \mathcal{D}\mathbf{k}^2 + 1\right)\epsilon_{\mathbf{k}} & -\left(\tau s + \tau \mathcal{D}\mathbf{k}^2 + 1\right)\hbar s \\ \left(\tau s + \tau \mathcal{D}\mathbf{k}^2 + 1\right)\hbar s - 2\tilde{\mu}_P & \left(\tau s + \tau \mathcal{D}\mathbf{k}^2 + 1\right)\epsilon_{\mathbf{k}} + 2\mu_T \end{pmatrix}, \end{aligned} \tag{6.32}$$

where all possible singular terms appear in the prefactor. Before proceeding, we need to consider the general definition of the inverse Laplace transformation of a function $f(t)$. This is defined via the Bromwich integral [84]

$$f(t) = \frac{1}{2\pi i} \int_{c-i\infty}^{c+i\infty} ds\ \breve{f}(s) e^{st}. \tag{6.33}$$

According to reference [84, Ch. 9.2] the inverse Laplace transformation of a function $\breve{f}(s)$ that has n singular points λ_i, can be calculated by the residuum theorem:

$$f(t) = \sum_{i=1}^{n} \operatorname*{Res}_{s=\lambda_i} \left[\breve{f}(s) e^{st} \right]. \tag{6.34}$$

We mention that inserting (6.23) in (6.34) directly yields (6.22). In our case, this has the consequence, that we need to find all roots of the prefactor in (6.32), i.e. the equation

$$\left(\tau s + \tau \mathcal{D}\mathbf{k}^2 + 1\right)\det(L(\mathbf{k},s)) = 0 \tag{6.35}$$

needs to be solved. We can distinguish two cases. In the first case we find, that

$$s = -\mathcal{D}\mathbf{k}^2 - 1/\tau, \tag{6.36}$$

with a purely real frequency, i.e. only damping is present. Note, that this corresponds to a resonance of the propagator (5.6). Therefore, this mode is a pure excitation of the temperature. The corresponding piece in the sum (6.34) is given by

$$\begin{pmatrix} \tilde{u}(\mathbf{k},t) \\ \\ \tilde{v}(\mathbf{k},t) \end{pmatrix} = \begin{pmatrix} 0 & 0 \\ \\ -2\tilde{\mu}_P & 2\mu_T \end{pmatrix} \begin{pmatrix} \tilde{u}(\mathbf{k},0) \\ \\ \tilde{v}\mathbf{k},0) \end{pmatrix} e^{-\left(1/\tau+\mathcal{D}\mathbf{k}^2\right)t}. \tag{6.37}$$

Therefore, in this mode $\tilde{u}(\mathbf{k},t)$ vanishes for all parameters, meaning that only the imaginary part in the wave function survives. But up to first order the photon density $\mathfrak{n}$ is due to (6.3) given by

$$\mathfrak{n} = \mathfrak{n}_0 + \sqrt{\mathfrak{n}_0}\left(\delta\psi^* + \delta\psi\right), \tag{6.38}$$

so only the real part of the perturbations u can contribute. Thus, this mode describes pure temperature perturbations.
The second case

$$0 = \det(L(\mathbf{k},s)) \tag{6.39}$$

provides us with excitations of the whole system. The determinant from (6.28)

$$0 = (\hbar s)^2 - \hbar s\frac{\tilde{\mu}_P}{\tau}\breve{\breve{\mathcal{G}}}(\mathbf{k},s) + \epsilon_{\mathbf{k}}^2 + \epsilon_{\mathbf{k}}\frac{\mu_T}{\tau}\breve{\breve{\mathcal{G}}}(\mathbf{k},s). \tag{6.40}$$

Inserting the definition of the propagator (5.6) and multiplying by it yields a polynomial of third order:

$$0 = s^3 + s^2\left(\mathcal{D}\mathbf{k}^2 + \frac{1}{\tau}\right) + s\left(\frac{\epsilon_{\mathbf{k}}^2}{\hbar^2} - \frac{\mu_p}{\hbar\tau}\right) + \frac{\epsilon_{\mathbf{k}}^2}{\hbar^2}\left(\mathcal{D}\mathbf{k}^2 + \frac{1}{\tau}\right) + \frac{\epsilon_{\mathbf{k}}}{\hbar^2\tau}\mu_T. \tag{6.41}$$

By comparing with (3.55) we see by identifying $s = i\omega$, that this is exactly the same polynomial as derived in the case of the two equations, meaning that all the results that have been derived there are also valid here. In particular, we refer to Figure 3.4 and the subsequent discussion.
Let us discuss now the contribution of the steady state. According to (6.30) this can only contribute in case of $\mathbf{k} \to \mathbf{0}$ due to the Dirac delta function and imprints then the frequency $s = -1/\tau$ upon the solution. But as $s = -1/\tau$ is already a solution of (6.36) in this limit the steady state has no influence.
Finally, the question on, how the coupling to higher frequencies changes the results, is left. This question is numerically tackled by solving (6.41) with the replacement $s \to s + j/\tau$. The result is shown in Figure 6.1. At first we note in panel (a), that the frequency is not shifted noteworthy. The same applies for the damping. This can be explained by the value of the relaxation time, which is the longest time scale we have. Thus, l we be needed to be large enough in order to introduce some effect. But as for increasing j also the order in the expansion (6.30) grows. However, the mode for $j = 0$ is always present, since it is a common prefactor in (6.30). Thus, the instability from this mode determines in every case the spectrum.

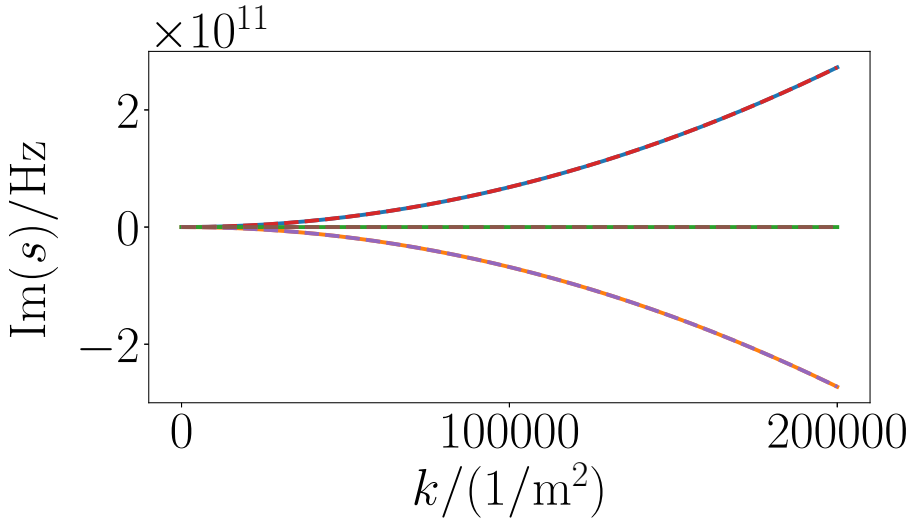

(a)

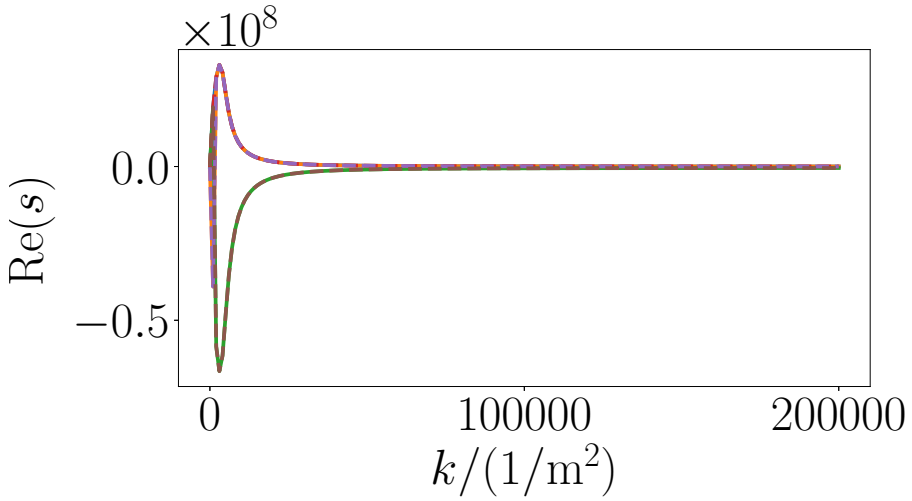

(b)

FIG. 6.1: Numerical solution of (6.41) for $s \to s + j/\tau$. The solid lines represent the result for $l = 0$, whereas the dashed lines represent the results for $l = 10$. Panel **(a)** shows the imaginary part of s, which is the oscillation frequency, whereas panel **(b)** shows the real part of s which is the damping.

7. Condensate in Harmonic Trap

Und an dem Ufer steh ich lange Tage,
Das Land der Griechen mit der Seele suchend;
Und gegen meine Seufzer bringt die Welle
Nur dumpfe Töne brausend mir herüber.

Johann Wolfgang von Goethe Iphigenie auf Tauris, Act I, Scene 1

And day by day upon the shore I stand,
My soul still seeking for the land of Greece.
But to my sighs, the hollow-sounding waves
Bring, save their own hoarse murmurs, no reply.

In this Chapter we turn towards the calculation of the lowest-lying collective frequencies. As we have discussed in the introduction to Chapter 4 their knowledge reveals deep information about the nature of the interparticle interaction. The main purpose of this Chapter is to reformulate Chapter 4 by means of the Green's function approach that is worked out in Chapter 5 and to investigate, whether the previous Gaussian ansatz for the temperature is valid or not.
In Section 7.1 it turns out, that the Gaussian ansatz for the temperature distribution performed in Chapter 4 only works, if the temperature diffusion has small effects. The equation for the photon number is calculated in Section 7.2. In Section 7.3 the cumulant equations of motion are derived, which are linearised afterwards in Section 7.4. Also here the Laplace transformation plays a basic role in order to dissolve the temporal convolutions. This yields a set of three algebraic equations in the frequency domain. Their steady state is then analysed in Section 7.5. The dynamical stability of this steady state is investigated in Section 7.6 with respect to perturbations of the centre-of-mass and in Section 7.7 with respect to variations of the widths.

7.1. Ansatz

We consider now again the case of a harmonically trapped photon BEC. According to (5.12) the condensate equation is in this case given by

$$i\hbar\partial_t\psi = \left[-\frac{\hbar^2}{2m}\nabla^2 + \frac{m\Omega^2}{2}\mathbf{x}^2 + g_T B\mathcal{G} * |\psi|^2\right]\psi + \frac{i\hbar}{2}\left[\aleph p - \Gamma + P\mathcal{G} * |\psi|^2\right]\psi. \tag{7.1}$$

As the perturbations that arise through the interaction and the pump are still considered to be small, it is valid to consider a Gaussian ansatz for the photon wave function

$$\psi(\mathbf{x},t) = \sqrt{\frac{N(t)}{\pi q_1(t) q_2(t)}} \exp\left\{ \sum_{j=1}^{2} \left[\left(-\frac{1}{2q_j(t)^2} + iA_j(t) \right) (x_j - x_{0j}(t))^2 + ix_j C_j \right] \right\}, \tag{7.2}$$

whereas we specify the pump to the experimental relevant case of a homogeneous pump spot as mentioned in the end of Section 4.4

$$p = \frac{P_0}{A_{\text{cavity}}}. \tag{7.3}$$

The notations are the same as in Chapter 4.
This ansatz for the photon wave function is now the advantage of the approach using a propagator, as no assumption upon the temperature function is needed any more. Instead, the temperature T is determined by inserting the ansatz (7.2) into the convolution (5.7) and after performing the spatial integrals, we obtain the remaining time integral

$$T(\mathbf{x},t) = B \int_0^t dt' \, \frac{N' \exp\left(-\frac{t-t'}{\tau}\right)}{\pi \sqrt{[4\mathcal{D}(t-t') + q_1'^2][4\mathcal{D}(t-t') + q_2'^2]}} \exp\left[-\sum_{j=1}^{2} \frac{(x_j - x_{0j}')^2}{4\mathcal{D}(t-t') + q_j'^2} \right]. \tag{7.4}$$

Here and throughout the rest of the chapter the prime denotes quantities that are taken at time t'.
The question is now how large the temperature distribution deviates from the Gaussian ansatz (4.4) performed in Chapter 4. For this purpose, we calculate the time-dependent moment generating function M of the temperature. This is defined by

$$M(\alpha_1, \alpha_2; t) = \int d^2x \, \exp\left(\sum_{j=1,2} \alpha_j x_j \right) T(\mathbf{x}, t). \tag{7.5}$$

After inserting the temperature function (7.4) and performing the spatial integrals we arrive at

$$M(\alpha_1, \alpha_2; t) = B \int_0^t dt' \; N' e^{-(t-t')/\tau} \exp\left\{ \sum_{j=1,2} \alpha_j x_{0j}' + \alpha_j^2 \left[\mathcal{D}(t-t') + \frac{q_j'^2}{4} \right] \right\}. \tag{7.6}$$

We assume now the quantities to vary slightly around the steady state. Therefore we take $q_j(t) = q_0 + \delta q_j(t)$, $N(t) = N_0 + \delta N(t)$ as well as $x_{0j}(t) = \delta x_j(t)$, where δ denotes small perturbations around the steady state. Inserting these expansions into (7.6) and keeping only terms up to first order in the perturbations, we find

$$M(\alpha_1, \alpha_2; t) \approx M_0(\alpha_1, \alpha_2; t) + \delta M(\alpha_1, \alpha_2; t). \tag{7.7}$$

The contribution $M_0(\alpha_1, \alpha_2; t)$ to the generating function is given by

$$M_0(\alpha_1, \alpha_2; t) = T_0 \exp\left[\frac{\left(\alpha_1^2 + \alpha_2^2\right) q_0^2}{4} \right] \frac{1 - \exp\left\{ -t \left[\frac{1}{\tau} + \left(\alpha_1^2 + \alpha_2^2\right) \mathcal{D} \right] \right\}}{1 + \tau \mathcal{D} (\alpha_1^2 + \alpha_2^2)}, \tag{7.8}$$

where we define $T_0 = \tau B N_0$ according to (4.29). In the long-time limit $t \to \infty$ Equation (7.8) approaches the equilibrium value

$$M_0(\alpha_1, \alpha_2) = T_0 \exp\left[\frac{\left(\alpha_1^2 + \alpha_2^2\right) q_0^2}{4}\right] \frac{1}{1 + \tau\mathcal{D}(\alpha_1^2 + \alpha_2^2)}. \tag{7.9}$$

Thus, the generating function deviates from a Gaussian due to the presence of diffusion in the system. In case of $\tau D \to 0$ (7.9) reduces to the moment generating function of a Gaussian distribution. Note, that the α_i have the dimension of an inverse length. Therefore, we can use $\tau\mathcal{D}/l_{\text{osc}}^2$ in order to quantify the deviation from the usual Gaussian distribution. Using the experimental values, the deviation is given by

$$\frac{\tau\mathcal{D}}{l_{\text{osc}}^2} = 3.9 \times 10^{-3} \tag{7.10}$$

and is, thus, small. Note that (7.10) coincides with the modification of the thermo-optic interaction due to the temperature diffusion in Section 4.4.1. Therefore, the ansatz with the two Gaussian functions from Chapter 4 is valid in the experimental case, but breaks down, if a strong diffusion would be present in the system. In Figure 7.1 the temperature distribution (7.4) is shown. In panel (a) we see the time evolution of the temperature distribution that reaches, indeed, a steady state during the time scale of τ. This steady state is shown in panel (b). In comparison to the normal distribution, that is here plotted for a standard deviation of 4, the width is smaller, but the tails are larger. In order to quantify this, we calculate the excess γ [85], that is defined as the kurtosis κ adjusted by the kurtosis of the normal distribution $\kappa_n = 3$. Therefore, the steady state excess of (7.4) is given by

$$\gamma_T = \frac{3}{\left(\frac{q^2}{4\mathcal{D}\tau} - 1\right)^2}. \tag{7.11}$$

As $\gamma_T > 0$ the distribution is leptokurtic, meaning that the tails are fatter, as we have already observed in Figure 7.1(b).
Now, we check, whether the part linear in the perturbations contributes to a deviation from a Gaussian temperature distribution:

$$\begin{aligned}\delta M(\alpha_1, \alpha_2; t) = B \int_0^t dt'\ e^{-(t-t')/\tau} \exp\left\{\left(\alpha_1^2 + \alpha_2^2\right)\left[4\mathcal{D}(t-t') + \frac{q_0^2}{4}\right]\right\} \delta N' \\ + B \int_0^t dt'\ e^{-(t-t')/\tau}\left[\alpha_1 \delta x_1' + \alpha_2 \delta x_2' + \frac{q_0}{2}\left(\alpha_1^2 \delta q_1' + \alpha_2^2 \delta q_2'\right)\right] e^{(\alpha_1^2+\alpha_2^2) q_0^2/4}.\end{aligned} \tag{7.12}$$

A Laplace transformation of the perturbations yields

$$\begin{aligned}\mathcal{L}\left[\delta M\right](\alpha_1, \alpha_2; s) = \frac{\tau B \delta \breve{N}(s) e^{(\alpha_1^2+\alpha_2^2) q_0^2/4}}{\tau s + 4\tau\mathcal{D}(\alpha_1^2 + \alpha_2^2) + 1} \\ + \frac{\tau B N_0}{\tau s + 1}\left[\alpha_1 \delta \breve{x}_1 + \alpha_2 \delta \breve{x}_2 + \frac{q_0}{2}\left(\alpha_1^2 \delta \breve{q}_1 + \alpha_2^2 \delta \breve{q}_2\right)\right] e^{(\alpha_1^2+\alpha_2^2) q_0^2/4}.\end{aligned} \tag{7.13}$$

In the first line we see the same effect as in the case of the steady state, namely a change of the momentum generating function due to the diffusion. From the second line we can conclude that in the dynamical case a Gaussian ansatz is still valid.

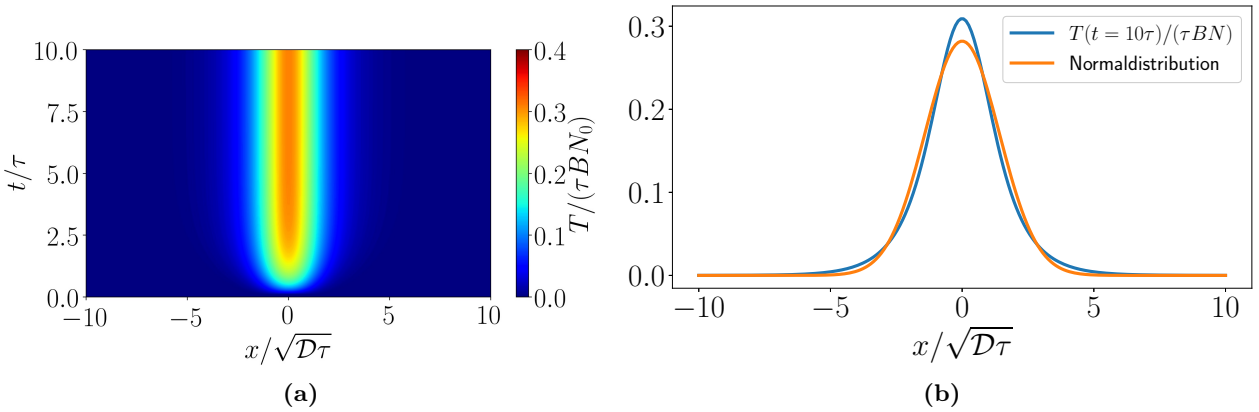

FIG. 7.1: Plot of the temperature according to (7.4). Panel **(a)** shows the time evolution of the temperature distribution until it reaches the steady state. This very steady state is shown in Panel **(b)**. For reasons of comparison also the normal distribution for standard deviation 4 is drawn.

We are now in the position to redo the steps of Chapter 4 from the point of view of an integro-differential equation that is capable to describe the influences of the temperature diffusion more accurate.

7.2. Normalisation

The first step is to calculate the normalisation of the photon wave function. This is done by integrating the continuity equation of (7.1) and leads to an integro-differential equation for the photon number:

$$\partial_t N = (\aleph p - \Gamma)N + P \int d^2x \ \left(\mathcal{G} * |\psi|^2\right) |\psi(\mathbf{x},t)|^2, \tag{7.14}$$

where the number of photons is defined according to

$$N(t) = \int d^2x \ |\psi(\mathbf{x},t)|^2. \tag{7.15}$$

Inserting the ansatz (7.2) and performing the remaining spatial integrals yields

$$\partial_t N = (\aleph p - \Gamma)N + PN \int_0^t dt' \frac{N' \exp\left(-\frac{t-t'}{\tau}\right) \exp\left[-\sum_{j=1}^{2} \frac{(x_{0j}-x'_{0j})^2}{4\mathcal{D}(t-t')+q_j'^2+q_j^2}\right]}{\pi\sqrt{[4\mathcal{D}(t-t')+q_1'^2+q_1^2][4\mathcal{D}(t-t')+q_2'^2+q_2^2]}}. \tag{7.16}$$

7.3. Cumulants Equations

In the following we derive the equations governing the evolution of the first and the second cumulant. For this purpose (7.1) is multiplied by the conjugated wave function ψ^* as well as by the weights that are also used in Chapter 4 and in Appendix C.
In order to find the equation for the first cumulant, we multiply (7.1) by $x_k - x_{0k}$ and find after integrating the resulting equation

$$\begin{aligned} i\hbar \int d^2x\ (x_k - x_{0k})\psi^* \partial_t \psi = &- \frac{\hbar^2}{2m} \int d^2x\ (x_k - x_{0k})\psi^* \nabla^2 \psi \\ &+ \frac{m\Omega^2}{2} \int d^2x\ (x_k - x_{0k})\mathbf{x}^2 |\psi(\mathbf{x},t)|^2 \\ &+ \left(g_T B + \frac{i\hbar}{2} P \right) \int d^2x\ (x_k - x_{0k}) \left(\mathcal{G} * |\psi|^2 \right) |\psi(\mathbf{x},t)|^2. \end{aligned} \tag{7.17}$$

Inserting (7.2) and performing the spatial integrals yields

$$\begin{aligned} i\hbar \left(\frac{\dot{x}_{0k}}{2} - iA_k q_k^2 \dot{x}_{0k} + i\frac{q_k^2}{2}\dot{C}_k \right) = &\frac{\hbar^2}{2m}(iC_k + 2A_k C_k q_k^2) + \frac{m\Omega^2}{2} x_{0k} q_k^2 \\ &+ \left(g_T B + \frac{i\hbar}{2} P \right) q_k^2 \int_0^t dt'\ G_k(t,t') N'(x'_{0k} - x_{0k}), \end{aligned} \tag{7.18}$$

with the memory kernel

$$G_k(t,t') = \frac{\exp\left[-\sum_{j=1}^{2} \frac{(x_{0j} - x'_{0j})^2}{4\mathcal{D}(t-t') + q_j'^2 + q_j^2} - \frac{t-t'}{\tau} \right]}{\pi \sqrt{[4\mathcal{D}(t-t') + q_1'^2 + q_1^2][4\mathcal{D}(t-t') + q_2'^2 + q_2^2]}\left[(4\mathcal{D}(t-t') + q_k'^2 + q_k^2 \right]}, \tag{7.19}$$

that does not only depend on the time difference $t - t'$ but also on the centres-of-mass and the widths at both times t and t'.
From the imaginary part of (7.18) we find

$$C_k = \frac{m\dot{x}_{0k}}{\hbar} - \frac{mPq_k^2}{\hbar} \int_0^t dt'\ G_k(t,t') N'(x'_{0k} - x_{0k}). \tag{7.20}$$

Reinserting this into the real part of (7.18) yields a second order integro-differential equation of second kind for the centre-of-mass evolution:

$$\ddot{x}_{0k} + \Omega^2 x_{0k} = 2PI_k - \frac{2\hbar^2 \tilde{g}}{m^2 \tau} \int_0^t dt'\ N' G_k(t,t')(x'_{0k} - x_{0k}), \tag{7.21}$$

where we inserted the dimensionless interaction strength (3.20). The remaining pump influence is determined by the quantities

$$I_k = -\frac{1}{\hbar q_k^2} \frac{d}{dt} q_k^2 \int_0^t dt'\ G_k(t,t') N'(x'_{0k} - x_{0k}) + \frac{\hbar A_k q_k^2}{m} \int_0^t dt'\ G_k(t,t') N'(x'_{0k} - x_{0k}). \tag{7.22}$$

Thus, the centre-of-mass coordinates obey an equation of motion for a harmonic oscillator that is perturbed by the pump on the one hand and by the temporally retarded interaction on the

other hand.

Now we turn our attention towards the second cumulant. Multiplying (7.1) by the conjugated wave function and by $(x - x_{0k})^2 - q_k^2/2$ yields after integration

$$\begin{aligned} i\hbar \int d^2x \left[(x_k - x_{0k}) - \frac{q_k^2}{2}\right] \psi^* \partial_t \psi = &-\frac{\hbar^2}{2m} \int d^2x \left[(x_k - x_{0k}) - \frac{q_k^2}{2}\right] \psi^* \nabla^2 \psi \\ &+ \frac{m\Omega^2}{2} \int d^2x \left[(x_k - x_{0k}) - \frac{q_k^2}{2}\right] \mathbf{x}^2 |\psi(\mathbf{x},t)|^2 \\ &+ (g_T B + \frac{i\hbar}{2} P) \int d^2x \left[(x_k - x_{0k}) - \frac{q_k^2}{2}\right] \left(\mathcal{G} * |\psi|^2\right) |\psi(\mathbf{x},t)|^2. \end{aligned} \tag{7.23}$$

Inserting also here the ansatz (7.2) and performing the integrals yields

$$\begin{aligned} i\hbar \left(\frac{q_k \dot{q}_k}{2} + i\frac{q_k^4 \dot{A}_k}{2}\right) = &-\frac{\hbar^2}{2m}\left(\frac{1}{2} + 2iA_k q_k^2 - 2A_k^2 q_k^4\right) + \frac{m\Omega^2}{4} q_k^4 \\ &+ \left(g_T B + \frac{i\hbar}{2} P\right) q_k^4 \int_0^t dt' \; N' G_k(t,t') \left[\frac{(x'_{0k} - x_{0k})^2}{4\mathcal{D}(t-t') + q_k'^2 + q_k^2} - \frac{1}{2}\right]. \end{aligned} \tag{7.24}$$

Also here we separate real and imaginary part. The latter results in an equation for A_k in terms of the widths:

$$A_k = -\frac{m\dot{q}_k}{2\hbar q_k} + \frac{mPq_k^2}{2\hbar} \int_0^t dt' \; N' G_k(t,t') \left[\frac{(x'_{0k} - x_{0k})^2}{4\mathcal{D}(t-t') + q_k'^2 + q_k^2} - \frac{1}{2}\right]. \tag{7.25}$$

Inserting this into the real part yields after several steps of simplification

$$\ddot{q}_k + \Omega^2 q_k = \frac{\hbar^2}{m^2 q_k^3} - \frac{4\hbar^2 \tilde{g} q_k}{m^2 \tau} \int_0^t dt' \; N' G_k(t,t') \left[\frac{(x'_{0k} - x_{0k})^2}{4\mathcal{D}(t-t') + q_k'^2 + q_k^2} - \frac{1}{2}\right] - q_k^3 J_k. \tag{7.26}$$

To shorten the equation we denote the pump influence upon the width dynamics by

$$\begin{aligned} J_k = &P^2 q_k \left\{ \int_0^t dt' \; N' G_k(t,t') \left[\frac{(x'_{0k} - x_{0k})^2}{4\mathcal{D}(t-t') + q_k'^2 + q_k^2} - \frac{1}{2}\right] \right\}^2 \\ &+ P \frac{d}{dt} \int_0^t dt' \; N' G_k(t,t') \left[\frac{(x'_{0k} - x_{0k})^2}{4\mathcal{D}(t-t') + q_k'^2 + q_k^2} - \frac{1}{2}\right]. \end{aligned} \tag{7.27}$$

Finally, (7.16), (7.21) and (7.26) represent the system of equations that is analysed in the remainder of this section in order to find the frequencies of the lowest-lying collective excitations.

7.4. Linearisation and Laplace Transformation

In the following we proceed by linearising the system (7.16), (7.21) and (7.26) in the neighbourhood of the fixed points. Afterwards, the equations are Laplace transformed in order to get rid of the remaining time integrals. In this way, algebraic equations for the collective frequencies

are obtained.
In order to linearise the equations we write the photon number as $N(t) = N_0 + \delta N(t)$, where N_0 denotes the steady state and $\delta N(t)$ small perturbations around this steady state. The same is done for the centre-of-mass coordinates $x_{0k}(t) = x_0^{(0)} + \delta x_{0k}(t)$ and for the widths $q_k = q_0 + \delta q_{0k}$, where already an isotropic trap is assumed, as the steady state values for both coordinate directions are the same.

The linearised version of (7.16) is given by

$$\begin{aligned}\partial_t \delta N \approx (\aleph p - \Gamma)(N_0 + \delta N) + P N_0 \left[(G_0 * 1) N_0 + (G * \delta N') + (G_0 * 1)\delta N\right] \\ - P N_0^2 q_0 \left[(G_1 * 1)(\delta q_1 + \delta q_2) + G_1 * \left(\delta q_1' + \delta q_2'\right)\right],\end{aligned} \tag{7.28}$$

where the convolution, see (5.8), is understood with respect to t' and the propagators $G_i(t)$ are given by

$$G_i(t) = \frac{e^{-t/\tau}}{\pi \left(4\mathcal{D}t + 2q_0^2\right)^{i+1}}. \tag{7.29}$$

In order to deal with the convolutions appearing in (7.28), this linear equation is Laplace transformed. Thus, the convolutions appearing in the equation are replaced by products of the Laplace transformed functions. With this, we obtain

$$\begin{aligned}&s\delta\breve{N}(s) - \delta N(0) = (\aleph p - \Gamma)\left(\frac{N_0}{s} + \delta\breve{N}(s)\right) + P N_0 \left\{\breve{G}_0(s)\left(\frac{N_0}{s} + \delta\breve{N}(s)\right)\right. \\ &+\mathcal{L}\left[(G_0 * 1)\delta N(t)\right](s) - N_0 q_0 \breve{G}_1(s)\left(\delta\breve{q}_1(s) + \delta\breve{q}_2(s)\right) \\ &\left.-N_0 q_0 \mathcal{L}\left[(G_1 * 1)\left(\delta q_1(t) + \delta q_2(t)\right)\right](s)\right\},\end{aligned} \tag{7.30}$$

where $\mathcal{L}[f](s)$ denotes the operator of the Laplace transformation acting on the function f at frequency s. Moreover, it is used that the Laplace transform of a constant C is given by C/s. The Laplace transformation of the propagators (7.29) is calculated as follows. First, we note that due to the Taylor expansion the identity

$$(1 + x)^{-l} = \sum_{n=0}^{\infty} \binom{-l}{n} x^n \tag{7.31}$$

holds. Here, the definition of the binomial coefficient is extended to negative upper numbers [86], such that the relation

$$\binom{-l}{n} = (-1)^n \binom{l + n - 1}{n}, \quad \text{for } n \in \mathbb{N},\ l \in \mathbb{N} \tag{7.32}$$

holds. By using (7.31) the Laplace transformation

$$\breve{G}_i(s) = \frac{1}{\pi}\mathcal{L}\left[e^{-t/\tau}\left(4\mathcal{D}t + 2q_0^2\right)^{-i-1}\right] \tag{7.33}$$

can be written as

$$\breve{G}_i(s) = \frac{1}{\pi(2q_0^2)^{i+1}} \sum_{n=0}^{\infty} \binom{-(i+1)}{n} \left(\frac{2\mathcal{D}}{q_0^2}\right)^n \mathcal{L}\left[e^{-t/\tau} t^n\right]. \tag{7.34}$$

Therefore the Laplace transformation is finally given by

$$\breve{G}_i(s) = \frac{\tau}{\pi(2q_0^2)^{i+1}} \sum_{n=0}^{\infty} \binom{-(i+1)}{n} \left(\frac{2\mathcal{D}\tau}{q_0^2}\right)^n \frac{n!}{(\tau s+1)^{n+1}}. \tag{7.35}$$

Thus, we find that the propagator is given by a Taylor series in the parameter $\mathcal{D}\tau/q_0^2$, that has already appeared in Section 7.1 as a smallness parameter for determining when a Gaussian ansatz for the temperature fails. Up to first order in $\mathcal{D}\tau/q_0^2$ the propagator reads:

$$\breve{G}_i(s) \approx \frac{\tau}{\pi(2q_0^2)^{i+1}} \left[\frac{1}{\tau s+1} - \frac{2\mathcal{D}\tau}{q_0^2} \frac{i+1}{(\tau s+1)^2}\right]. \tag{7.36}$$

Moreover, in (7.30) terms of the form $\mathcal{L}\left[(G_i * 1) f(t)\right]$, which are not a convolution, occur, as already in Chapter 6. There they led to couplings to higher frequencies. As in the present case the definition of the propagator is more complicated, also the coupling to higher frequencies turns out to be more involved. First we need to calculate the integral

$$\int_0^t dt'\; G_i(t-t') = \int_0^t dt'\; \frac{e^{-(t-t')/\tau}}{\pi\left[4\mathcal{D}(t-t') + 2q_0^2\right]^{i+1}}. \tag{7.37}$$

After applying the substitution $\theta = t - t'$ we can do the same steps as in the calculation above and find

$$\int_0^t dt'\; G_i(t-t') = \frac{1}{\pi(2q_0^2)^{i+1}} \sum_{n=0}^{\infty} \binom{-(i+1)}{n} \left(\frac{2\mathcal{D}}{q_0^2}\right)^n \int_0^t d\theta\; e^{-\theta/\tau} \theta^n. \tag{7.38}$$

Hence, the convolution of the propagator with unity is given by

$$(G_i * 1)(t) = \frac{\tau}{\pi(2q_0^2)^{i+1}} \sum_{n=0}^{\infty} \binom{-(i+1)}{n} \left(\frac{2\mathcal{D}\tau}{q_0^2}\right)^n n! \left[1 - e^{-t/\tau} \sum_{l=0}^{n} \frac{(t/\tau)^l}{l!}\right]. \tag{7.39}$$

Therefore, the Laplace transformation $\mathcal{L}\left[(G_i * 1) f(t)\right]$ yields

$$\mathcal{L}\left[(G_i * 1) f(t)\right] = \frac{\tau}{\pi(2q_0^2)^{i+1}} \sum_{n=0}^{\infty} \binom{-(i+1)}{n} \left(\frac{2\mathcal{D}\tau}{q_0^2}\right)^n n! \left[\breve{f}(s) - \sum_{l=0}^{n} \frac{1}{l!\tau^l} \frac{d^l}{ds^l} \breve{f}(s+1/\tau)\right], \tag{7.40}$$

which is also a series in the parameter $\mathcal{D}\tau/q_0^2$. Moreover, we also find that derivatives of $\breve{f}$ occur, which is due to the finite sum in the curly brackets. Up to first order in the diffusion (7.40)

simplifies to

$$\mathcal{L}\left[(G_i * 1)f(t)\right] \approx \frac{\tau}{\pi(2q_0^2)^{i+1}} \left\{ \breve{f}(s) - \breve{f}(s+1/\tau) - \frac{2(i+1)\mathcal{D}\tau}{q_0^2} \left[\breve{f}(s) - \breve{f}(s+1/\tau) - \frac{1}{\tau}\frac{d}{ds}\breve{f}(s+1/\tau) \right] \right\}. \tag{7.41}$$

We assume further that τ represents a long time scale, as was already figured out in Chapter 2. Then $1/\tau$ amounts to a small frequency and we can absorb the derivative $\frac{d}{ds}\breve{f}(s+1/\tau)$ in (7.41) by the first two terms of the expansion of the translation operator $\exp\left(\frac{1}{\tau}\frac{d}{ds}\right)$:

$$\mathcal{L}\left[(G_i * 1)f(t)\right] \approx \frac{\tau}{\pi(2q_0^2)^{i+1}} \left\{ \breve{f}(s) - \breve{f}(s+1/\tau) - \frac{2(i+1)\mathcal{D}\tau}{q_0^2} \left[\breve{f}(s) - \breve{f}(s+2/\tau) \right] \right\}. \tag{7.42}$$

This can be rewritten by using the Laplace transformed propagator $\breve{G}_i$ from (7.35) as

$$\mathcal{L}\left[(G_i * 1)f(t)\right] \approx \breve{G}_i(0)\breve{f}(s) - \frac{\tau}{\pi(2q_0^2)^{i+1}} \left[\breve{f}(s+1/\tau) - \frac{2(i+1)\mathcal{D}\tau}{q_0^2}\breve{f}(s+2/\tau) \right]. \tag{7.43}$$

Linearising the centre-of-mass equation (7.21) thus yields

$$\delta\ddot{x}_{0k} + \Omega^2(x_{0k}^{(0)} + \delta x_{0k}) = 2P\delta I_k - \frac{\hbar^2\tilde{g}N_0}{m^2\tau}\left[G_1 * \delta x'_{0k} - (G_1 * 1)\,\delta x_{0k}\right], \tag{7.44}$$

where the linear pump influence is given by

$$\delta I_k = -\frac{N_0}{\hbar}\partial_t\left[G_1 * \delta x'_{0k} - (G_1 * 1)\delta x_{0k}\right] + \frac{\hbar A_k q_k^2 N_0}{m}\left[G_1 * \delta x'_{0k} - (G_1 * 1)\delta x_{0k}\right]. \tag{7.45}$$

From this equation we see, that the photon wave function is centred around the origin, i.e. $x_{0k}^{(0)} = 0$. As done above for the normalisation, we perform also here a Laplace transformation and find

$$\begin{aligned} s^2\delta\breve{x}_{0k} - \delta\dot{x}_{0k}(0) - s\delta x_{0k}(0) + \Omega^2\delta\breve{x}_{0k} =& 2P\mathcal{L}[\delta I_k] \\ & - \frac{2\hbar^2\tilde{g}N_0}{m^2\tau}\left(\breve{G}_1\delta\breve{x}_{0k} - \mathcal{L}\left[(G_1 * 1)\delta x_{0k}\right]\right), \end{aligned} \tag{7.46}$$

where the transformation of the pump term is given by

$$\begin{aligned} \mathcal{L}[\delta I] =& -\frac{N_0}{\hbar q_0^4}\left\{ s\breve{G}_1(s)\delta\breve{x}_{0k}(s) - G_1(0)\delta x_{0k}(0) - \mathcal{L}\left[\frac{d}{dt}(G_1 * 1)\delta x_{0k}\right] \right\} \\ & + \frac{\hbar N_0 A_0 q_0^2}{m}\left\{ \breve{G}_1\delta\breve{x}_{0k} - \mathcal{L}\left[(G_1 * 1)\delta x_{0k}\right] \right\}. \end{aligned} \tag{7.47}$$

Note, that we write down the explicit form of these equations in the next Sections, when we go for the collective frequencies.

Finally, the width equation (7.26) is left to be linearised. Here, we find

$$\begin{aligned}\delta\ddot{q}_k + \Omega^2(q_0+\delta q_k) = &\frac{\hbar^2}{m^2 q_0^3} - \frac{3\hbar^2\delta q_k}{m^2 q_0^4} + \frac{2\hbar^2\tilde{g}}{m^2\tau}\left\{(G_1*1)N_0 q_0\right.\\ &+G_2*\left[2q_0^2\delta N' - q_0^2 N_0\left(\delta q_1' + \delta q_2' + 2\delta q_k'\right)\right] - (G_2*1)q_0^2 N_0\left(\delta q_1+\delta q_2\right)\\ &\left.4\mathcal{D}\left((G_2 t)*1\right)\left(q_0\delta N + N_0\delta q_k\right)\right\} + q_0^3 J_0 + q_0^3\delta J_k + 3q_0^2 J_0\delta q_k. \end{aligned} \tag{7.48}$$

The pump influence is given by

$$J_0 = \frac{P^2 q_0 N_0^2}{4}\left(G_3*1\right) - \frac{PN_0}{2}\frac{d}{dt}\left(G_2*1\right) \tag{7.49}$$

and the part linear in the perturbations reads

$$\begin{aligned}\delta J_k = &- P^2 N_0\left\{G_4*\left[-q_0^3\delta N' + \frac{N}{2}\left(2\delta q_k' + \delta q_1' + \delta q_2'\right)\right] + \frac{N}{2}(G_4*1)(\delta q_1+\delta q_2)\right.\\ &\left.-\mathcal{D}\left((G_4 t)*1\right)q_0\delta N + N_0\delta q_k\right\} - \frac{P}{2}\frac{d}{dt}\left\{G_2*\left[2q_0^2\delta N' - N_0\left(2\delta q_k' + \delta q_1' + \delta q_2'\right)\right]\right.\\ &\left.-(G_2*1)N_0(2\delta q_k+\delta q_1+\delta q_2) + 4\mathcal{D}\left((G_2 t)*1\right)\delta N\right\}. \end{aligned} \tag{7.50}$$

Performing a Laplace transformation yields

$$\begin{aligned}&s^2\delta\breve{q}_k - \delta\dot{q}_k(0) + s\delta q_k(0) + \Omega^2(\frac{q_0}{s} + \delta\breve{q}_k) = \frac{\hbar^2}{sm^2 q_0^3} - \frac{3\hbar\delta\breve{q}_k}{m^2 q_0^4}\\ &+\frac{2\hbar^2\tilde{g}}{m^2\tau}\left\{\frac{\breve{G}_1(s)}{s}N_0 q_0 + \breve{G}_2\left[2q_0^2\delta\breve{N} - q_0^2 N_0\left(\delta\breve{q}_2 + \delta\breve{q}_1 + 2\delta\breve{q}_k\right)\right]\right\}\\ &+\mathcal{L}\left[G_2(t-t')\left[4\mathcal{D}(t-t')\left(q_0\delta N(t) + N_0\delta q_k(t)\right) - q_0^2 N_0\left(\delta q_2(t)+\delta q_1(t)\right)\right]\right]\\ &+q_0^3\mathcal{L}[J_0] + q_0^3\mathcal{L}\left[\delta J_k\right] + 3q_0^2\mathcal{L}\left[J_0\delta q_k\right]. \end{aligned} \tag{7.51}$$

The Laplace transformed pump terms are given by

$$\mathcal{L}[J_0] = \frac{P^2 q_0 N^2}{4}\frac{\breve{G}_3}{s} - \frac{PN_0}{2}\breve{G}_2 \tag{7.52}$$

and

$$\begin{aligned}\mathcal{L}[\delta J_k] = &- P^2 N_0\left\{\breve{G}_4\left[-q_0^3\delta\breve{N} + \frac{N}{2}\left(2\delta\breve{q}_k + \delta\breve{q}_1 + \delta\breve{q}_2\right)\right] + \frac{N}{2}\mathcal{L}\left[G_4*(\delta q_1+\delta q_2)\right]\right.\\ &\left.-\mathcal{D}q_0[G_4 t]\delta\breve{N} + N_0\mathcal{D}\mathcal{L}\left[(G_4 t)*\delta q_k\right]\right\} - \frac{P}{2}\left\{4\mathcal{D}\mathcal{L}\left[(G_4 t)*\delta N\right]\right.\\ &\left.sG_2\left[2q_0^2\delta\breve{N} - N_0\left(2\delta\breve{q}_k + \delta\breve{q}_1 + \delta\breve{q}_2\right)\right] - N_0\mathcal{L}\left[G_2*(2\delta q_k+\delta q_1+\delta q_2)\right]\right\} \end{aligned} \tag{7.53}$$

Note, that the terms quadratic in P can be neglected in practical calculations, as they are proportional to $\left(\frac{\partial n}{\partial T}\right)^2$ and we consider only a theory that is of first order in $\frac{\partial n}{\partial T}$, cf. Chapter 4.

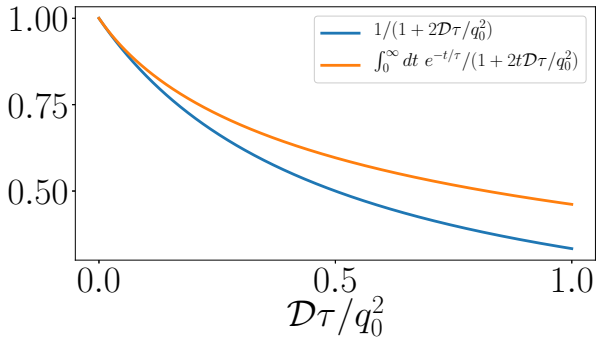

FIG. 7.2: Functional dependencies of the propagators (7.56) on the diffusion. In the current experimental case we have $\mathcal{D}\ \tau/q_0^2 \sim 1 \times 10^{-3}$.

7.5. Steady State

We start by evaluating the equations in case of the steady state, i.e. in the limit $s \to 0$. From (7.30) we find in the limit $s \to 0$ for the steady state of the photon number

$$N_0 = \frac{(\Gamma - \aleph p)}{P\breve{G}_0(0)} \tag{7.54}$$

and of the condensate width

$$0 = -\frac{1}{l_{\mathrm{osc}}^4} + \frac{1}{q_0^4} + \frac{2\tilde{g}N_0}{\tau}\breve{G}_1(0), \tag{7.55}$$

where we introduced the harmonic oscillator length $l_{\mathrm{osc}} = \sqrt{\hbar/(m\Omega)}$. Comparing (7.54) to the corresponding equation of the two Gaussian approach (4.46), we can identify that $\tau G^0_{\mathrm{T}\psi}$ corresponds to $\breve{G}_0(0)$ in the above equation. In order to compare these two quantities, we write down the respective formulas next to each other

$$G^0_{\mathrm{T}\psi} = \frac{1}{2\pi q_0^2}\frac{1}{1+2\mathcal{D}\tau/q_0^2}, \tag{7.56a}$$

$$\breve{G}_0(0) = \frac{1}{2\pi q_0^2}\int_0^\infty dt\ \frac{e^{-t}}{1+2\mathcal{D}\tau t/q_0^2}, \tag{7.56b}$$

where we changed the integration constant in the latter equation from t to t/τ. It can be seen in (7.56) that the diffusion is taken into account quite differently. Whereas in the approach with two Gaussians the diffusion only influences via the steady state, in the propagator approach the whole history of the diffusion plays a role in the photon steady state. The functional dependences of these two approaches on the diffusion is plotted in Figure 7.2. The two-Gaussian approach overestimates the influence of the diffusion especially in the case of a strong, but finite diffusion, as we have $\breve{G}_0(0) \geq G^0_{\mathrm{T}\psi}$ according to Figure 7.2. Although, in the current experiments, where $\mathcal{D}\tau/q_0^2 \sim 1 \times 10^{-3}$, see (7.29), the difference between these approaches is negligible, in future experiments the difference between the two approaches may become important. For a detailed discussions we refer to Section 4.4.

Next we investigate the stability of this steady state. For this purpose we proceed as in Chapter 4 by first analysing the dipole mode and, afterwards, examining the quadrupole together with the breathing mode.

7.6. Dipole Mode

As we have already seen in (7.44), the centre-of-mass equation does not couple to the other dynamical degrees of freedom. Therefore, we will analyse in this subsection the oscillation frequency of the dipole mode. It is again given by the singularities of the Laplace transformation of $\delta x_{0k}(t)$. The equation for the dipole mode is given by

$$\begin{aligned}
&\delta\breve{x}_{0k}(s)\left\{s^2+\Omega^2+\frac{2\hbar^2\tilde{g}N_0}{m^2\tau}\left[\breve{G}_1(s)-\breve{G}_1(0)\right]-2P\left(-\frac{N_0 s}{\hbar q_0^4}+\frac{\hbar N_0 A_0 q_0^2}{m}\right)\left(\breve{G}_1(s)-\breve{G}_1(0)\right)\right\}\\
=&\delta\dot{x}_{0k}(0)+s\delta x_{0k}(0)-\frac{\tau\delta x_{0k}(s+1/\tau)}{\pi(2q_0^2)^2}\left\{\frac{2\hbar^2\tilde{g}N_0}{m^2\tau}+2PN_0\left[\frac{s+1/\tau}{\hbar q_0^4}+\frac{\hbar A_0 q_0^2}{m}\right]\right\}\\
&+\frac{\tau\delta\breve{x}_{0k}(s+2/\tau)}{\pi(2q_0^2)^2}\left\{\frac{2\hbar^2\tilde{g}N_0}{m^2\tau}\frac{4\mathcal{D}\tau}{q_0^2}+2PN_0\frac{4\mathcal{D}\tau}{q_0^2}\left[\frac{s+2/\tau}{\hbar q_0^4}+\frac{\hbar A_0 q_0^2}{m}\right]\right\}. \qquad (7.57)
\end{aligned}$$

From the analysis of the homogeneous case in the previous Section we know that the most relevant frequencies of the inverse Laplace transformation, i.e. the lowest order in the thermo-optic perturbation series, are already calculated by only considering the initial conditions of the perturbation on the right-hand side of (7.57). Therefore, we find from (7.57) the lowest order solution

$$\delta\breve{x}_{0k}(s)=\frac{\delta\dot{x}_{0k}(0)+s\delta x_{0k}(0)}{s^2+\Omega^2+\frac{2\hbar^2\tilde{g}N_0}{m^2\tau}\left[\breve{G}_1(s)-\breve{G}_1(0)\right]-2P\left(-\frac{N_0 s}{\hbar q_0^4}+\frac{\hbar N_0 A_0 q_0^2}{m}\right)\left[\breve{G}_1(s)-\breve{G}_1(0)\right]}. \qquad (7.58)$$

The singularities of (7.58) are provided by the roots of the denominator:

$$0=s^2+\Omega^2+\frac{2\hbar^2\tilde{g}N_0}{m^2\tau}\left[\breve{G}_1(s)-\breve{G}_1(0)\right]-2P\left(-\frac{N_0 s}{\hbar q_0^4}+\frac{\hbar N_0 A_0 q_0^2}{m}\right)\left[\breve{G}_1(s)-\breve{G}_1(0)\right]. \qquad (7.59)$$

Again, only in case of a strong diffusion, this equation differs from the one in Section 4.5, as this difference is due to the propagators. To compare this in more detail with the results of Section 4.5 it is convenient to integrate (4.66), as this is the quantity, which is in the current approach hidden in the propagator. We find

$$\delta y_{0k}=\int_0^t\frac{dt'}{\tau}\,e^{-(t-t')/\tau}\delta x_{0k}(t'). \qquad (7.60)$$

Note, that in this equation no diffusion is present. This means that the diffusion only enters through the steady state, as can also be seen by inserting (7.60) into (4.67). Therefore, we conclude that the main difference between the approach presented in this part and the previous approach using two equations is that, due to using a propagator, the effects brought in by the diffusion are taken into account dynamically, whereas in the other method only static diffusion effects are considered. Both approaches coincide if only a small diffusion is present, as it is,

indeed, the case in the current experiments, but in future experiments, the diffusion might be much larger.

7.7. Breathing and Quadrupole Modes

As the width dynamics couples linearly to the dynamics of the photon number, we have to take into account the coupled system of the equations for the photon number and for both widths. Due to (7.30) the photon number obeys the equation

$$\begin{aligned}
&\delta\breve{N}(s)\left\{s-\left[\aleph p-\Gamma+P_0N_0\left(\breve{G}_0(s)+\breve{G}_0(0)\right)\right]\right\}+\left(\delta\breve{q}_1(s)+\delta\breve{q}_2(s)\right)P_0N_0^2q_0\left[\breve{G}_1(s)+\breve{G}_1(0)\right]\\
=&\delta N(0)+\left(\aleph p-\Gamma+PN_0\breve{G}_0(s)\right)\frac{N_0}{s}+\frac{\tau PN_0}{2\pi q_0^2}\left[-\delta\breve{N}(s+\frac{1}{\tau})+\frac{4\mathcal{D}\tau}{q_0^2}\delta\breve{N}(s+\frac{2}{\tau})\right]\\
&-\frac{N_0q_0\tau PN_0}{\pi(2q_0^2)^2}\left[-\delta\breve{q}_1(s+\frac{1}{\tau})-\delta\breve{q}_2(s+\frac{1}{\tau})+\frac{4\mathcal{D}\tau}{q_0^2}\left(-\delta\breve{q}_1(s+\frac{2}{\tau})-\delta\breve{q}_2(s+\frac{2}{\tau})\right)\right]. \qquad (7.61)
\end{aligned}$$

From (7.48) we find for the width in the 1-direction the equation

$$\begin{aligned}
&\delta\breve{q}_1(s)\left\{s^2+\Omega^2+\frac{3\hbar^2}{m^2q_0^4}+\left[\frac{2q_0^2N_0\hbar^2\tilde{g}}{m^2\tau}-\frac{q_0^3Ps}{2}\right]\left[3\breve{G}_2(s)+\breve{G}_2(0)\right]\right\}\\
&+\delta\breve{q}_2(s)\left\{\left[\frac{2q_0^2N_0\hbar^2\tilde{g}}{m^2\tau}-\frac{q_0^3Ps}{2}\right]\left[\breve{G}_2(s)+\breve{G}_2(0)\right]\right\}+\delta\breve{N}(s)\breve{G}_2(s)q_0^2\left[-\frac{4\hbar^2\tilde{g}}{\tau m^2}+Ps\right]\\
=&\delta\dot{q}_1(0)+s\delta q_1(0)+\frac{1}{s}\left[-\Omega^2q_0+\frac{\hbar^2}{m^2q_0^3}+\frac{2\hbar^2\tilde{g}}{m^2\tau}\breve{G}_1(s)\right]\\
&+\frac{2\hbar^2\tilde{g}}{m^2\tau}\left\{4\mathcal{D}\frac{d}{ds}\left[\breve{G}_2(0)\left(q_0\delta\breve{N}(s)+N_0\delta\breve{q}_1(s)\right)-\frac{\tau}{\pi(2q_0^2)^3}\left(q_0\delta\breve{N}(s+\frac{1}{\tau})+N_0\delta\breve{q}_1(s+\frac{1}{\tau})\right.\right.\right.\\
&\left.\left.\left.-\frac{4\mathcal{D}\tau}{q_0^2}\left\{q_0\delta\breve{N}(s+\frac{2}{\tau})+N_0\delta\breve{q}_1(s+\frac{2}{\tau})\right\}\right)\right]\right\}-q_0^3\frac{PN_0s}{2}\breve{G}_2(s)\\
&+q_0^3\frac{PN_0s}{2}\frac{\tau}{\pi(2q_0^2)^3}\left\{3\delta\breve{q}_1(s+\frac{1}{\tau})+\delta\breve{q}_2(s+\frac{1}{\tau})-\frac{4\mathcal{D}\tau}{q_0^2}\left[3\delta\breve{q}_1(s+\frac{2}{\tau})+\delta\breve{q}_2(s+\frac{2}{\tau})\right]\right\}\\
&+4\mathcal{D}\frac{d}{ds}\left[\breve{G}_4(s)\delta\breve{N}(s)-\frac{\tau}{\pi(2q_0^2)^5}\left(\delta\breve{N}(s+\frac{1}{\tau})+\frac{4\mathcal{D}\tau}{q_0^2}\delta\breve{N}(s+\frac{2}{\tau})\right)\right]. \qquad (7.62)
\end{aligned}$$

From (7.62) we conclude that a similar equation for the width in the 2-direction can be found by interchanging the indices $1 \leftrightarrow 2$. The widths do not only couple to higher frequencies but, due to terms that are proportional to the time variable, also derivatives in the frequency variable occur on the right-hand side. But from the previous Sections we learned that the terms involving the initial conditions yield already the dominant frequencies of the oscillations. Therefore, we consider only those terms in the following analysis. The resulting system can be written in

vector-matrix form as

$$L(s)\begin{pmatrix}\delta\breve{N}(s)\\ \delta\breve{q}_1(s)\\ \delta\breve{q}_2(s)\end{pmatrix}=\begin{pmatrix}\delta N(0)\\ \delta\dot{q}_1(0)+s\delta q_1(0)\\ \delta\dot{q}_2(0)+s\delta q_2(0)\end{pmatrix}. \tag{7.63}$$

Note, that the variable s on the right-hand side, yields simply the phase between the velocity of the width and the width itself. The entries of the system matrix are given by

$$L_{N,N}=s-\left[\aleph p-\Gamma+P_0N_0\left(\breve{G}_0(s)+\breve{G}_0(0)\right)\right], \tag{7.64a}$$

$$L_{N,q_1}=P_0N_0^2q_0\left[\breve{G}_1(s)+\breve{G}_1(0)\right]=L_{N,q_2}, \tag{7.64b}$$

$$L_{q_1,N}=\breve{G}_2(s)q_0^2\left[-\frac{4\hbar^2\tilde{g}}{\tau m^2}+Ps\right]=L_{q_2,N}, \tag{7.64c}$$

$$L_{q_1,q_1}=s^2+\Omega^2+\frac{3\hbar^2}{m^2q_0^4}+\left[\frac{2q_0^2N_0\hbar^2\tilde{g}}{m^2\tau}-\frac{q_0^3Ps}{2}\right]\left[3\breve{G}_2(s)+\breve{G}_2(0)\right]=L_{q_1,q_1}, \tag{7.64d}$$

$$L_{q_1,q_2}=\left[\frac{2q_0^2N_0\hbar^2\tilde{g}}{m^2\tau}-\frac{q_0^3Ps}{2}\right]\left[\breve{G}_2(s)+\breve{G}_2(0)\right]=L_{q_2,q_1}. \tag{7.64e}$$

Here again we are looking for the roots of the determinant of the system matrix $L(s)$. The numerical results are shown in Figure 7.3. We encounter that also the breathing mode is shifted to lower frequencies in contrast to the case of a contact interaction, cf. Appendix C, which is the same behaviour as in 7.3. Moreover, we see that the quadrupole mode is basically undamped, whereas the breathing mode is slightly damped. In contrast to these two modes, the perturbation of the photon number, that can only undergo a diffusive motion, is damped strongest and cannot oscillate at all. Contrarily to all results we got before, the modes of the widths turn out to be stable for all photon numbers.

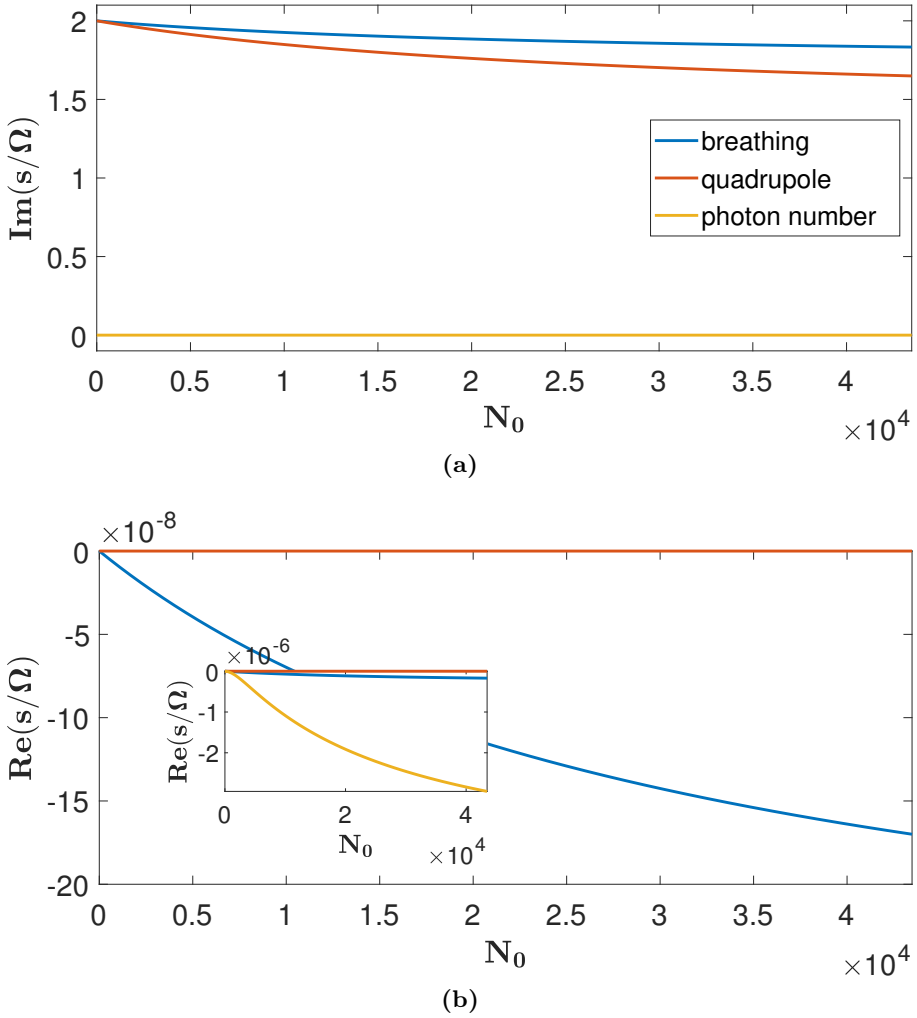

FIG. 7.3: Breathing and quadrupole modes. In **(a)** the frequency is plotted, whereas in **(b)** the corresponding damping is shown. The inlet shows also the damping of the photon number.

8. Conclusion

The web of our life is of a mingled yarn, good and ill together:
our virtues would be proud, if our faults whipped them not;
and our crimes would despair, if they were not cherished by our virtues.

William Shakespeare, All's Well that Ends Well, Act IV, Scene 3

Inspired by the simple mean-field theory for exciton-polariton condensates in reference [34], the aim of this thesis is to find a description of a photon Bose-Einstein condensate that is of similar ease and able to describe the effective photon-photon interaction which arises due to the thermo-optic effect. With this we then investigate the influence of the thermo-optic nonlinearity on collective excitation frequencies, which have not yet been found experimentally.

For this purpose we start in Chapter 2 with Maxwell's equations and take also a temperature dependence of the refractive index of the dye solution into account. We then obtain a system of two coupled partial differential equation in three spatial dimensions. However, as the longitudinal modes for both the temperature and the electric field are fixed, a corresponding system of evolution equations (2.81) and (2.82) in the remaining two transversal degrees of freedom is derived. This system also incorporates the pump and loss processes. It turns out, that these two equations are similar to the corresponding mean-field equations for the exciton-polariton condensate, see Table 2.1.
As a first step in the analysis we investigate the homogeneous condensate. For this purpose we perform in Chapter 3 a linear stability analysis of the system (2.81) and (2.82), where the trap is neglected. We find that the condensate is possibly unstable in the long wavelength limit, cf. (3.40) and the subsequent discussion. Moreover, an eigenvalue zero is always present in this limit, such that the Goldstone theorem is valid, see also Figure 3.4. However, for slightly smaller wavelengths the condensate tends to get unstable due to the thermo-optic interaction, but it gets stable again in the small wavelength limit, as described by the formulas (3.49) and (3.56). In Chapter 6 we point out, that the same results can also be derived by using an approach, where the temperature equation (2.82) is eliminated by means of a Green's function, see Chapter 5.
The case of a harmonically trapped condensate is addressed in Chapter 4. Here, we aim for the imprint of the thermo-optic interaction upon the lowest-lying collective frequencies, that are usually calculated via a variational approach relying on the action principle [77]. Nonetheless, this approach cannot be used here, as no action principle for open-dissipative systems exists. Instead we use a method that is based on calculating the cumulants equations of motion [81]. In Appendix C we show that this method coincides with the variational approach in case of an ordinary Gross-Pitaevskii equation. With this method and the assumption that the temperature is also Gaussian shaped (4.4) as the condensate wave function, we can then calculate the steady state of the trapped condensate as well as its stability. However, in Chapter 7 we show that the ansatz for the temperature is only valid, if the diffusion has a small influence, as (7.9) and

Figure 7.1 demonstrate. It turns out that the steady state is the one of a closed Gross-Pitaevskii equation with a contact interaction modified by the temperature diffusion, as a comparison of (C.22) and (4.41) and Figure 7.2 shows. Therefore, we conclude, that the usual experimental procedure for measuring the interaction strength [35,53], which relies on (C.22), has a systematic error of ignoring the temperature diffusion.
The analysis of the perturbations of the trapped steady state, which is done in Sections 4.5 and 4.6 as well as in Sections 7.6 and 7.7, reveals that the thermo-optic interaction affects modes that are not influenced by a usual contact interaction. In this manner Figure 4.7 shows that the dipole mode breaks the Kohn theorem, so that the frequency of the dipole mode becomes smaller then the trapping frequency. Moreover, also the breathing mode, that is according to (C.24a) always twice the trapping frequency, experiences a shift to lower frequencies, as Figure 4.8 indicates. Finally, also the quadrupole mode undergoes a frequency shift to smaller values, see Figure 4.8. In Section 4.7 two possible experiments on how to detect those modes are discussed.

To sum up, in this thesis a mean-field description for photon Bose-Einstein condensates under the influence of a thermo-optic photon-photon interaction is derived. With this theory at hand, the lowest-lying collective frequencies of a harmonically trapped condensate are calculated, inter alia. Those frequencies can be measured via a streak camera or by investigating the eigenfrequencies of the dye-filled cavity.

9. Outlook

If we shadows have offended,
Think but this, and all is mended,
That you have but slumber'd here
While these visions did appear.
And this weak and idle theme,
No more yielding but a dream,
Gentles, do not reprehend:
if you pardon, we will mend:

William Shakespeare, A Midsummer Night's Dream, ll. 2275-2282

As the mean-field equations, which are derived in Chapter 2, have been extensively investigated, we briefly discuss points that still offer prospects for future works.

9.1. Matter Degrees of Freedom

At first we share thoughts on how the matter degrees of freedom can be included in order to complete the analysis of the system. For this purpose, it is more convenient to describe the condensate wave function $\psi(\mathbf{x}, t)$ by its projections on the unperturbed cavity eigenmodes, i.e. the eigenmodes of the two-dimensional harmonic oscillator, see (4.93). The corresponding expansion of the condensate wave function is already given in (4.98). As the harmonic oscillator eigenfunctions (4.93) are real, we can also expand the temperature distribution in those eigenfunctions

$$T(\mathbf{x}, t) = \sum_{\beta} b_{\beta}(t)\phi_{\beta}(\mathbf{x}), \tag{9.1}$$

where b_β are real-valued expansion coefficients defined by

$$b_{\beta}(t) = \int d^2x \; T(\mathbf{x}, t)\phi_{\beta}(\mathbf{x}, t). \tag{9.2}$$

The aim is now to propose a minimal model, that is able to describe the thermo-optic effect and the spectral dynamics of the molecules. For this purpose we take the coherent part from equations (2.81) and (2.82) and project those reduced equations on the eigenstates (4.93) in order to find the equations of motion for the expansion coefficients (4.98) and (9.2), respectively.

For the condensate wave function we find:

$$i\hbar\dot{a}_\alpha = \hbar\omega_\alpha a_\alpha + g_T \sum_{\mu\nu} c_{\alpha\mu\nu} t_\mu a_\nu, \tag{9.3}$$

where the eigenfrequency ω_α is defined in (4.100), furthermore

$$c_{\lambda\mu\nu} = \int d^2x \; \phi_\lambda(\mathbf{x})\phi_\mu(\mathbf{x})\phi_\nu(\mathbf{x}) \tag{9.4}$$

are the coupling constants that arise due to the nonlinear coupling of the temperature to the photon equation of motion. Similarly, we find for the temperature

$$\dot{t}_\beta = -\frac{1}{\tau} t_\beta + B \sum_{\mu\nu} c_{\beta\mu\nu} a^*_\mu a_\nu. \tag{9.5}$$

We model now the occupation numbers of the ground and the excited state of the molecules by a two-level system, where the emission and absorption rate obey the Kennard-Stepanov relation (A.17). Thus, the rate equation for the occupation number N_2 of the upper state is given by

$$\dot{N}_2 = \sum_\alpha \left[-B_{21}(\omega_\alpha) N_2 |a_\alpha|^2 + B_{12}(\omega_\alpha) N_1 |a_\alpha|^2 \right] + P N_1 - \gamma N_2. \tag{9.6}$$

Here, $B_{21}(\omega)$ and $B_{12}(\omega)$ denotes the stimulated emission and absorption coefficient at the frequency ω, whereas P and γ are the rate coefficients for the pump and the nonradiative decay of the molecules, respectively. The corresponding rate equation for the lower molecular energy state reads

$$\dot{N}_1 = -\dot{N}_2. \tag{9.7}$$

Note, that these equations are a generalisation of the usual laser rate equations, compare to [87]. The material degrees of freedom are coupled to the coefficients of the photon wave function by adding the corresponding photon number rate equation in the imaginary part of (9.3):

$$i\hbar\dot{a}_\alpha = \hbar\omega_\alpha a_\alpha + g_T \sum_{\mu\nu} c_{\alpha\mu\nu} t_\mu a_\nu + \frac{i\hbar}{2} \left[B_{21}(\omega_\alpha) N_2 - B_{12}(\omega_\alpha) N_1 - \kappa \right] a_\alpha, \tag{9.8}$$

where κ denotes the cavity decay. As the total number of molecules $N = N_1 + N_2$ is constant in time due to (9.7), the matter degrees of freedom are fully described by one equation for the population inversion $D = N_2 - N_1$. Finally, with the definition of the vacuum population inversion

$$D_0 = N \frac{P - \gamma}{P + \gamma} \tag{9.9}$$

and the relaxation time of the population inversion

$$\theta = \frac{1}{P + \gamma}, \tag{9.10}$$

we end up with the following system of equations

$$\dot{D} = \frac{D_0 - D}{\theta} + \sum_{\alpha} \left[\left(N B_{-}^{\alpha} - D B_{+}^{\alpha} \right) |a_\alpha|^2 \right], \tag{9.11a}$$

$$i\hbar \dot{a}_\alpha = \hbar \omega_\alpha a_\alpha + g_T \sum_{\mu\nu} c_{\mu\nu\alpha} t_\mu a_\nu + \frac{i\hbar}{4} \left[-B_{-}^{\alpha} N + B_{+}^{\alpha} D - 2\kappa \right] a_\alpha, \tag{9.11b}$$

$$\dot{t}_\beta = -\frac{1}{\tau} t_\beta + B \sum_{\mu\nu} c_{\mu\nu\beta} a_\mu^* a_\nu. \tag{9.11c}$$

Here, we introcued the rates

$$B_{\pm}^{\alpha} = B_{12}(\omega_\alpha) \pm B_{21}(\omega_\alpha). \tag{9.12}$$

By using the Kennard-Stepanov (A.17) relation, (9.12) can be brought to the form

$$B_{\pm}\alpha = B_{12}(\omega_\alpha) \left(1 \pm e^{-\xi_\alpha} \right), \tag{9.13}$$

with the Kennard-Stepanov exponent $\xi_\alpha = -\hbar(\omega_\alpha - \omega_{\mathrm{ZPL}})/(k_B T)$. From (9.12) we see, that in the case of a laser, where we have $\xi_\alpha = 0$, the coefficient B_{-}^{α} vanishes. As we are looking for the lowest-lying frequencies, we proceed as in Section 3.4 by only considering the modes with the three lowest energies. Preliminary results of a simulation of (9.11) are shown in Figure 9.1. Here we use the initial state that the main contribution of photons is in the ground state ϕ_{00} and only a very small amplitude of the first excited state ϕ_{01} is present. The parameters are adjusted in a way, that the main features of the model can still be found, but the computation time stays short. In panels (a) and (b), where the corresponding projection of the photon distribution is plotted, one can see that in the x_1 direction only the width of the condensate changes, whereas in the x_2 direction also the centre-of-mass oscillates. The latter stems from the initial condition that also a little contribution of the ϕ_{01} mode is in the total state. The first stems from the thermo-optic interaction, since the dominating part of the initial state is the ground state ϕ_{00}. But due to the interaction, the condensate broadens up and the widths start to oscillate. Due to the initial conditions these oscillations can be identified with the breathing mode. The corresponding temperature distribution can be found in panels (c) and (d), respectively. Panel (e) shows to centre-of-mass motion, which corresponds to the dipole mode once the temperature reaches its equilibrium. As it appears, the centre-of-mass oscillation gets damped as the time evolves. Finally, in panel (f) the temporal evolution of the widths is shown. Thus, the width grows with time which is attributed to the thermo-optic interaction building up. Moreover, this growth comes together with some oscillations that experience a damping during time, as we already mentioned.
In total, we have shown that including the matter degrees of freedom yields a stabilisation of the condensate, as the absorption rate of the higher modes are larger, but the emission rates are smaller due to the Kennard-Stepanov relation. Therefore, photons are removed from the higher modes and inserted into the ground mode.

However, this model is neither able to describe the thermalisation of the uncondensed photon gas nor can it describe the effects of polarisation, because the spontaneous emission is not included. For the first one needs the spontaneous emission in order to introduce a Bose-Einstein distribution, see Section 1.1. For the latter one needs to include spontaneous emission to have also

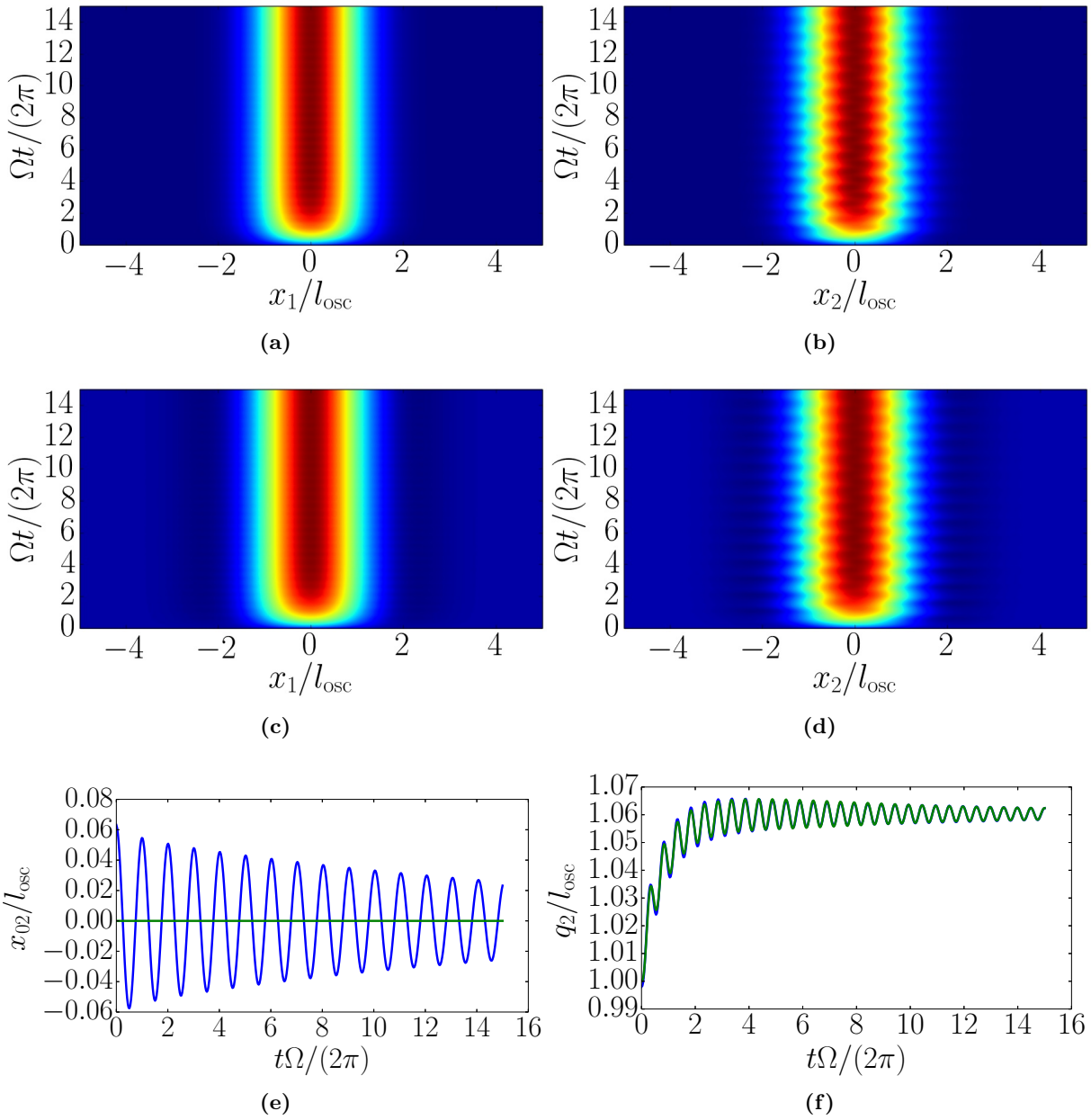

FIG. 9.1: Solutions to system (9.11). Panels **(a)** and **(b)** show the projection of the condensate distribution to the x and y axis, respectively. The same is plotted in Panels **(c)** and **(d)** for the temperature distribution. The evolution of the centre-of-mass coordinate is drawn in Panel **(e)**, whereas the dynamics of the widths can be found in Panel **(f)**. In the last both pictures, blue (green) corresponds to the 1 (2) direction.
The numerical parameters are chosen as: $\tau\Omega = 0.2$, $B = l_{\mathrm{osc}}^2 k_{\mathrm{B}}/\hbar$, $g_T = 0.9\ k_{\mathrm{B}}$. For the material we have the parameters $\gamma = 0.5\ \Omega$, $\kappa = 0.2\ \Omega$. The absorption rates are chosen to be $B(\omega_{00}) = \Omega$, $B(\omega_{10}) = B(\omega_{01}) = 1.01\ \Omega$ and $B(\omega_{20}) = B(\omega_{02}) = 1.02\ \Omega$, with the corresponding Kennard-Stepanov exponents $\xi_{00} = -3$, $\xi_{01} = \xi_{10} = -2.95$ as well as $\xi_{02} = \xi_{20} = -2.9$.

processes that change the polarisation of a photon [88]. A possible way to include spontaneous emission into a mean-field model is to include an additive Gaussian white noise as it is shown in [89].
Moreover, also the coherent light-atom coupling is missing, meaning that the model (9.11) only yields the envelope of the full time evolution as coherent absorption-emission processes happen continuously. In order to incorporate that, the semiclassical laser equations [87] need to be considered. Generalising this theory to molecular absorption and emission spectra, i.e. taking into account the Kennard-Stepanov equation this should lead to the model that is used in [57]. Nevertheless, one can also ask the question, whether a temporal nonlocal interaction is, indeed, due to the thermo-optics and does not stem from the Kerr effect. In the end, this is a question of competing time scales, as the condensate life time is about $5 \times 10^{-7}\,\mathrm{s}$, whereas the time scale of the thermo-optic interaction on the other hand is in the order of $1 \times 10^{-6}\,\mathrm{s}$. This means that the condensate does not live long enough in order to reach the steady state that is provided by the thermo-optic interaction. On the other hand, the fluorescence lifetime of Rhodamine 6G is of the order of $1 \times 10^{-9}\,\mathrm{s}$ [90], which yields the time scale of the thermo-optic effect. Therefore, it is possible that due to this fast time scale of the Kerr effect a nonlocality in time is due to this effect and not due to the thermo-optic interaction. This argumentation holds at least for one single photon BEC. If many experiments are conducted after each other in a row, then it may come to an accumulation of heat and, thus, the condensate may reach a thermo-optic equilibrium. However, in [90] it is also shown that the life time drops with increasing dye concentration. Possibly, a first attempt to a mean-field theory describing a nonlocal Kerr effect may have the same form as our model (2.81) with (2.82), where the temperature may be interpreted as the density of electronic population inversion. Therefore, the interaction strength would be determined by the life time of the electronic excitations. As this lifetime gets smaller with increasing dye concentration, one could possibly explain the behaviour of the interaction constant from [53], where the interaction decreases at larger concentrations. But here one also needs to take the solvatochromatic shift of the fluorescence maximum [91] into account, i.e. a shift due to the interactions between the dye and its solvent, as this changes the rates and also the interaction.

9.2. Polarisation

The experiments presented in Section 1.3 show that the condensate is polarised according to the pump beam, whereas the thermal cloud is not polarised at all. The same results are theoretically obtained in [88]. However, what is missing is a thorough analysis of the underlying Stokes parameters as these parameters are also used experimentally to determine the polarisation [51]. Moreover, so far no dynamical analysis of a two-component photon BEC has been done, neither corresponding equations have been set up so far. A possible approach is again found in the literature of exciton-polariton condensates [92]. There the authors used the mean-field model from [34] and extended the model by a second species of polaritons. Moreover, they also allow the species to merge into each other.
In the case of a photon BEC it is, in principle, also possible to extend the model presented in this thesis, but this model may not be able to describe the experimental findings of a condensate polarisation being the same as the pump laser polarisation. For this one needs to take the matter degrees of freedom into account. However, in order to describe also dynamical processes between

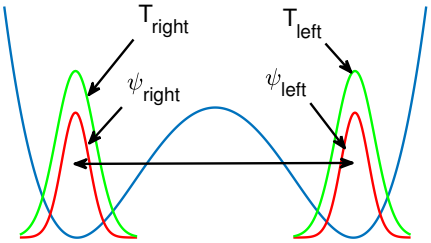

FIG. 9.2: Double well potential. Both the wave function and the temperature distribution decompose into a part that is settled in the left well and one that is centred in the right well.

the two species, such as interaction or a change of polarisation, spontaneous emission needs to be taken into account, as this is independent from the polarisation.

9.3. Double Well Potential

As already mentioned in Section 1.4 it is experimentally possible to generate double well potentials for photon BECs [52]. In such potentials the wave function falls into two pieces, namely one per well, if the wells are separated far enough from each other, see Figure 9.2. In case of atomic BECs this system is well studied and known to undergo Josephson oscillations, see [21, 93, 94]. What happens in the case of a photon BEC? The main difference is that a photon BEC is an open-dissipative system, meaning that the condensate not only oscillates back and forth between the sites in the double well, but also the coherent and incoherent interaction with the bath plays a crucial role for the dynamics. In addition there still is the thermo-optic interaction present, whose strength could oscillate in time as it depends on the heating due to imperfect absorption processes of photons by the dye. Mathematically, the envelope of the oscillations can be described by the nonlocal Gross-Pitaevskii equation from Part III:

$$i\hbar\partial_t\psi = \left\{ -\frac{\hbar^2\nabla^2}{2m} + V(\mathbf{x}) + g_T B\mathcal{G} * |\psi|^2 + \frac{i\hbar}{2}\left[\aleph p - \Gamma + 2(\aleph p + \Gamma)G * |\psi|^2\right] \right\}, \tag{9.14}$$

where $V(\mathbf{x})$ denotes the double well potential. The condensate wave function ψ can be expressed in basis of the functions ψ_i centred in each well:

$$\psi(\mathbf{x}, t) = a_1(t)\psi_1(\mathbf{x}) + a_2(t)\psi_2(\mathbf{x}), \tag{9.15}$$

where the basis functions ψ_i are given by the steady state calculated in Chapter 7.5. Inserting (9.15) in (9.14) then yields a system of two coupled integro-differential equations, that can be analysed by performing a Laplace transformation of the linearised equations as it was done in Chapter 4. From [93] it is known that in case of a usual Gross-Pitaevskii equation the resulting equations can be described by means of the Hamilton function of a pendulum. Here the two possible eigenmodes describe either a condensate oscillating back and forth between the single sites or a condensate that is trapped in one of the sites, respectively. However, this description is not possible anymore in our case, as we have a system that also contains pump and loss

processes.
The matter degrees of freedom can be brought in by using the ideas from Section 9.1. One can then also think of duplicating the matter degrees of freedom, such that each well has its own bath.

9.4. Vortices

Vortex physics is well known from three-dimensional atomic Bose-Einstein condensates both theoretically and experimentally [21]. In our case the situation is quite different, not only that the photon BEC exists in two dimensions but in addition loss and pump processes and a nonlocal interaction are present. Also in exciton-polariton condensates vortices are examined experimentally, cf. [95, 96] as well as theoretically. The most recent theoretical work [97] investigates the interaction of vortices and is based on the mean-field equations from [34]. The main difference to vortices in closed systems is that in exciton-polariton condensates vortices function as a source of polaritons. This stems from the fact that the losses are due to polariton-polariton scattering, meaning that a loss can only happen at coordinates with nonzero polariton density, i.e. losses cannot occur inside a vortex. On the other hand the pump inside a vortex is less suppressed than the loss. The produced polaritons leave the vortex radially. This mechanism has a high influence on the dynamics of vortex pairs, as is shown in Figure 9.3. The panels (a) and (b) show the case of a vortex-vortex pair. The equilibrium, that is marked by the white points and represents also the initial condition, is perturbed by the polariton flows out of the vortices. Due to that a new orbit evolves that is stabilised by the interplay between these flows and the influence of the von-Neumann boundary conditions, which are assumed by the authors. The pictures in the second row show the corresponding motion of a vortex-antivortex pair. Instead of moving parallel to each other, the distance between the vortex and the antivortex increases, showing that they repel each other.
Similar results can be suspected in the mean-field description of the photon BEC as the equations are nearly the same. However, the spontaneous emission may change some of the results as it does not depend on the local condensate density.

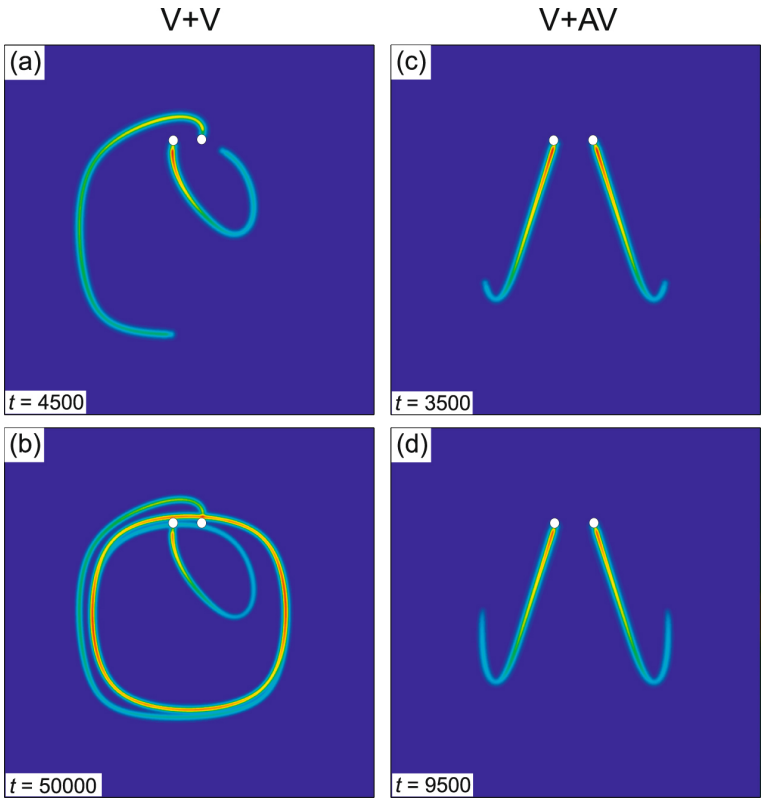

FIG. 9.3: Some of the results from [97]. The pictures (a) and (b) show the motion of a vortex-vortex pair, whereas in (c) and (d) the trajectories for a vortex-antivortex pair is plotted. In all pictures a red coloured trajectory means that the vortex passed this point in recent time.

Appendix

A. Lorentz Model for Dye and Kennard–Stepanov Relation

The purpose of this appendix is to give an overview on how the dye susceptibility could possibly be calculated on the basis of the Lorentz oscillator model and by taking into account the relation between absorption and emission spectrum which is provided by the so-called Kennard-Stepanov relation.

A.1. Lorentz Model

Within the Lorentz model one usually approximates an electronic transition between energy levels of a two-level system under the influence of an incident driving field $\mathbf{E}$ by a driven and damped harmonic oscillator with its frequency being the transition frequency Ω [60, 61]. Thus, for the position vector of the electron $\mathbf{x}$ we have the equation

$$\ddot{\mathbf{x}} + \beta\dot{\mathbf{x}} + \Omega^2\mathbf{x} = -\frac{e}{m}\mathbf{E}, \tag{A.1}$$

where β denotes the damping constant. By performing a half-sided Fourier transformation, which is a special case of the Laplace transformation (5.3) with $s = i\omega$, we find an algebraic equation for the Laplace transformed position $\breve{\mathbf{x}}$

$$\breve{\mathbf{x}} = -\frac{e}{m}\Gamma(\omega)\breve{\mathbf{E}}, \tag{A.2}$$

where we assumed, that the electron is at rest at initial time $t = 0$. Moreover, the Green's function for a harmonic oscillator is defined by

$$\Gamma(\omega) = \frac{1}{\Omega^2 - \omega^2 - i\beta\omega}. \tag{A.3}$$

Since in case of a linear susceptibility the relation between polarisation P of single molecule and incident electrical field is according to (2.3) given by

$$\mathbf{P} = \varepsilon_0\chi^{(1)}\mathbf{E}, \tag{A.4}$$

we find for the linear susceptibility within the Lorentz model

$$\breve{\chi}^{(1)}(\omega) = -\frac{e}{\varepsilon_0 m}\Gamma(\omega) \tag{A.5}$$

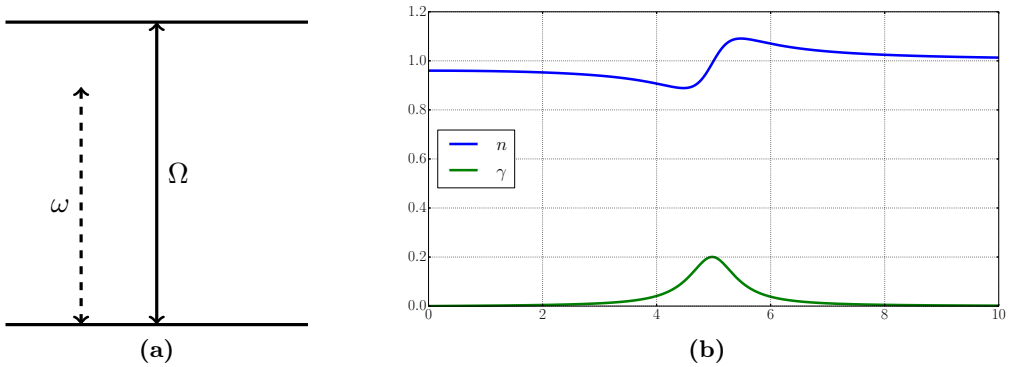

FIG. A.1: Optical properties of a two-level system. Panel **(a)** shows the level scheme of the two-level system. The energy levels differ by an energy of $\hbar\Omega$, whereas light at energy $\hbar\omega$ is shined in. The resulting refractive index n and extinction coefficient γ according to (A.7) is shown in Panel **(b)**. The parameters are chosen as $e/(\varepsilon_0 m) = 1 = \beta$.

and so for the dielectric function

$$\breve{\epsilon}(\omega) = 1 + \breve{\chi}^{(1)} = 1 - \frac{e}{\varepsilon_0 m}\Gamma(\omega). \tag{A.6}$$

Following (2.6) refractive index and extinction coefficient are given by

$$\breve{n}(\omega) = \mathrm{Re}\left(\sqrt{1 - \frac{e}{\varepsilon_0 m}\Gamma(\omega)}\right) \text{ and } \breve{\gamma}(\omega) = \mathrm{Im}\left(\sqrt{1 - \frac{e}{\varepsilon_0 m}\Gamma(\omega)}\right). \tag{A.7}$$

How the resulting refractive index and extinction coefficient look, can be seen in panel (b) of Figure A.1. Note here, that the suspected exact absorption line is blurred out due to the damping. Therefore, we can conclude that refractive index n and extinction coefficient γ only play a role near the resonance frequency and far from the resonance the refractive index approaches 1, whereas the extinction coefficient vanishes. It should be mentioned that in more complex material the refractive index usually tends towards some certain background value n_{bag}.
In the case of a solution consisting of two components, the refractive index is a sum over both dielectric functions $\epsilon_{1(2)}$ of the species 1(2), where the weights are proportional to the respective concentration $c_{1(2)}$ provided that the interaction between the two species is small enough, as their the emission/absorption rates are not affected:

$$\epsilon(\omega) \propto c_1\epsilon_1(\omega) + c_2\epsilon_2(\omega). \tag{A.8}$$

In the experimental situation of the photon BEC, the concentration of the solvent ethylene glycol is much larger than the one of the Rhodamine 6G. Moreover, the experiment is in a frequency region that is far away from any resonances of the solvent, such that only the background value ϵ_{bag} matters. Note, that this background value is real, as no absorption processes happen. On the other hand, we are right at the resonances of the dye. Since the concentration of the dye is small compared to the concentration of the solvent, the real part of the total dielectric function $\epsilon(\omega)$ is given entirely by the background value of ethylene glycol and the imaginary part of the total dielectric function is completely determined by the absorption emission spectrum of

Rhodamine 6G. Therefore, the total dielectric function is given by

$$\epsilon(\omega) \propto c_1 \epsilon_{\text{bag}} + i c_2 \text{Im}\left(\epsilon_{\text{R6G}}(\omega)\right). \tag{A.9}$$

In real time, the polarisation P is provided by a convolution of the response, i.e. the dielectric function, with the incident field $\mathbf{E}$:

$$\mathbf{P} = \varepsilon_0 \epsilon * \mathbf{E}. \tag{A.10}$$

For the definition of the convolution see (5.8), but note, that we here only consider the temporal convolution. As the real part of the dielectric function is a constant, the inverse Laplace transformation is a simple Dirac delta function. For the imaginary part of the convolution we assume, that the incident field $\mathbf{E}$ is dominated by one frequency and has only minor contributions of near lying frequencies, such that the dielectric function is nearly constant in this frequency range. Thus, also in the imaginary part the convolution is resolved by a Dirac delta function and we find for the linear polarisation

$$\mathbf{P}(t) \approx \varepsilon_0 \epsilon \mathbf{E}(t). \tag{A.11}$$

Therefore, the question arises what one knows about the spectrum of the dye molecules. This is the topic of the next section.

A.2. Kennard-Stepanov Relation

In this section we derive the Kennard-Stepanov relation [39–42], as this plays a crucial role in the thermalisation of photon Bose-Einstein condensates. The starting point is Figure A.2, where the Jablonski diagram of a molecule with two electronic levels is shown. The transition frequency is assumed to be ω_{ZPL}, where ZPL stands for zero-phonon-line, as this indicates a pure electronic transition. Due to the possible vibrations of the molecule, the levels themselves obtain many sublevels. Since the molecule can interact with its surrounding, the vibrational levels are occupied according to the Boltzmann distribution

$$p(\Delta\omega_1) = e^{-\hbar\Delta\omega_1/(k_B T)} \tag{A.12}$$

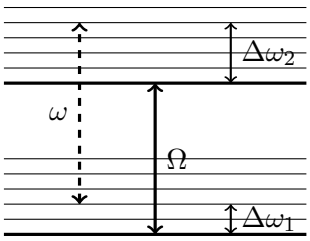

FIG. A.2: Jablonski diagram of a molecule with two electronic levels. The thick lines show the bare transition, whereas the thin lines correspond to the phononic excitations of the dye.

for the lower manifold and

$$p(\Delta\omega_2) = e^{-\hbar\Delta\omega_2/(k_B T)} \tag{A.13}$$

for the upper manifold. Due to the conservation of energy $\omega_{\mathrm{ZPL}} + \Delta\omega_2 = \Omega + \Delta\omega_1$, we can express the latter by the distribution for the lower manifold:

$$p(\Delta\omega_2) = p(\Delta\omega_1) e^{-\hbar(\Omega-\omega_{\mathrm{ZPL}})/(k_B T)}. \tag{A.14}$$

The aim is now to generalise the Einstein coefficients for the transitions between total upper and total lower manifold. For this purpose consider the Einstein coefficients $B_{12}(\Omega, \Delta\omega_1)$ for the transition from some certain state of the lower manifold at energy $\hbar\Omega + \hbar\Delta\omega_1$ to the upper manifold. As we assume that the states in the lower manifold are thermally occupied, the total absorption coefficient $B_{12}(\Omega)$ can be found by averaging over all microscopic coefficients:

$$B_{12}(\Omega) = \int d\Delta\omega_1 \; g(\Delta\omega_1) B_{12}(\Omega, \Delta\omega_1) p(\Delta\omega_1), \tag{A.15}$$

where $g(\Delta\omega_q)$ is the density of states in the lower manifold. By the same reasoning for the upper manifold we find by using (A.14) for the induced emission Einstein coefficient

$$B_{21}(\Omega) = e^{-\hbar(\Omega-\omega_{\mathrm{ZPL}})/(k_B T)} \int d\Delta\omega_2 \; g(\Delta\omega_2) B_{21}(\Omega, \Delta\omega_2) p(\Delta\omega_1). \tag{A.16}$$

From the analysis of a simple two-level system the detailed balancing condition $g(\Delta\omega_1) B_{12}(\Omega, \Delta\omega_1) = g(\Delta\omega_2) B_{21}(\Omega, \Delta\omega_2)$ is known. Using this, we find from (A.16) the Kennard-Stepanov relation

$$B_{21}(\Omega) = e^{-\hbar(\Omega-\omega_{\mathrm{ZPL}})/(k_B T)} B_{12}(\Omega). \tag{A.17}$$

The temperature that emerges in the exponent is called spectral temperature. For the photon BEC it is crucial, that this temperature is constant in the experimental frequency range, as the photon gas thermalises to this temperature.

B. Gaussian Integrals

In this appendix we shortly comment on how to solve integrals of products of Gaussian functions, which possess different centres-of-masses. For this purpose we make use of a technique that is called integration by differentiation and goes back to [98,99]. As this technique is not commonly known, a short overview is given in Section B.1. Afterwards we will use this particular method and solve the general form of Gaussian integrals that appear in 4 and 7 in Section B.2.

B.1. Integration by Differentiation

Consider an analytic function $f : \mathbb{R} \to \mathbb{R}$ and the definite integral $I = \int_a^b dx\ f(x)$. In order to introduce the method, we create now an exponential term by inserting the unity in form of $\lim_{\epsilon\to 0} e^{\alpha\epsilon x}$:

$$I = \lim_{\epsilon\to 0} \int_a^b dx\ f(x) e^{\alpha\epsilon x}. \tag{B.1}$$

After replacing the integration variable by the corresponding derivative with respect to ϵ yields

$$I = \lim_{\epsilon\to 0} f\left(\frac{1}{\alpha}\partial_\epsilon\right) \int_a^b dx\ e^{\alpha\epsilon x}, \tag{B.2}$$

which can be integrated to

$$I = \lim_{\epsilon\to 0} f\left(\frac{1}{\alpha}\partial_\epsilon\right) \frac{e^{\alpha\epsilon b} - e^{\alpha\epsilon a}}{\alpha\epsilon}. \tag{B.3}$$

These three steps describe the fundamental steps of the integration by differentiation method.

B.2. Gaussian Integrals

As in the this thesis Gaussian integrals play a crucial role, we turn now on how to calculate them within the framework of integration by differentiation. As in the text we deal with products of Gaussian functions with different centres-of-mass, we deal with the general form of those.
In order to ease our work we will make use of the following identity

$$e^{a\partial_\epsilon^2}\delta(\epsilon) = \frac{1}{\sqrt{4\pi a}} e^{-\epsilon^2/(4a)}. \tag{B.4}$$

This can be proofed by using the integral representation of the delta function

$$e^{a\partial_\epsilon^2}\delta(\epsilon) = \frac{1}{2\pi}\int_{-\infty}^{\infty} dx\; e^{a\partial_\epsilon^2} e^{i\epsilon x} \tag{B.5}$$

Replacing ∂_ϵ by ix and performing the remaining integrals yields

$$e^{a\partial_\epsilon^2}\delta(\epsilon) = \frac{1}{\sqrt{4\pi a}} e^{-\epsilon^2/(4a)}. \tag{B.6}$$

Consider now an integral I of E Gaussian functions in D dimensions

$$I = \int d^D x \exp\left[-\sum_{j=1}^{D}\sum_{k=1}^{E}\frac{(x_j-\xi_{jk})^2}{q_{jk}^2}\right]. \tag{B.7}$$

After introducing for each coordinate x_j an auxiliary variable ϵ_j and multiplying out the square in the exponential the integral takes the form

$$I = \prod_{j=1}^{D} 2\pi \lim_{\epsilon_j\to 0} \exp\left[-\sum_{k=1}^{E}\frac{\xi_{jk}^2 - 2i\xi_{jk}\partial_{\epsilon_j} - \partial_{\epsilon_j}^2}{q_{jk}^2}\right]\delta(\epsilon_j). \tag{B.8}$$

We can now apply the differential operators and arrive at

$$I = \prod_{j=1}^{D}\frac{2\pi}{\sqrt{4\pi\sum_{k=1}^{E} 1/q_{jk}^2}} \exp\left[-\sum_{k=1}^{E}\frac{\xi_{jk}^2}{q_{jk}^2}\right] \lim_{\epsilon_j\to 0}\exp\left[-\frac{1}{4\sum_{k=1}^{E}1/q_k^2}\left(\epsilon_j - 2i\sum_{k=1}^{E}\frac{\xi_{jk}}{q_{jk}^2}\right)^2\right] \tag{B.9}$$

yielding finally, after performing the limit

$$I = \sqrt{\frac{\pi^D}{\prod_{j=1}^{D}\sum_{k=1}^{E}1/q_{jk}^2}} \exp\left\{\sum_{j=1}^{D}\sum_{k=1}^{E}\left[\frac{1}{\sum_{k=1}^{D}1/q_{jk}^2}\sum_{l=1}^{E}\frac{\xi_{jk}\xi_{jl}}{q_{jk}^2 q_{jl}^2} - \frac{\xi_{jk}^2}{q_{jk}^2}\right]\right\}. \tag{B.10}$$

This also provides us with the solution for some smooth function in front of the Gaussians, namely

$$\int d^D x\; f(\mathbf{x}) \exp\left[-\sum_{j=1}^{D}\sum_{k=1}^{E}\frac{(x_j-\xi_{jk})^2}{q_{jk}^2}\right] \tag{B.11}$$

$$= \sqrt{\frac{\pi^D}{\prod_{j=1}^{D}\sum_{k=1}^{E}1/q_{jk}^2}} \lim_{\epsilon\to\mathbf{0}} f(-i\partial_\epsilon) \exp\left\{-\sum_{j=1}^{D}\left[\frac{1}{4\sum_{k=1}^{E}1/q_k^2}\left(\epsilon_j - 2i\sum_{k=1}^{E}\frac{\xi_{jk}}{q_{jk}^2}\right)^2 + \sum_{k=1}^{E}\frac{\xi_{jk}^2}{q_{jk}^2}\right]\right\}$$

For further calculations let us write this in a slightly shorter way

$$\begin{aligned}&\int d^D x\ f(x) \exp\left\{-\sum_{j=1}^{D}\left[\sum_{k=1}^{E}\frac{(x_j - x_{jk})^2}{q_{jk}^2}\right]\right\}\\ =&\mathcal{N}\lim_{\epsilon\to 0} f(-i\partial_\epsilon)\exp\left\{-\sum_{j=1}^{D}\left[A_j^{(E)}\left(\epsilon_j - 2iB_j^{(E)}\right)^2 + C_j^{(E)}\right]\right\},\end{aligned} \tag{B.12}$$

with the abbreviations

$$A_j^{(E)} = \frac{1}{4\sum_{k=1}^{E} 1/q_{jk}^2}, \tag{B.13a}$$

$$B_j^{(E)} = \sum_{k=1}^{E}\frac{\xi_{jk}}{q_{jk}^2}, \tag{B.13b}$$

$$C_j^{(E)} = \sum_{k=1}^{E}\frac{\xi_{jk}^2}{q_{jk}^2}, \tag{B.13c}$$

$$\mathcal{N} = \sqrt{\frac{\pi^D}{\prod_{j=1}^{D}\sum_{k=1}^{E} 1/q_{jk}^2}} = \pi^{D/2}\prod_{j=1}^{D}\frac{\prod_{l=1}^{E} q_{jl}}{\sqrt{\sum_{k=1}^{E}\prod_{l\neq k}^{E} q_{jk}^2}}. \tag{B.13d}$$

In the concrete calculation, f will be a polynomial with at most fourth order terms. Thus, we consider the following calculation, where we do not denote the superscripts and shift the variable according to $x_j = \epsilon_j - 2iB_j^{(E)}$,

$$\frac{\partial^4}{\partial x_1\partial x_2\partial x_3\partial x_4} e^{-\sum(A_j x_j^2 + C_j)} \tag{B.14a}$$

$$= \frac{\partial^3}{\partial x_1\partial x_2\partial x_3}\left[-2A_4 x_4\right] e^{-\sum(A_j x_j^2 + C_j)} \tag{B.14b}$$

$$= \frac{\partial^2}{\partial x_1\partial x_2}\left[-2A\delta_{34} + 4A_4A_3x_4x_3\right] e^{-\sum(A_j x_j^2 + C_j)} \tag{B.14c}$$

$$= \frac{\partial}{\partial x_1}\left[4A_4A_3\left(x_3\delta_{42} + x_4\delta_{32}\right) - 8A_4A_3A_2x_4x_3x_2\right] e^{-\sum(A_j x_j^2 + C_j)} \tag{B.14d}$$

$$\begin{aligned}=&\left[4A_4A_3\left(\delta_{31}\delta_{42} + \delta_{41}\delta_{32}\right) - 8A_4A_3A_2\left(x_4x_3\delta_{21} + x_4x_2\delta_{31} + x_3x_2\delta_{41}\right)\right.\\ &\left.+16A_4A_3A_2A_1x_4x_3x_2x_1\right] e^{-\sum(A_j x_j^2 + C_j)}.\end{aligned} \tag{B.14e}$$

In this notation the limit $\epsilon_j \to 0$ corresponds to the substitution $x_j \to -2iB_j$. But this means, we can replace in the integral (B.12) the monomial powers according to Table B.1.

Table B.1.: Monomial replacement in Gaussian integrals. The lines are determined by the corresponding lines in (B.14).

Monomial	**Replacement**
x_4	$4A_4B_4$
x_3x_4	$2A_4\delta_{34} + 16A_4A_3B_4B_3$
x_4^2	$2A_4 + 16A_4^2B_4^2$
$x_2x_3x_4$	$2A_4A_3(B_3\delta_{42} + B_4\delta_{32}) + 64A_4A_3A_2B_4B_3B_2$
$x_2x_3^2$	$4A_3^2B_3\delta_{23} + 64A_2A_3^2B_2B_3^2$
$x_1x_2x_3x_4$	$4A_4A_3(\delta_{31}\delta_{42} + \delta_{41}\delta_{32}) + 32A_4A_3A_2(B_4B_2\delta_{21} + B_4B_2\delta_{31}B_3B_2\delta_{41}) + 256A_4A_3A_2A_1B_4B_3B_2B_1$
$x_2^2x_4^2$	$8A_4^2\delta_{42} + 32A_4^2A_2(B_4^2 + B_4B_2 + B_4B_2\delta_{42}) + 256A_4^2A_2^2B_4^2B_2^2$

Table B.2.: Calculation of the A, B, C coefficients according to the definitions (B.13).

E	$A_j^{(E)}$	$B_j^{(E)}$	$C_j^{(E)}$
1	$\frac{q_{j1}^2}{4}$	$\frac{x_{j1}}{q_{j1}^2}$	$\frac{x_{j1}^2}{q_{j1}^2}$
2	$\frac{q_{j1}^2q_{j2}^2}{4(q_{j1}^2+q_{j2}^2)}$	$\frac{x_{j1}q_{j2}^2 + x_{j2}q_{j1}^2}{q_{j1}^2q_{j2}^2}$	$\frac{x_{j1}^2q_{j2}^2 + x_{j2}^2q_{j1}^2}{q_{j1}^2q_{j2}^2}$
3	$\frac{q_{j1}^2q_{j2}^2q_{j3}^2}{4(q_{j2}^2q_{j3}^2 + q_{j1}^2q_{j3}^2 + q_{j1}^2q_{j2}^2)}$	$\frac{x_{j1}q_{j2}^2q_{j3}^2 + x_{j2}q_{j1}^2q_{j3}^2 + x_{j3}q_{j1}^2q_{j2}^2}{q_{j1}^2q_{j2}^2q_{j3}^2}$	$\frac{x_{j1}^2q_{j2}^2q_{j3}^2 + x_{j2}^2q_{j1}^2q_{j3}^2 + x_{j3}^2q_{j1}^2q_{j2}^2}{q_{j1}^2q_{j2}^2q_{j3}^2}$

C. Cumulants Method

In this appendix we answer the questions after the shape and after the lowest-lying collective excitations of a harmonically trapped D-dimensional Bose-Einstein condensate whose particles underlie a weak contact interaction. The usual way to tackle those issues is, that the condensate wave function is assumed to be Gaussian shaped as this is the solution to the noninteracting case. In the present ansatz the widths are allowed to be affected due to the presence of a weak interaction. One usually proceeds by inserting this ansatz into the condensate action functional. As now the action functional depends on the widths of the condensate, Hamilton's principle can be used to find the corresponding evolution equations for the widths. As the spatial degrees of freedom have been eliminated due to the ansatz, the quest after solving a D-dimensional nonlinear partial differential equation is reduced to solving D coupled nonlinear ordinary differential equations for the widths, see e.g. [77, 79, 82].
In this appendix a different approach that yields the same results as the standard variational method is presented. The procedure is based on the statistical properties of the Gauss function, namely that a Gauss function is described by the first two cumulants, i.e. the width and the centre-of-mass. The equations governing their temporal evolution are derived by calculating the average of Gross-Pitaevskii equation weighted with certain factors. Along this path the same equations for the widths as in the standard procedure can be derived. This method has the advantage that no action is needed to derive the width equations which means that it can also be used to calculate such variational equations for open-dissipative systems as it is the case with the photon BEC. In Chapter 4 as well as in Chapter 7, this method will be used to calculate the collective frequencies of the photon condensate. A similar method has first been used in [100] to describe a system of two interacting BECs that may undergo losses and that are harmonically trapped. Therefore, they also use Gaussian ansatzes for the BECs, but here only the width dynamics is considerd. In [81] this method is extended to also be able to describe the nonequilibrium dynamics of the centre-of-mass of a condensate, which is part of hybrid atom-optomechanical system.
The purpose of this chapter is to introduce the reader to the cumulants method and to show that it yields the same results as the variational approach. To this end this appendix is structured as follows. In Section C.1 the cumulants equations for a D-dimensional condensate are derived. As the photon condensate is a two-dimensional object, in Section C.2 the findings of Section C.1 are specified to two spatial dimensions and discussed further. Those results are compared to to results obtained by solving the Gross-Pitaevskii equation numerically in Section C.3. Finally, as numerous integrals appear, especially in Chapters 4 and 7 during the averaging of the Gross-Pitaevskii equation, we provide an overview of those integrals in Section C.4.

C.1. Collective Frequencies of Atomic Bose-Einstein Condensate

In this section, we analyse the lowest-lying collective frequencies of a BEC, that is described by a closed Gross-Pitaevskii equation in D spatial dimensions

$$i\hbar\partial_t\psi = -\frac{\hbar^2}{2m}\nabla^2\psi + \frac{m}{2}\sum_{i=1}^{D}\Omega_i^2 x_i^2\psi + g|\psi|^2\psi. \tag{C.1}$$

As the purpose of this appendix is only to introduce the reader to the cumulants method, we transform this equation to dimensionless quantities by rescaling the lengths with the harmonic oscillator length $l_{\text{osc}} = \sqrt{\hbar/(m\Omega)}$ and the time by the inverse frequency scale $1/\Omega$ that determines the frequencies in the various dimensions by $\Omega_i = \lambda_i\Omega$, with $\lambda \in \mathbb{R}_+$. Thus we can restate (C.1) as

$$i\partial_t\psi = -\frac{1}{2}\nabla^2\psi + \frac{1}{2}\sum_{i=1}^{D}\lambda_i^2 x_i^2\psi + \tilde{g}|\psi|^2\psi. \tag{C.2}$$

Here, we define the dimensionless interaction strength by

$$\tilde{g} = \frac{g}{\hbar\Omega}\left(\frac{m\Omega}{\hbar}\right)^D. \tag{C.3}$$

In the following we first determine the ansatz for the wave function and discuss the resulting cumulants equations as well as the arising consequences for the lowest-lying collective frequencies.

C.1.1. Ansatz

Since small interaction strengths are considered, a Gaussian ansatz for the condensate wave function is considered, as this solves the non-interacting case. In detail this reads

$$\psi = \sqrt{\frac{N_0}{\pi^{D/2}\prod_{i=1}^{D} q_i(t)}}\exp\left\{\sum_{j=1}^{D}\left[-\left(\frac{1}{2q_j(t)^2} + iA_j(t)\right)\left(x_j - x_{0j}(t)\right)^2 + ix_jC_j(t)\right]\right\}. \tag{C.4}$$

This ansatz allows us to examine $2D$ eigenmodes, namely D modes where only the widths q_j oscillate and D modes where only the centres-of-mass x_{0j} oscillate, see Figure 4.1 for the special case $D = 2$.

C.1.2. Cumulants Equations

In order to calculate the cumulants equation of motion we average over the Gross-Pitaevskii equation (C.1) with the weight f_{ik}:

$$\begin{aligned} i\int d^D x\ f_{ik}\psi^*\partial_t\psi =& \frac{1}{2}\int d^D x\ \psi^*\nabla f_{ik}\cdot\nabla\psi + \frac{1}{2}\int d^D x\ f_{ik}|\nabla\psi|^2 \\ &+ \frac{1}{2}\sum_{i=1}^{D}\lambda_i^2\int d^D x\ x_i^2 f_{ik}|\psi|^2 + \tilde{g}\int d^D x\ f_{ik}|\psi|^4, \end{aligned} \tag{C.5}$$

where the kinetic term has been partially integrated.
As the ansatz (C.4) is a Gaussian function, it is enough to calculate the first two central moments, meaning we consider on the one hand, see [81]

$$f_{1k} = x_k - x_{0k} \tag{C.6}$$

to find the equations governing the centre-of-mass motion. On the other hand

$$f_{2k} = (x_k - x_{0k})^2 - \frac{q_k^2}{2} \tag{C.7}$$

is considered, in order to find the system governing the widths motion.

C.1.3. Dipole Mode and Kohn Theorem

First, we inspect the case of f_{1k} that encodes the centre-of-mass motion. Performing the integrals yields the complex differential equation

$$\frac{i}{2}\dot{x}_{0k} + A_k q_k^2\dot{x}_{0k} - \dot{C}_k\frac{q_k^2}{2} = \frac{i}{2}C_k + A_k C_k q_k^2 + \frac{1}{2}\lambda_k^2 x_{0k} q_k^2. \tag{C.8}$$

As all the coefficients are real, (C.8) is decomposed into real and imaginary part. The imaginary part results in the relation between x_{0k} and C_k:

$$C_k = \dot{x}_{0k}. \tag{C.9}$$

The real part on the other hand leads to

$$A_k q_k^2\dot{x}_{0k} - \dot{C}_k\frac{q_k^2}{2} = A_k C_k q_k^2 + \frac{1}{2}\lambda_k^2 x_{0k} q_k^2. \tag{C.10}$$

By inserting (C.9) into (C.10) these two equations yield one harmonic oscillator equation for the centre-of-mass x_{0k}:

$$\ddot{x}_{0k} + \lambda_k^2 x_{0k} = 0. \tag{C.11}$$

The dipole-mode frequency of the kth direction $\omega_{\mathrm{dip}}^{(k)}$ is directly read off from this equation to be

$$\omega_{\mathrm{dip}}^{(k)} = \lambda_k. \tag{C.12}$$

Remarkably enough, this frequency does only depend on the trap frequency in the kth direction and is completely unconnected to the interaction of the BEC particles. This result is referred to as **Kohn theorem** [78, 79] that has been first stated by Walter Kohn in the realm of an interacting electron gas in a magnetic field [101]. In this setting Kohn showed, that the cyclotron frequency of the gas is independent of the electron-electron interaction.

C.1.4. Breathing- and Quadrupole Mode

As next the case of f_{2k} is considered. Executing the corresponding integrals in (C.5) yields also here a complex differential equation

$$i\frac{\dot{q}_k q_k}{2} + \frac{\dot{A}_k q_k^4}{2} = -\frac{1}{2}\left(1 + 2iA_k q_k^2\right) + \frac{1}{4} + A_k^2 q_k^4 + \frac{1}{4}\lambda_k^2 q_k^4 - \frac{N\tilde{g}q_k^2}{2^{D/2+2}\pi^{D/2}\prod_{j=1}^{D} q_j}. \tag{C.13}$$

The imaginary part of this equation reveals the relation between A_k and q_k

$$A_k = -\frac{\dot{q}_k}{2q_k}. \tag{C.14}$$

The real part of (C.13) results in a differential equation for $\dot{A}_k$

$$\frac{\dot{A}_k q_k^4}{2} = \frac{1}{2} + A_k^2 q_k^4 + \frac{1}{4}\lambda_k^2 q_k^4 - \frac{N\tilde{g}q_k^2}{2^{D/2+2}\pi^{D/2}\prod_{j=1}^{D} q_j}. \tag{C.15}$$

By using (C.14), (C.15) can be turned into a differential equation of second order for q_k

$$\ddot{q}_k + \lambda_k^2 q_k = \frac{1}{q_k^3} + \frac{N_0\tilde{g}}{(2\pi)^{D/2} q_k \prod_{i=1}^{D} q_i}. \tag{C.16}$$

This equation is completely decoupled from the centre-of-mass motion, but in contrast to the dipole mode, this equation still inherits information on the interaction and the widths in the different directions are coupled.
The equations of motion can also be summarised by writing down a potential

$$V^{(D)} = \frac{1}{2}\sum_{k=1}^{D}\left(\lambda_k^2 q_k^2 + \frac{1}{q_k^2}\right) + \frac{N_0\tilde{g}}{(2\pi)^{D/2}\prod_{i=1}^{D} q_i}, \tag{C.17}$$

which can be directly compared to [77, (13)]. The potential in the reference agrees with the here calculated potential $V^{(3)}$ by identifying $q_i = u_i$ and $P = N_0\tilde{g}/(2\pi)^{3/2}$.

C.2. Two-Dimensional Atomic Bose-Einstein Condensate

As the focus of the present thesis lies upon two-dimensional condensates in an isotropic harmonic trap, the results of the preceding section are specialised in this section to two spatial dimensions. The trap isotropy finds its expression in choosing $\lambda_1 = \lambda_2 \equiv 1$.

The first observation is, that the result for the dipole mode (C.12) is not changed. Also here the condensate oscillates with the trap frequency. The system of equations for the widths (C.16) takes now the form

$$\ddot{q}_1 + q_1 = \frac{1}{q_1^3} + \frac{N_0 g}{2\pi q_1^2 q_2}, \tag{C.18a}$$

$$\ddot{q}_2 + q_2 = \frac{1}{q_2^3} + \frac{N_0 g}{2\pi q_1 q_2^2}. \tag{C.18b}$$

In order to find also in this case an oscillation frequency, (C.18a) will be linearised by the ansatz

$$q_k(t) = q_0 + \delta q_k e^{-i\omega t},\ k = 1, 2, \tag{C.19}$$

where q_0 describes the steady state and is the same in both directions due to the isotropy. Small perturbations of this steady state are described by δq_k, $k = 1, 2$.
Inserting (C.19) into (C.18a) and keeping only terms up to first order in the perturbations leads to

$$-\omega^2 \delta q_1 + q_0 = \frac{1}{q_0^3} + \frac{N_0 \tilde{g}}{2\pi q_0^3} - \left(1 + \frac{3}{q_0^4} + \frac{N_0 \tilde{g}}{\pi q_0^4}\right) \delta q_1 - \frac{N_0 \tilde{g}}{2\pi q_0^4} \delta q_2, \tag{C.20}$$

$$-\omega^2 \delta q_2 + q_0 = \frac{1}{q_0^3} + \frac{N_0 \tilde{g}}{2\pi q_0^3} - \left(1 + \frac{3}{q_0^4} + \frac{N_0 \tilde{g}}{\pi q_0^4}\right) \delta q_2 - \frac{N_0 \tilde{g}}{2\pi q_0^4} \delta q_1. \tag{C.21}$$

Thus, the steady state is described by

$$q_0^4 = 1 + \frac{N \tilde{g}}{2\pi} \tag{C.22}$$

depending on the interaction. According to this result, the condensate width grows, if the particle number or the interaction strength is increased. This result is plotted in panel (a) of Figure C.1.
In order to get the squares of the corresponding eigenmode frequencies, the coefficient matrix

$$S = \begin{pmatrix} 1 + \frac{3}{q_0^4} + \frac{N_0 \tilde{g}}{\pi q_0^4} & + \frac{N_0 \tilde{g}}{2\pi q_0^4} \\ + \frac{N_0 \tilde{g}}{2\pi q_0^4} & 1 + \frac{3}{q_0^4} + \frac{N_0 \tilde{g}}{\pi q_0^4} \end{pmatrix} \tag{C.23}$$

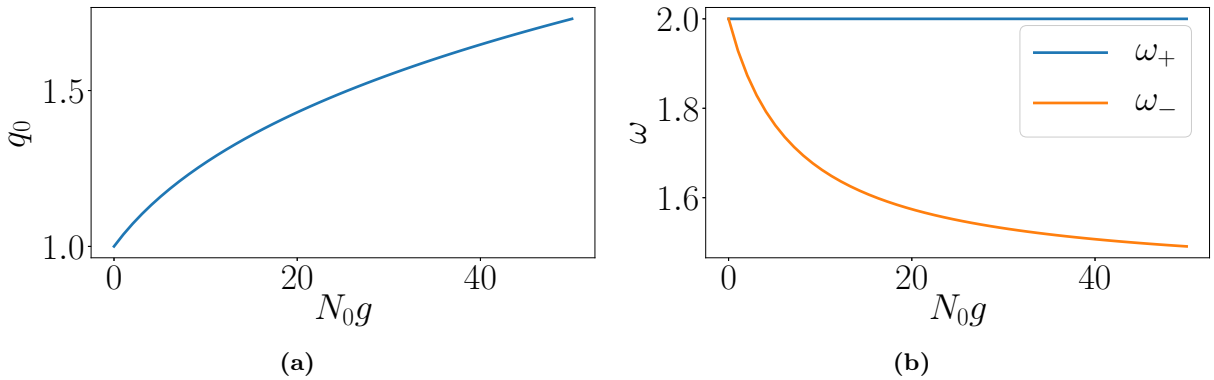

(a) **(b)**

FIG. C.1: Results for linear stability analysis of (C.18a). Panel **(a)** shows the steady state solution as calculated in (C.22). In panel **(b)** the frequencies of oscillatory solutions as calculated in (C.24) are drawn.

is diagonalised. Therefore, we find

$$\omega_+ = 2, \tag{C.24a}$$

$$\omega_- = \sqrt{1 + \frac{6\pi + N_0\tilde{g}}{2\pi + N_0\tilde{g}}}\,. \tag{C.24b}$$

Surprisingly, only one of those modes, namely the "-"-mode, depends on the interaction. In case of vanishing interaction, i.e. $N_0\tilde{g} \to 0$, both modes share the same frequency, but in the limit $N_0\tilde{g} \to \infty$, the "-"-mode tends to $\sqrt{2}$. This behaviour can also be seen in panel (b) of Figure C.1.
The corresponding eigenvectors are given by

$$\chi_+ = \frac{1}{\sqrt{2}} \begin{pmatrix} 1 \\ 1 \end{pmatrix}, \tag{C.25}$$

meaning that the width perturbation oscillate in phase. As this makes the condensate look like as it is breathing, this mode is referred to as breathing mode. The second eigenvector is provided by

$$\chi_- = \frac{1}{\sqrt{2}} \begin{pmatrix} 1 \\ -1 \end{pmatrix}. \tag{C.26}$$

In this case, the widths oscillate with a phase of π, therefore, this mode is called quadrupole mode.

C.3. Numerical Results

The Gross-Pitaevskii equation (C.2) can also be solved numerically. With this numerical solution at hand we can then check, how well the approach that is presented in the preceding Section works. For the numerical implementation we chose a Split-Step Fourier method, see e.g. Reference [102]. Within this method one propagates the kinetic term in the Fourier space, where the application of the Laplacian is only a multiplication by a real number, whereas the rest is propagated in real space. In order to explain what is meant by that in more detail, we derive now heuristically the iteration equation.
The formal solution of the Gross-Pitaevskii (C.2) is provided by

$$\psi(t,\mathbf{x}) = \exp\left[\int_0^t dt' \ \left(-\frac{\nabla^2}{2} + V(\psi(t',\mathbf{x}))\right)\right]\psi(t=0,\mathbf{x}), \tag{C.27}$$

where we defined $V(\psi) = \frac{1}{2}\sum_{i=1}^{D}\lambda_i^2 x_i^2\psi^2 + \tilde{g}|\psi|^2\psi$. For an infinitesimal time step Δt, the integral can be approximated such that the formal solution reads

$$\psi(t+\Delta t) \approx \exp\left[\left(-\frac{\nabla^2}{2} + V(\psi(t))\right)\Delta t\right]\psi(t), \tag{C.28}$$

where we left off the spatial index. Application of Baker-Campbell-Hausdorff formula in the lowest order yields

$$\psi(t+\Delta t) \approx \exp\left[-\frac{\nabla^2}{2}\Delta t\right]\exp\left[V\Delta t\right]\psi(t). \tag{C.29}$$

We apply now the spatial Fourier transformation $\mathcal{F}[\cdot]$ to get rid of the Laplacian operator

$$\psi(t+\Delta t) = \mathcal{F}^{-1}\left[e^{-\mathbf{k}^2\Delta t/2}\mathcal{F}\left[e^{V\Delta t}\psi(t)\right]\right]. \tag{C.30}$$

This is already the basic form of the Split-Step Fourier method and one can see how the name of the method is chosen as the propagation step is split into propagation in real space and propagation in Fourier space.

With this numerical solution at hand the centre-of-mass and the widths can be calculated from the numerical data by performing the integrals

$$x_{0k}(t) = \int d^2x \ x_k^2 \ |\psi(\mathbf{x},t)|^2 \tag{C.31}$$

and

$$\frac{q_k^2}{2} = \int d^2x \ (x_k - x_{0k})^2 \ |\psi(\mathbf{x},t)|^2 \tag{C.32}$$

numerically. The resulting curves are then fitted by $f(x) = a + b\cos(cx+d)$, where $a,\ b,\ c$ and d are the respective fitting parameters. For the widths the parameter a yields the equilibrium width q_0 and c the oscillation frequency. The mode is selected by choosing appropriate initial conditions.
For the concrete simulation we take a rectangular grid with regularly ordered grid points. We

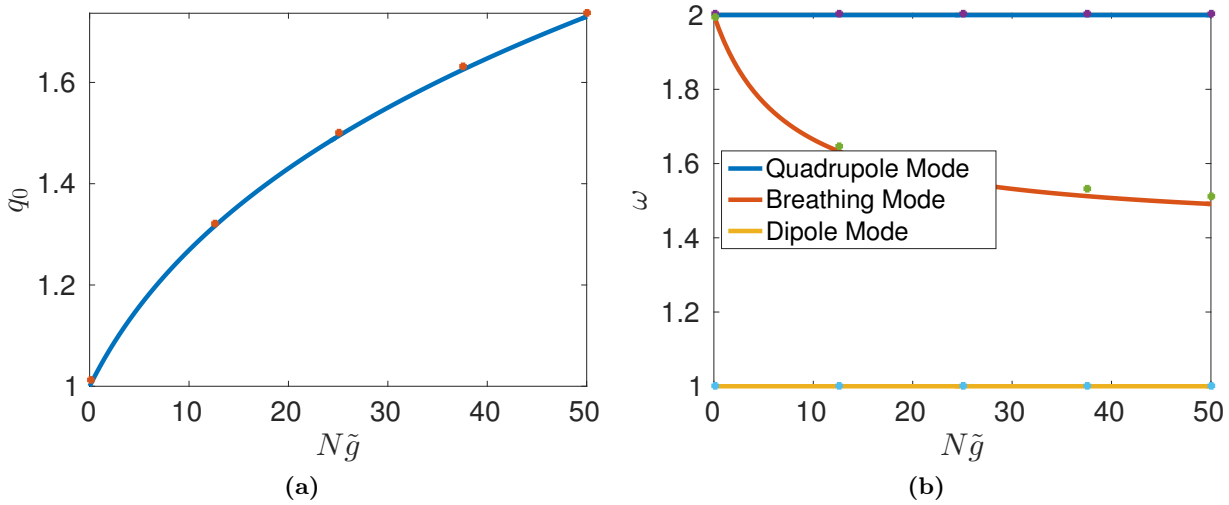

FIG. C.2: Comparison of numerical and analytical results. In Panel **(a)** the results for the equilibrium width is plotted. The blue curve is the analytical solution provided by (C.22). The red dots mark the numerical results. Panel **(b)** deals with the oscillation frequencies, whereas the curves show the analytical results as calculated in (C.12) and in (C.24). The crosses mark the numerical results.

work with 1024^2 grid points which amounts to a distance of 0.0196 between two neighboured points. We evolute one full period that is set by the centre-of-mass oscillation where one time step is 2^{-8}.
The resulting frequencies are shown in Figure C.2. As one can see the agreement between the numerical data from this Section agree with the analytical results from the last Section. However, a small devitiation can be seen for larger interaction strengths $N\tilde{g}$. In this region the ansatz (C.4) gets worse, as the Gaussian ansatz is still based on small interaction strengths. For larger interaction strength the Gaussian ansatz is supposed to bend over into the parabolic form of the Thomas-Fermi limit, where the kinetic energy can be neglected in comparison to the interaction energy.

C.4. Table of Appearing Integrals

This Sectionprovides a table of the integrals appearing by performing the moments approach. They are solved with the methods provided in Appendix B, especially by using Table B.1.

C.4.1. Photon Equation

First Moments

1.
$$\int d^2x\ (x_k - x_{0k})\psi^* \partial_t \psi = N_0 \left(\frac{\partial_t x_{0k}}{2} - iA_k q_k^2 \partial_t x_{0k} + i\frac{q_k^2}{2}\partial_t C_k \right) \tag{C.33}$$

2.
$$\int d^2x\ (x_k - x_{0k})\psi^* \nabla^2 \psi = -N_0 \left(iC_k + 2A_k C_k q_k^2 \right) \tag{C.34}$$

3.
$$\int d^2x\ (x_k - x_{0k})\mathbf{x}^2 |\psi|^2 = N_0 x_{0k} q_k^2 \tag{C.35}$$

4.
$$\int d^2x\ (x_k - x_{0k})T|\psi|^2 = N_0 T_0 G_{\mathrm{T}\psi} \frac{q_k^2 (y_{0k} - x_{0k})}{q_k^2 + r_k^2} \tag{C.36}$$

5.
$$\int d^2x\ (x_k - x_{0k})|\psi|^4 = 0 \tag{C.37}$$

6.
$$\int d^2x\ (x_k - x_{0k})p|\psi|^2 = -N_0 P_0 G_{\mathrm{P}\psi} \frac{q_k^2 x_{0k}}{q_k^2 + s^2} \tag{C.38}$$

7.
$$\int d^2x\ (x_k - x_{0k})pT|\psi|^2 = N_0 P_0 T_0 G_{\mathrm{TP}\psi} \frac{(y_{0k} - x_{0k})q_k^2 s^2 - x_{0k} q_k^2 r_k^2}{(s^2 + r_k^2)q_k^2 + r_k^2 s^2} \tag{C.39}$$

8.
$$\int d^2x\ (x_k - x_{0k})|\psi|^2 = 0 \tag{C.40}$$

Second Moments

1.
$$\int d^2x \ \left[(x_k - x_{0k})^2 - \frac{q_k^2}{2}\right] \psi^* \partial_t \psi = N_0 \frac{q_k \partial_t q_k}{2} + N_0 i \frac{q_k^4 \partial_t A_k}{2} \tag{C.41}$$

2.
$$\int d^2x \ \left[(x_k - x_{0k})^2 - \frac{q_k^2}{2}\right] \psi \nabla^2 \psi = -N_0 \left(-\frac{1}{2} - 2iA_k q_k^2 + 2A_k^2 q_k^4\right) \tag{C.42}$$

3.
$$\int d^2x \ \left[(x_k - x_{0k})^2 - \frac{q_k^2}{2}\right] \mathbf{x}^2 |\psi|^2 = N_0 \frac{q_k^4}{2} \tag{C.43}$$

4.
$$\int d^2x \ \left[(x_k - x_{0k})^2 - \frac{q_k^2}{2}\right] T|\psi|^2 = N_0 T_0 G_{\mathrm{T}\psi} \left[\left(\frac{(y_{0k} - x_{0k}) q_k^2}{r_k^2 + q_k^2}\right)^2 - \frac{q_k^4}{2(q_k^2 + r_k^2)}\right] \tag{C.44}$$

5.
$$\int d^2x \ \left[(x_k - x_{0k})^2 - \frac{q_k^2}{2}\right] |\psi|^4 = -\frac{N_0^2 q_k^2}{8\pi q_1 q_2} \tag{C.45}$$

6.
$$\int d^2x \ \left[(x_k - x_{0k})^2 - \frac{q_k^2}{2}\right] p|\psi|^2 = N_0 P_0 G_{\mathrm{P}\psi} \left[\left(\frac{x_{0k} q_k^2}{s^2 + q_k^2}\right)^2 - \frac{q_k^4}{2(q_k^2 + s^2)}\right] \tag{C.46}$$

7.
$$\int d^2x \ \left[(x_k - x_{0k})^2 - \frac{q_k^2}{2}\right] pT|\psi|^2 = T_0 N_0 I_0 G_{\mathrm{TP}\psi} \left\{\left[\frac{(x_{0k} - y_{0k}) q_k^2 s^2 + x_{0k} q_k^2 p_k^2}{s^2 r_k^2 + q_k^2 (r_k^2 + s^2)}\right]^2 - \frac{q_k^4 (s^2 + r_k^2)}{2[q_k^2 (s^2 + r_k^2) + r_k^2 s^2]}\right\} \tag{C.47}$$

C.4.2. Temperature Equation

First Moments

1.
$$\int d^2x \ x_k \partial_t T = \partial_t (T_0 y_{0k}) \tag{C.48}$$

2.
$$\int d^2x \ x_k \nabla^2 T = 0 \tag{C.49}$$

3.
$$\int d^2x\ x_k T = T_0 y_{0k} \tag{C.50}$$

4.
$$\int d^2x\ x_k |\psi|^2 = N_0 x_{0k} \tag{C.51}$$

Second Moments

1.
$$\int d^2x\ (x_k - y_{0k})^2 \partial_t T = \partial_t \left(T_0 \frac{r_k^2}{2} \right) \tag{C.52}$$

2.
$$\int d^2x\ 2(x_k - y_{0k})^2 \nabla^2 T = 2T_0 \tag{C.53}$$

3.
$$\int d^2x\ (x_k - x_{0k})^2 T = \frac{T_0 r_k^2}{2} \tag{C.54}$$

4.
$$\int d^2x\ (x_k - y_{0k})^2 |\psi|^2 = N_0 \frac{q_k^2}{2} + N_0 (x_{0k} - y_{0k})^2 \tag{C.55}$$

D. Overview of Used Notations and Experimental Values

In this appendix we will list all the necessary quantities, their corresponding symbol and –insofar known– their experimental and theoretical value.

D.1. Natural Constants

Quantity	Symbol	Value
Light velocity	c	$299\,792\,458\,\mathrm{m/s}$
Planck's constant	$\hbar$	$1.054\,571\,8 \times 10^{-34}\,\mathrm{J\,s}$
Boltzmann's constant	k_b	$1.380\,648\,52 \times 10^{-23}\,\mathrm{J/K}$
Vacuum permittivity	ε_0	$8.854\,187\,817 \times 10^{-12}\,\mathrm{C^2/(N\,m^2)}$

D.2. Dye Solution and Temperature Field

D.2.1. Fundamental Constants (R6G in Ethylene Glycol)

Quantity	Symbol	Experimental Value
Refractive index	n	1.46 [103]
Exctinction coefficient	γ	-
Thermal conductivity	κ	$0.258\,\mathrm{W/(m\,K)}$ [103]
Molar weight	-	62.07 g/mol
Specific heat	c_p	$149.5\,\mathrm{J/(mol\,K)} = 2408\,\mathrm{J/(kg\,K)}$ [103]

Density	ρ	$1110\,\mathrm{kg/m^3}$ [103]
Thermo-optic coefficient	$\frac{\partial n}{\partial T}$	$-4.68 \times 10^{-4}/\mathrm{K}$ [44]
Absorption rate	Γ_{abs}	$1 \times 10^{9}\,\mathrm{Hz}$ to $1 \times 10^{10}\,\mathrm{Hz}$ [104]
Quantum yield	η	0.95 [44]

D.2.2. Derived Quantities

Quantity	Symbol	Formula	Theoretical Value
Thermal diffusion coefficient	$\mathcal{D}$	$\lambda_w/(c_p\rho)$	$9.16 \times 10^{-8}\,\mathrm{m^2/s}$
Effective temperature mass	m_T	$\hbar/(2\mathcal{D})$	$5.75 \times 10^{-28}\,\mathrm{kg}$
Effective temp. trap frequency	$\Omega_{\nu T}$	$2\mathcal{D}\nu\pi/L_0\sqrt{2/(L_0R)}$	313.43 Hz
Decay time	τ_1	$1/(\mathcal{D}k_{01}^2)$	$2.49 \times 10^{-6}\,\mathrm{s}$
Effective absorbtion rate	Γ	$(1-\eta)\Gamma_{\mathrm{abs}}$	

D.3. Cavity and Electrical Field

D.3.1. Fundamental Constants

Quantity	Symbol	Experimental Value
Unperturbed length	L_0	$1.5 \times 10^{-6}\,\mathrm{m}$ [44]
Mirror curvature	R	1 m [44]

D.3.2. Derived Quantities

Quantity	Symbol	Formula	Theoretical Value
Photon mass	m_7	$7\pi\hbar n_0/(L_0c)$	$7.53 \times 10^{-36}\,\mathrm{kg}$

Photon trap	Ω	$c/n_0\sqrt{2/(L_0R)}$	$2.37 \times 10^{11}\,\mathrm{Hz}$

D.3.3. Coupling Constants

Quantity	Symbol	Formula	Theoretical Value
Temperature-photon coupling	g_T	$-m_7c^2a\frac{\partial n}{\partial T}/n_0^2$	$-1.13 \times 10^{-22}\,\mathrm{J/K}$
Heating rate	B	$2am_7c^2/(Ln_0c_p\rho)$	$2.73 \times 10^{-10}\,\mathrm{K\,m^2/s}$
Dimensionless thermo-optic interaction	$\tilde{g}_T$	$\tau g_T B$	2.56×10^{-4}

Bibliography

[1] W. Capelle. *Die Vorsokratiker*, volume 119 of *Kröners Taschenausgabe*. Kröner, 9th edition (2008).

[2] H. E. Burton. *The Optics of Euclid. Journal of the Optical Society of America*, **33**, 357 (1943).

[3] T. Lucretius. *De Rerum Natura*. Akademie-Verlag Berlin (1972).

[4] L. de Broglie. *Licht und Materie, Ergebnisse der neuen Physik*. H. Goverts Verlag, Hamburg, 5th edition (1943).

[5] S. I. Newton. *Opticks: Or, A Treatise of the Reflections, Refractions, Inflections and Colours of Light*. Fourth, corrected edition (1730).

[6] C. Huygens. *Abhandlung über das Licht*, volume 20 of *Ostwalds Klassiker der exakten Wissenschaften*. Verlag Harri Deutsch (1996).

[7] A. Sommerfeld. *Vorlesungen über theoretische Physik*, volume III, Elektrodynamik. Akademische Verlagsgesellschaft Geest & Portig K.-G. (1949).

[8] J. C. Maxwell. *A Treatise on Electricity and Magnetism*, volume I. Oxford, 2nd edition (1881).

[9] A. Einstein. *Zur Elektrodynamik bewegter Körper. Annalen der Physik und Chemie*, **Jg. 17**, 891 (1905).

[10] M. Planck. *Über eine Verbesserung der Wienschen Spektralgleichung (1). Verhandlungen der Deutschen Physikalischen Gesellschaft*, **2**, 202 (1900).

[11] M. Planck. *Zur Theorie des Gesetzes der Energieverteilung im Normalspektrum. Verhandlungen der Deutschen Physikalischen Gesellschaft*, **2**, 237 (1900).

[12] M. Planck. *Über das Gesetz der Energieverteilung im Normalspektrum. Drudes Annalen*, p. 553 (1901).

[13] A. Einstein. *Über einen die Erzeugung und Verwandlung des Lichtes betreffenden heuristischen Gesichtspunkt. Drudes Annalen*, p. 132 (1905).

[14] L. de Broglie. *Recherches sur la theorie des quanta. Annale de Physique*, **10**, 22 (1925).

[15] E. Schrödinger. *Quantisierung als Eigenwertproblem I. Annalen der Physik*, **79**, 361 (1926).

[16] E. Schrödinger. *Quantisierung als Eigenwertproblem II. Annalen der Physik*, **79**, 489 (1926).

[17] P. A. M. Dirac. *The Quantum Theory of the Emission and Absorption of Radiation. Proceedings of the Royal Society A*, **114**, 243 (1927).

[18] T. H. Maiman. *Stimulated Optical Radiation in Ruby. Nature*, **187**, 493 (1960).

[19] M. H. Anderson, J. R. Ensher, M. R. Matthews, C. E. Wieman, and E. A. Cornell. *Observation of Bose-Einstein Condensation in a Dilute Atomic Vapor. Science*, **269**, 198 (1995).

[20] K. B. Davis, M. O. Mewes, M. R. Andrews, N. J. van Druten, D. S. Durfee, D. M. Kurn, and W. Ketterle. *Bose-Einstein Condensation in a Gas of Sodium Atoms. Physical Review Letters*, **75**, 3969 (1995).

[21] C. J. Pethick and H. Smith. *Bose-Einstein Condensation in Dilute Gases.* Cambridge University Press, second edition (2008).

[22] O. Lahav, A. Itah, A. Blumkin, C. Gordon, S. Rinott, A. Zayats, and J. Steinhauer. *Realization of a Sonic Black Hole Analog in a Bose-Einstein Condensate. Physical Review Letters*, **105**, 240401 (2010).

[23] J. Anglin. *Quantum Optics: Particles of Light. Nature*, **468**, 517 (2010).

[24] K. Staliunas. *Laser Ginzburg-Landau Equation and Laser Hydrodynamics. Physical Review A*, **48**, 1573 (1993).

[25] H. Haken. *Laser Theory.* Springer-Verlag Berlin Heidelberg, 1st edition (1984).

[26] J. G. A. Swartzlander and C. T. Law. *Optical Vortex Solitons Observed in Kerr Nonlinear Media. Physical Review Letters*, **69**, 2503 (1992).

[27] T. Roger, C. Maitland, K. Wilson, N. Westerberg, D. Focke, E. M. Wright, and D. Faccio. *Optical analogues of the Newton–Schrödinger Equation and Boson Star Evolution. Nature Communications*, **7**, 13492 (2016).

[28] Q. Fontaine, T. Bienaimé, S. Pigeon, E. Giacobino, A. Bramati, and Q. Glorieux. *Observation of the Bogoliubov Dispersion Relation in a Fluid of Light. arXiv: 1807.10242v1* (2018).

[29] H. Deng, H. Haug, and Y. Yamamoto. *Exciton-Polariton Bose-Einstein Condensate. Reviews of Modern Physics*, **82**, 1489 (2010).

[30] I. Carusotto and C. Ciuti. *Quantum Fluids of Light. Reviews of Modern Physics*, **85**, 299 (2013).

[31] H. Deng, G. Weihs, C. Santori, J. Bloch, and Y. Yamamoto. *Condensation of Semiconductor Microcavity Exciton Polaritons. Science*, **298**, 199 (2002).

[32] C. Ciuti, P. Schwendimann, B. Deveaud, and A. Quattropani. *Theory of the Angle-Resonant Polariton Amplifier. Physical Review B*, **62**, R4825 (2000).

[33] J. Kasprzak, M. Richard, S. Kundermann, A. Baas, P. Jeambrun, J. M. J. Keeling, F. M. Marchetti, M. H. Szymanska, R. Andre, J. L. Staehli, V. Savona, P. B. Littlewood, B. Deveaud, and L. S. Dang. *Bose–Einstein Condensation of Exciton Polaritons. Nature*, **443**, 409 (2006).

[34] M. Wouters and I. Carusotto. *Excitations in a Nonequilibrium Bose-Einstein Condensate of Exciton Polaritons. Physical Review Letters*, **99**, 140402 (2007).

[35] J. Klaers, J. Schmitt, F. Vewinger, and M. Weitz. *Bose-Einstein Condensation of Photons in an Optical Microcavity. Nature*, **468**, 545 (2010).

[36] R. A. Nyman and B. T. Walker. *Bose-Einstein Condensation of Photons from the Thermodynamic Limit to Small Photon Numbers. Journal of Modern Optics*, **65**, 754 (2018).

[37] J. Schmitt. *Dynamics and Correlations of a Bose-Einstein Condensate of Photons. arXiv:1807.08747v1* (2018).

[38] A. Einstein. *Strahlungs-Emission und -Absorption nach der Quantentheorie. Verhandlungen der Deutschen Physikalischen Gesellschaft*, **18**, 318 (1916).

[39] B. I. Stepanov and V. P. Gribkovski. *Theory of Luminiscence.* Iliffe Books Ltd (1968).

[40] E. H. Kennard. *On the Thermodynamics of Fluorescence. Physical Review*, **11**, 29 (1918).

[41] R. C. Gilmore. *A Reexamination of the Kennard-Stepanov Relation.* Ph.D. thesis, Department of Physics and Astronomy, University of Rochester (1994).

[42] D. A. Sawicki and R. S. Knox. *Universal Relationship between Optical Emission and Absorption of Complex Systems. Physical Review A*, **54**, 4837 (1996).

[43] J. Schmitt. *Dynamik und Korrelationen eines Bose-Einstein-Kondensats aus Licht.* Ph.D. thesis, Rheinische Friedrich-Wilhems-Universität Bonn (2015).

[44] J. Klaers, J. Schmitt, T. Damm, F. Vewinger, and M. Weitz. *Bose–Einstein Condensation of Paraxial Light. Applied Physics B*, **105**, 17 (2011).

[45] M. Weitz. *Calorimetry of a Bose-Einstein-Condensed Photon Gas.* Talk at "Quantum Fluids of Light and Matter " (2018).

[46] J. Schmitt, T. Damm, D. Dung, F. Vewinger, J. Klaers, and M. Weitz. *Thermalization Kinetics of Light: From Laser Dynamics to Equilibrium Condensation of Photons. Physical Review A*, **92**, 011602 (2015).

[47] J. Klaers, J. Schmitt, T. Damm, F. Vewinger, and M. Weitz. *Statistical Physics of Bose-Einstein-Condensed Light in a Dye Microcavity. Physical Review Letters*, **108**, 160403 (2012).

[48] J. Schmitt, T. Damm, D. Dung, F. Vewinger, J. Klaers, and M. Weitz. *Observation of Grand-Canonical Number Statistics in a Photon Bose-Einstein Condensate. Physical Review Letters*, **112**, 030401 (2014).

[49] T. Damm, J. Schmitt, Q. Liang, D. Dung, F. Vewinger, M. Weitz, and J. Klaers. *Calorimetry of a Bose-Einstein-Condensed Photon Gas. Nature Communications*, **7**, 11340 (2016).

[50] B. T. Walker, L. C. Flatten, H. J. Hesten, F. Mintert, D. Hunger, J. M. Smith, and R. A. Nyman. *Driven-Dissipative Bose–Einstein Condensation of just a Few Photons. arXiv: 1711.11087* (2017).

[51] S. Greveling, F. van der Laan, H. C. Jagers, and D. van Oosten. *Polarization of a Bose-Einstein Condensate of Photons in a Dye-Filled Microcavity. arXiv: 1712.08426* (2017).

[52] D. Dung, C. Kurtscheid, T. Damm, J. Schmitt, F. Vewinger, M. Weitz, and J. Klaers. *Variable Potentials for Thermalized Light and Coupled Condensates. Nature Photonics*, **11**, 565 (2017).

[53] S. Greveling, F. van der Laan, K. L. Perrier, and D. van Oosten. *The Effective Interaction Strength in a Bose-Einstein Condensate of Photons in a Dye-Filled Microcavity. arXiv: 1712.079221* (2017).

[54] I. Bloch, J. Dalibard, and W. Zwerger. *Many-body Physics with Ultracold Gases. Review of Modern Physics*, **80**, 885 (2008).

[55] M. Calvanese Strinati and C. Conti. *Bose-Einstein Condensation of Photons with Nonlocal Nonlinearity in a Dye-Doped Graded-Index Microcavity. Physical Review A*, **90**, 043853 (2014).

[56] E. C. I. van der Wurff, A.-W. de Leeuw, R. A. Duine, and H. T. C. Stoof. *Interaction Effects on Number Fluctuations in a Bose-Einstein Condensate of Light. Physical Review Letters*, **113**, 135301 (2014).

[57] M. Radonjić, W. Kopylov, A. Balaž, and A. Pelster. *Interplay of Coherent and Dissipative Dynamics in Condensates of Light. New Journal of Physics*, **20**, 055014 (2018).

[58] M. Weitz. *Scanned Hand-Written Notes on Heat Transfer and Coupling to Photons* (2012).

[59] H. Alaeian, M. Schedensack, C. Bartels, D. Peterseim, and M. Weitz. *Thermo-Optical Interactions in a Dye-Microcavity Photon Bose-Einstein Condensate. New Journal of Physics*, **19**, 115009 (2017).

[60] A. Zangwill. *Modern Electromagnetism.* Cambridge University Press, 1st edition (2013).

[61] R. W. Boyd. *Nonlinear Optics*. Acadamic Press, 3rd edition (2008).

[62] M. Franko and C. D. Tran. *Analytical Thermal Lens Instrumentation. Review of Scientific Instruments*, **67**, 1 (1996).

[63] D. Vocke, K. Wilson, F. Marino, I. Carusotto, E. M. Wright, T. Roger, B. P. Anderson, P. Öhberg, and D. Faccio. *Role of Geometry in the Superfluid Flow of Nonlocal Photon Fluids. Physical Review A*, **94**, 013849 (2016).

[64] L. D. Landau and E. M. Lifschitz. *Lehrbuch der theoretischen Physik*, volume VI, Hydrodynamik. Akademie-Verlag, 3rd edition (1978).

[65] M. Lax, W. H. Louisell, and W. B. McKnight. *From Maxwell to Paraxial Wave Optics. Physical Review A*, **11**, 1365 (1975).

[66] L. A. Lugiato and R. Lefever. *Spatial Dissipative Structures in Passive Optical Systems. Physical Review Letters*, **58**, 2209 (1987).

[67] F. Marino. *Acoustic Black Holes in a Two-Dimensional "Photon Fluid". Physical Review A*, **78**, 063804 (2008).

[68] P. N. Butcher and D. Cotter. *The Elements of Nonlinear Optics*, volume 9. Cambridge University Press (1993).

[69] F. T. Arecchi and R. Bonifacio. *Theory of Optical Maser Amplifiers. IEEE Journal of Quantum Electronics*, p. 196 (1965).

[70] R. A. Nyman and M. H. Szymańska. *Interactions in Dye-Microcavity Photon Condensates and the Prospects for their Observation. Physical Review A*, **89**, 033844 (2014).

[71] N. D. Mermin and H. Wagner. *Absence of Ferromagnetism or Antiferromagnetism in One- or Two-Dimensional Isotropic Heisenberg Models. Physical Review Letters*, **17**, 1133 (1966).

[72] P. C. Hohenberg. *Existence of Long-Range Order in One and Two Dimensions. Physical Review*, **158**, 383 (1967).

[73] M. Ueda. *Fundamentals and New Frontiers of Bose-Einstein Condensation*. World Scientific (2010).

[74] Z. Hadzibabic and J. Dalibard. *Two-Dimensional Bose Fluids: An Atomic Physics Perspective. Rivista del Nuovo Cimento*, **34**, 389 (2011).

[75] J. Goldstone, A. Salam, and S. Weinberg. *Broken Symmetries. Physical Review*, **127**, 965 (1962).

[76] A. Hurwitz. *Ueber die Bedingungen, unter welchen eine Gleichung nur Wurzeln mit negativen reellen Theilen besitzt. Mathematische Annalen*, **46**, 273 (1895).

[77] V. M. Pérez-García, H. Michinel, J. I. Cirac, M. Lewenstein, and P. Zoller. *Dynamics of Bose-Einstein Condensates: Variational Solutions of the Gross-Pitaevskii Equations. Physical Review A*, **56**, 1424 (1997).

[78] A. L. Fetter and D. Rokhsar. *Excited States of a Dilute Bose-Einstein Condensate in a Harmonic Trap. Physical Review A*, **57**, 1191 (1998).

[79] H. Al-Jibbouri and A. Pelster. *Breakdown of the Kohn theorem near a Feshbach resonance in a magnetic trap. Physical Review A*, **88**, 033621 (2013).

[80] D. M. Stamper-Kurn, H.-J. Miesner, S. Inouye, M. R. Andrews, and W. Ketterle. *Collisionless and Hydrodynamic Excitations of a Bose-Einstein Condensate. Physical Review Letters*, **81**, 500 (1998).

[81] N. Mann, M. R. Bakhtiari, A. Pelster, and M. Thorwart. *Nonequilibrium Quantum Phase Transition in a Hybrid Atom-Optomechanical System. Phys. Rev. Lett.*, **120**, 063605 (2018).

[82] V. M. Pérez-García, H. Michinel, J. I. Cirac, M. Lewenstein, and P. Zoller. *Low Energy Excitations of a Bose-Einstein Condensate: A Time-Dependent Variational Analysis. Physical Review Letters*, **77**, 5320 (1996).

[83] Y. I. M. K. K. K. Akira Takahashi, Mitsunori Nishizawa. *New Femtosecond Streak Camera with Temporal Resolution of 180 fs* (1994).

[84] A. D. Polyanin and A. V. Manzhiro. *Handbook of Integral Equations.* Chapman & Hall/CRC, 2nd edition (2008).

[85] P. D. P. von der Lippe. *Deskriptive Statistik.* Gustav Fischer Verlag (1993).

[86] A. Z. Grinshpan. *Weighted Inequalities and Negative Binomials. Advances in Applied Mathematics*, **45**, 564 (2010).

[87] H. Haken. *Licht und Materie II, Laser.* B.I. Wissenschaftsverlag, 1st edition (1981).

[88] R. I. Moodie, P. Kirton, and J. Keeling. *Polarization Dynamics in a Photon Bose-Einstein Condensate. Physical Review A*, **96**, 043844 (2017).

[89] M. Wouters and V. Savona. *Stochastic Classical Field Model for Polariton Condensates. Physical Review B*, **79**, 165302 (2009).

[90] K. A. Selanger, J. Falnes, and T. Sikkeland. *Fluorescence Lifetime Studies of Rhodamine 6G in Methanol. The Journal of Physical Chemistry*, **81**, 1960 (1977).

[91] C. V. Bindhu, S. S. Harilal, V. Nampoori, and C. Vallabhan. *Solvent Effect on Absolute Fluorescence Quantum Yield of Rhodamine 6G Determined Using Transient Thermal Lens Technique. Mordern Physics Letters B*, **13**, 563 (1999).

[92] X. Xu, Y. Hu, Z. Zhang, and Z. Liang. *Spinor Polariton Condensates under Nonresonant Pumping: Steady states and Elementary Excitations. Physical Review B*, **96**, 144511 (2017).

[93] A. Smerzi, S. Fantoni, S. Giovanazzi, and S. R. Shenoy. *Quantum Coherent Atomic Tunneling between Two Trapped Bose-Einstein Condensates. Physical Review Letters*, **79**, 4950 (1997).

[94] M. W. Jack, M. J. Collett, and D. F. Walls. *Coherent Quantum Tunneling between two Bose-Einstein Condensates. Physical Review A*, **54**, R4625 (1996).

[95] G. Roumpos, M. D. Fraser, A. Löffler, S. Höfling, A. Forchel, and Y. Yamamoto. *Single Vortex–Antivortex Pair in an Exciton-Polariton Condensate. Nature Physics*, **7**, 129 (2011).

[96] L. Dominici, R. Carretero-González, A. Gianfrate, J. Cuevas-Maraver, D. J. Frantzeskakis, G. Lerario, D. Ballarini, M. De Giorgi, G. Gigli, P. G. Kevrekidis, and D. Sanvitto. *Interactions and Scattering of Quantum Vortices in a Polariton Fluid. Nature Communications*, **9**, 1467 (2018).

[97] V. N. Gladilin and M. Wouters. *Interaction and Motion of Vortices in Nonequilibrium Quantum Fluids. New Journal of Physics*, **19**, 105005 (2017).

[98] A. Kempf, D. M. Jackson, and A. H. Morales. *New Dirac delta Function Based Methods with Applications to Perturbative Expansions in Quantum Field Theory. Journal of Physics A: Mathematical and Theoretical*, **47**, 415204 (2014).

[99] A. Kempf, D. M. Jackson, and A. H. Morales. *How to (path-) Integrate by Differentiating. Journal of Physics: Conference Series*, **626**, 012015 (2015).

[100] T. Busch, J. I. Cirac, V. M. Pérez-García, and P. Zoller. *Stability and Collective Excitations of a Two-Component Bose-Einstein Condensed Gas: A Moment Approach. Physical Review A*, **56**, 2978 (1997).

[101] W. Kohn. *Cyclotron Resonance and de Haas-van Alphen Oscillations of an Interacting Electron Gas. Physical Review*, **123**, 1242 (1961).

[102] T. R. Taha and M. J. Ablowitz. *Analytical and Numerical Aspects of Certain Nonlinear Evolution Equations. II. Numerical, Nonlinear Schrödinger Equation. Journal of Computational Physics*, **55**, 203 (1984).

[103] *Ethylene Glycol, MEGlobal Product Guide.*

[104] R. A. Nyman. *Absorption and Fluorescence spectra of Rhodamine 6G* (2017).

Danksagung

Da die Arbeit nun zusammen mit den vergangenen fünf Jahren meines Studiums das Ende findet, möchte ich die Gelegenheit nutzen und einigen Menschen meinen tiefsten Dank aussprechen.
An erster Stelle möchte ich meiner Familie und vor allem meinen Eltern Werner und Claudia danken. Ohne diese bedingungslose Unterstützung, die ihr mir immer zugesichert und auch gezeigt habt, hätte ich das Studium niemals schaffen können.
Mein nächster Dank gilt meinem Betreuer Priv.-Doz. Dr. Axel Pelster, der mir die Möglichkeit gegeben hat, diese Arbeit anzufertigen und mit seiner motivierenden Art und mit Rat und Tat mich durch die vergangenen beiden Jahre wissenschaftlich begleitet hat und es mir auch ermöglichte, zu vielen interessanten Konferenzen zu fahren.
Als nächstes gilt mein Dank meinen Kommilitonen, mit denen es immer Spaß machte, zusammen zu studieren. Mein besonderer Dank gilt Christoph Dauer und Alexej Gaidukov, die mir das ganze Studium über beistanden und auch große Teile dieser Arbeit gegen gelesen haben. Mein Dank gilt auch meinen Kommilitonen von der jungen DPG, ohne deren Projekte ich nicht der Mensch wäre, der ich jetzt bin.
Des Weiteren möchte ich auch den experimentellen Kollegen für die vielen interessanten Diskussionen danken.
Schließlich geht mein Dank auch an Sebastian Eggert, der es mir ermöglicht hat, diese Diplomarbeit in seiner Gruppe anzufertigen, und an die gesamte Arbeitsgruppe, die mir immer eine freundliche, konzentrierte und hilfsbereite Umgebung geboten hat.
Finally, I want also to thank my international colleagues Milan Radonjic and Antun Balaz for the helpful and in inspiring discussions and the pleasant stays in Belgrade.

Selbstständigkeitserklärung

Ich versichere, dass ich die Arbeit selbständig verfasst und keine anderen als die angegebenen Hilfsmittel verwendet habe.

Kaiserslautern, den 30. Juli 2018

_____

Enrico Stein